Ph.D. THESIS

Probabilistic Stability Evaluation of Vehicles under Strong Winds for Bridge Traffic Control

강풍 시 교량의 교통통제를 위한 확률론적 차량안정성 평가

2020 년 2 월

서울대학교 대학원

건설환경공학부

김 세 진

ABSTRACT

Probabilistic Stability Evaluation of Vehicles under Strong Winds for Bridge Traffic Control

Se-Jin Kim
Department of Civil and Environmental Engineering
Seoul National University

This study aims to propose a probabilistic evaluation method of vehicle stability on bridges for strong winds so that can provide valuable information during decision-making process related to traffic restriction or construction of wind barrier. The proposed method consists of three main items: 1) measurement of the aerodynamic coefficients of a vehicle on a bridge girder through wind tunnel test, 2) estimation of critical wind speed and traffic control wind speed through vehicle simulation, and 3) evaluation of vulnerability level considering wind environment at bridge site. As a case study, the developed method is applied to Gwnagan Bridge which is a double-deck truss type suspension bridge. Three vehicle models, a sedan, a truck and a tractor-trailer, are investigated.

A new developed measurement system and special jig system are introduced which are to estimate the six aerodynamic coefficients of vehicles on bridge models. The aerodynamic coefficients of vehicle models are measured on the 2-D girder sectional model in order to reflect the effect of

girder shape on the wind flow. The variations of coefficients are obtained for every traffic lane and various wind incident angles. In the case of the Gwangan Bridge, experiments are conducted for the main and approaching span. The large differences in the measurement results between the road sections are observed, and the causes of this large gap are discussed.

Two vehicle simulation methods are introduced, the dynamic and quasi-static approach. The well-known commercial software CarSim and TruckSim are adopted as a dynamic approach, while the quasi-static approach is developed by the author based on equilibrium equations. The validity of the developed quasi-static model is verified by comparing the estimated tire reaction forces with those of the dynamic approach.

A method to estimate critical wind speed curve and establish traffic control guideline is proposed. Critical wind speed curve (CWC) is estimated by vehicle simulation based on the pre-defined accident criteria. The uncertainty of turbulence and road geometries such as cant and curvature are considered during the vehicle simulation. CWC is estimated for all considered traffic lanes and road sections, and both quasi-static and dynamic approaches are utilized to minimize the total simulation time. CWC is also estimated according to the vehicle speed and road conditions. Based on the estimated CWCs, traffic control guideline is determined according to the road condition. In the case of Gwangan Bridge, CWC estimation is performed for one main span and two approach spans, and a traffic control guideline is established for the most dangerous road section.

A vulnerability evaluation method is developed that takes into account the wind environment at the bridge site. Long-term measurement data are used to obtain probability density functions of wind speeds for 16 wind directions, and the frequency of exceeding the critical level per a year is estimated based on the estimated CWCs. The vulnerability index is estimated for all traffic lanes, and the most vulnerable traffic lane and road section is identified by comparing the results. According to the application results, the lower deck of approaching span 1 of Gwangan Bridge was identified as the most vulnerable section among the whole area due to the relative angle between driving direction and the dominant direction of strong wind. By conducting further experiments and simulations, it could be found that installation of wind barriers in this road section can remarkably reduce vulnerability level of the bridge by more than 75%.

It is expected that the proposed methodology can provide valuable and useful information for decision-making and planning to ensure the vehicle safety on bridges against strong winds.

Keywords: Strong wind; Bridge; Vehicle stability evaluation; Wind tunnel test; Traffic control;

Student Number: 2015-30275

TABLE OF CONTENTS

LIST OF FIGURES

LIST OF TABLES

CHAPTER 1

INTRODUCTION

1.1 Research background

Vehicles crossing long-span bridges are often exposed to strong side-winds. Accidents involving side-slipped and overturned vehicles occur often on bridges such as the Gwangan and Seohae Bridges in Korea. Typhoon Jebi hit Japan in 2018, and videos taken during Jebi showing a heavy truck overturned on a bridge are available on the internet (The Weather Network, 2018). As the number of long-span bridges increases throughout the world, this issue increases in importance, and many wind-induced vehicle accidents have been reported in past decades (Baker and Reynolds, 1992; Zhu et al., 2012).

In order to prevent these accidents, the installation of wind barrier or traffic control actions have been proposed for protecting vehicles from high-speed winds. These measures can effectively mitigate the vulnerability of vehicle crossing a bridge under a crosswind. However, excessive applications of wind barriers or traffic control guidelines can cause negative effect in terms of economic aspect. Hence, an appropriate vehicle stability assessment which adequately considers the surrounding environmental and effect of structural shapes of bridges is necessary to provide valuable information for decision-making process.

Therefore, this study aims to develop and propose a probabilistic method for evaluation of vehicle stability considering the aerodynamic characteristics of bridges and vehicles. The vehicle stability is assessed by estimating critical wind speed and frequency of exposure to strong wind. The proposed methodology includes three main items: 1) estimation of aerodynamic coefficients of the vehicle through wind tunnel tests, 2) estimation of critical wind speed curves (CWC) through vehicle simulations, and 3) vulnerability evaluation using long-term measured wind data. Before introducing the details of the developed method, the literatures on the relevant topic were reviewed in the next section.

1.2 Literature review

1.2.1 Aerodynamic coefficients of vehicle

The aerodynamic coefficient of the vehicle is one of the most important information when performing a vehicle simulation because it is used to simulate the wind load acting on a vehicle body. For decades, extensive researches has been carried out to accurately estimate the aerodynamic coefficients.

The wind tunnel test has been the most widely adopted method for estimating coefficients using scaled vehicle models (Baker, 1986a; Baker, 1991a; Cheli et al, 2011a). The basic configuration of the experiment used a

scale vehicle model fixed to the tunnel floor, and the wind load was measured by a force balance sensor. This method is simple and convenient to perform, so it can be applied in small wind tunnel sections. In order to simulate more realistic wind flows around the bodywork, more complex wind tunnel testing methods also have been developed that utilize moving vehicle models using a catapult and a special jig system (Dorigatti et al., 2015; Xiang et al., 2017; Wang et al., 2018). Differences between the static and moving test methods were observed particularly in the lift coefficient which is sensitive to underbody flow pattern (Baker and Humphrey, 1996). However, in the case of side force and rolling moment, the dominant parameters for vehicle accidents, only slight differences were observed between the two methods (Baker and Humphrey, 1996; Dorigatti et al., 2015). A comparison between the results of the wind tunnel test and the full-scale test was also performed by Sterling et al. (2010) and Baker et al. (2004), and their reports confirmed a reasonable agreement between the two test methods for the mean and peak values of the side force and the rolling moment coefficients despite large differences in lift force.

Cooper (1984), Baker (1991b and 2010), and Wu et al. (2014) studied the aerodynamic admittance effect of a vehicle body which is induced by uncorrelated gust wind over the length of a vehicle. They suggested the weighting function in the frequency domain which allows to simulate wind loads with consideration of frequency dependency. According to Baker

(1991b, 2009, and 2010), admittance effect can be also easily considered by filtering the wind fluctuation time periods less than around 0.5 ~ 3 seconds.

Research works on the change of vehicle aerodynamic coefficient according to the shape of infrastructure have also been carried out by several researchers. Suzuki et al. (2003) performed several wind tunnel tests using scaled bridge girder sections and vehicle models and showed changes in coefficients according to the thickness of the bridge girder. They emphasized that the aerodynamic characteristics of the vehicle depend not only on the shape of the vehicle but also on the shape of the infrastructure. Cheli et al. (2011b) also reported the sensitivity of coefficients to infrastructure geometries. They measured vehicle aerodynamic coefficients on viaducts and embankments and found that wakes behind the vehicle body were greatly influenced by the width of the infrastructure, which in turn affected the side force and rolling moment coefficients. Chen et al. (2015) and Zhu et al. (2012) also performed experiments on bridge decks and observed changes in aerodynamic coefficients according to traffic lanes.

1.2.2 Vehicle simulation for estimation of critical wind speed

Estimation of vulnerability of vehicles crossing bridges begins with an evaluation of the critical wind speed, which is defined as the wind speed at which vehicles will side-slip or overturn. Once the critical wind speed is estimated, the vulnerability of the bridge can be performed (Kim et al., 2016).

Accordingly, appropriate numerical analysis model is required for the evaluation of the critical wind speeds of vehicles.

Extensive studies for simulating of vehicle movements and evaluating critical wind speed for given conditions have been conducted. Baker (1986b, 1987, 1991a, 1991b, 1991c) constructed an analytical framework that can be applied to simulate aerodynamic forces and vehicle motion. He performed several wind tunnel tests to examine the aerodynamic forces of vehicles according to wind direction, and introduced safety analysis methods which is to estimate critical wind speed. Similarly, Batista and Perkovič (2014) also proposed a simple static analysis method for estimating critical wind speed based on the tire reaction forces.

Several vehicle simulation methods have been proposed with consideration of wind-bridge-vehicle interactions (Xu and Guo, 2003; Chen and Cai, 2004; Han et al., 2014; Chen et al., 2015). They developed dynamic vehicle models and performed time-domain analysis to evaluate vehicle movement on a bridge, and estimated critical wind speeds for various vehicle speeds. Chen and Wu (2011) also considered stochastic traffic flow to simulate the vehicle-bridge system more realistic. All of these achievements helped to simulate vehicle reactions more realistically by calculating the tire reaction force and displacement of the vehicle, taking into account the vibrations of the bridge girders. Most of these studies focused mainly on the simulation of a vehicle system on a bridge or the calculation of critical wind speeds. However, there are very limited research works which considers the effect of bridge girder on

the vehicle stability during estimation of critical wind speed. Besides, the influence of the wind direction and the road geometry which are considered to be important factors for vehicle stability (Baker, 1987; Kim et al., 2016), are also hardly considered.

1.2.3 Risk assessment through probabilistic analysis

Several studies have been carried out to assess the risk level of driving vehicles against strong winds. In general, two methods were widely used for risk assessment. The first one is estimation of reliability index by defining limit state for the vehicle hazards (Sigbjörnsson and Snæbjörnsson, 1998; Carrarini, 2007; Snæbjörnsson et al., 2007; Proppe and Wetzel, 2010; Chen and Chen, 2013; Baker, 2015). They used several probability models to assume the distribution of various parameters, such as gust factor, road friction coefficient, aerodynamic coefficient, and driving speed. Based on the distribution models, reliability index was estimated for various wind scenario.

Another method also employs a probabilistic approach to assess risk level but uses long-term measured wind data to reflect the wind environment at the survey location (Baker, 1991c; Coleman and Baker, 1992; Andersson et al., 2004; Diana et al., 2008; Kim et al., 2016). They derived probability distribution functions from long-term wind data for 16 different wind directions and estimated the frequency of occurrence of risk situation during a year. Misu and Ishihara (2018) developed a method for assessing risk by

considering wind correlation along the target road segment. They performed CFD (computational fluid dynamics) to derive the correlation function between the wind speeds between the selected points and derived virtual long-term wind data based on the obtained functions. As a result, wind speed data from multiple locations could be obtained from one single measurement point, and the risk level of the entire road could be estimated.

Kwon et al. (2011) and Kim et al. (2011) also presented a method for assessing the frequency of exposure to hazardous crosswinds in order to propose guidelines for the decision-making process with respect to the need for wind barriers. They estimated the expected days for vehicle accidents through stochastic analysis using long-term wind data, and estimated the total expected cost induced by accidents. Using this method, decisions for the construction of windscreens can be justified from an economic perspective.

Most of the foregoing studies provided reasonable methodologies to estimate the risk level of running vehicle but only focused on straight road and did not considers details such as the positions of running vehicles over a bridge deck, road geometry, and the effect of girder shape on the wind flow. Since vehicle stability highly depends on the road geometry and vehicle location (Kim et al., 2016), it is necessary to develop a vulnerability evaluation method which can consider not only wind distribution but also the structural details of target bridge.

1.2.4 Risk mitigation method

In order to reduce the level of risk of driving vehicles under strong winds, two mitigation methods, traffic control, and wind barrier installation have generally been considered. Very limited number of researches have been done for the first mitigation method. Baker (1987) estimated critical wind speeds of vehicles according to wind direction and proposed a traffic control guideline. He categorized the strategy into two levels: level 1) vehicle speed limit for high-sided vehicles, level 2) traffic restriction for all vehicles. He proposed wind speeds corresponding to each control step based on the estimated critical wind speeds. Also, Fujii et al. (1999) and Imai et al. (2002) showed a procedure for establishing a train traffic control strategy. Wind tunnel test was performed to take into account the impact of infrastructure geometry. They estimated critical wind speeds for various vehicle speeds and suggested traffic control wind speeds according to wind direction.

The effect of wind barrier has been studied for decades. Coleman and Baker (1992) measured the changes of side force and lift force coefficients of the vehicle by locating it behind wind fences. They observed large reductions in both force coefficients even for the lower protection barrier. Chen et al. (2015) also measured the change in the aerodynamic coefficients of a vehicle and applied them during the vehicle simulation. According to his results, the wind barrier increased the critical wind speed dramatically. Chu et al. (2013) examined the effect of the barrier on vehicle stability on a bridge through

CFD simulation. He mentioned that the influence of barrier porosity is negligible compared to that of the barrier's height.

1.3 Proposed probabilistic evaluation method of vehicle stability

The proposed vehicle stability evaluation method consists of three main parts of which the procedure and output of each part are shown in Fig. 1.1. The first part is the estimation of aerodynamic characteristics of vehicles on a bridge through the wind tunnel test. Since the aerodynamic coefficients highly depend on the shape of the girder section and vehicle location, the experiment is performed using 2D girder sectional model. Variation of aerodynamic coefficients of vehicles is estimated on all traffic lanes.

The second part is estimation of critical wind speed of vehicles through vehicle simulation. Computer simulations are performed to calculate the displacement and tire reaction force of vehicles and the wind speed at which the vehicle can overturn or side-slip is estimated. In carrying out the simulation, the aerodynamic coefficients obtained from the wind tunnel tests are utilized, and details of road geometries such as curvature and cant are considered. Since the turbulent component of the wind is a stochastic process, the critical wind speed is also determined by probability analysis. Based on the estimated critical wind speed, wind speeds for traffic control can be determined as the final outputs.

The last part is the vulnerability evaluation. In this study, the frequency of exceeding the critical level per year is adopted as the vulnerability index, and the evaluation is performed considering the wind environment at bridge site and the results of part 2. Long-term measured wind data is used to obtain wind distribution models for 16 wind directions. Vulnerability index is estimated for every traffic lane, and the most vulnerable location can be identified based on the evaluation results.

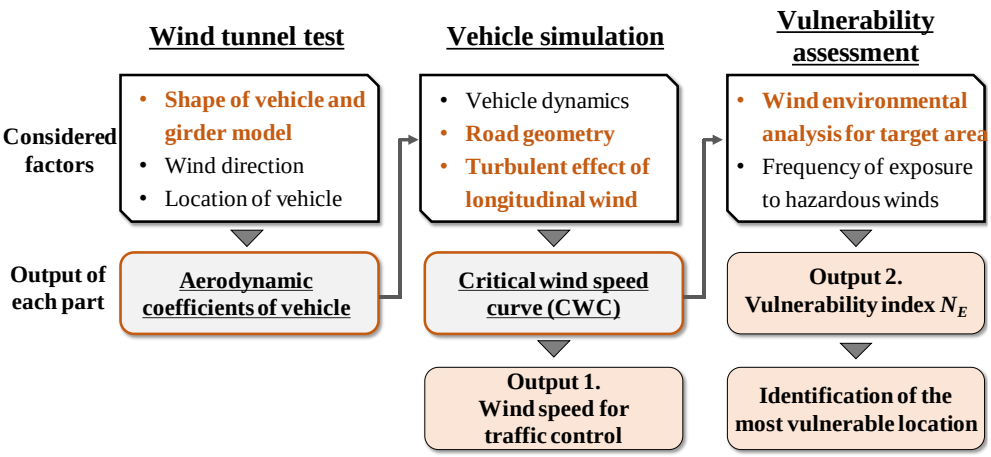

Fig. 1.1. The proposed methodology for evaluation of vehicle stability on a bridge for strong wind

1.4 Structure of the thesis

This thesis is organized into six chapters and structured in order to introduce each parts of the proposed methodology.

In this chapter, the background of this work and the brief introduction of the proposed method are described. Several related works of literature are also reviewed.

Next, in Chapter 2, a methodology to measure aerodynamic coefficients of vehicles on bridge girders is introduced. Scaled vehicle and girder models are utilized during wind tunnel test, and aerodynamic coefficients are obtained for various wind directions using a specially designed measurement system. Parameterization is performed to define six aerodynamic coefficients for whole wind direction.

Chapter 3 introduces two vehicle simulation methods, a dynamic and a quasi-static approach. Well-known commercial software, CarSim and TruckSim are adopted as the dynamic approach to simulate the vehicle system taking into account various components such as tires, suspension, driver. The quasi-static approach developed by the author is also described. Two vehicle types have been developed based on the equilibrium equations. The first type is a regular vehicle model with two axles and four wheels, and the other is a tractor-trailer model. The examination of feasibility of using these two quasi-static model in assessing the risk level of a vehicle under strong wind is performed.

Chapter 4 presents a method for estimating a critical wind speed curve (CWC). A probabilistic method is adopted to determine the CWC to consider the turbulence effect of wind. A determination procedure of wind speed for

traffic control using both dynamic and quasi-static approaches is also described.

In Chapter 5, a vulnerability evaluation method is proposed. Probability distributions of wind speed are derived for 16 different wind directions using long-term measured wind data. The vulnerability index of each traffic lane and road section is estimated based on the CWC obtained from Chapter 4. The most vulnerable section is determined by estimating the vulnerability index for separate road sections of the target bridge. The effect of wind barrier for reducing vulnerability level is also discussed.

Finally, in Chapter 6, the main results and contribution of this research is summarized, and several further research topics are discussed.

As a case study, the proposed framework is applied to an example bridge, Gwangan Bridge. This is a double-deck type suspension bridge located at Busan in Korea, and the total length is 5,120 m. Each deck has four traffic lanes, and the vertical distance between the two decks is about 9 m. The reason of this selection is the two consecutive wind-induced vehicle accidents that occurred on April, 3rd, 2012. The interesting point of these accidents is that both accidents occurred on the same road section which was the lower deck of approaching span rather than the main span. Therefore, the vehicle stability is estimated for Gwangan Bridge according to the road section and the influence of several factors which might be the main causes of the accident are investigated. The traffic control strategy is also suggested by applying the proposed methodology.

CHAPTER 2

ESTIMATION OF AERODYNAMIC COEFFICIENTS OF VEHICLES THROUGH WIND TUNNEL TEST

The aerodynamic coefficients of vehicle are the most important factors during vehicle simulation which can largely effect on the results of critical wind speed. Since the coefficients can change according to the shape of infrastructure (Suzuki et al., 2003; Zhu et al., 2012), realization of the environment of wind tunnel test or CFD simulation will be the one of the key issue in order to obtain reliable aerodynamic coefficients.

In this chapter, the measurement method was introduced which is to estimate aerodynamic coefficients of vehicle not only under the uniform wind but also on the 2D girder section. In section 2.1, the measurement system to estimate aerodynamic coefficients of vehicle and information of investigated vehicle models were introduced. In section 2.2, aerodynamic coefficients of three vehicle models were obtained under uniform wind condition. The adequacy of adopted experiment set-up was also examined by comparison with the results provided by several literatures. In section, section 2.3, the method to estimate aerodynamic coefficients of vehicle on the girder model for various wind incident angle was introduced. The coefficients of three vehicle models were obtained on the 2D sectional model of Gwangan Bridge for approaching and main span. In section 2.4, parameterization of

aerodynamic coefficients obtained under uniform wind and on girder section was performed to express the variation of the coefficients by form of sinusoidal function.

2.1 Measurement of aerodynamic forces and moments acting on vehicle models

There are two methods to measure the aerodynamic coefficients of vehicle model: static model test and moving model test. In general case, moving model test would be the best option because wind profile seen by a vehicle is skewed by vehicle own speed (Dorigatti et al. 2015; Ming et al. 2018) which causes the change of wind direction and amplitude of wind speed that vehicle experiences. Also, moving vehicle test can reproduce the ground flow under the bottom of the vehicle which effects on lift force and pitching moment. However, moving vehicle test has a high level of difficulty to perform because of the required size of test section and distortion of the measurement due to the mechanical noise induced by motor or track irregularity. Therefore, static vehicle model test has been still commonly adopted to many research works (Sterling et al., 2010; Zhu et al., 2012; Salati et al., 2017). According to results provided by previous research works (Baker and Humphrey,1986; Sterling et al., 2010; Dorigatti et al.,2015), interestingly, there are no significant difference in side force and rolling moments which are considered as the main causes of the vehicle accidents. Therefore, considering the size of the test

section, static model test was adopted in this paper rather than moving vehicle test.

2.1.1 Wind load measurement system

The experiment to measure the variations of aerodynamic coefficients of vehicle models was performed at the wind tunnel at Seoul National University. The wind tunnel is an opened circuit wind tunnel, and the available range of wind speed is from 1 m/s to 23 m/s. The width of the test section is 1.0 m, the height is 1.5 m, and the length is 4.0 m. Considering the size of the test section, all vehicle and bridge models were prepared to scale of 1/70.

Three aerodynamic forces and three aerodynamic moments acting on the vehicle models were measured using Nano17 SI-12-0.12 sensor which is a six-axis load cell manufactured by ATI Industrial Automation as shown in Fig. 2.1 (a). This sensor is optimized to measure small amplitude of external load and the maximum sensing ranges of the sensor are 12 N for forces and 0.12 N·m for moments and the accuracies is less than 1% of the capacity. The sensor was installed inside of the vehicle models as Fig. 2.1 (b), and mounted on the aluminum I-shape jig. The distance between the tires of the vehicle models and the girder sectional model were kept about 2 mm during the experiments.

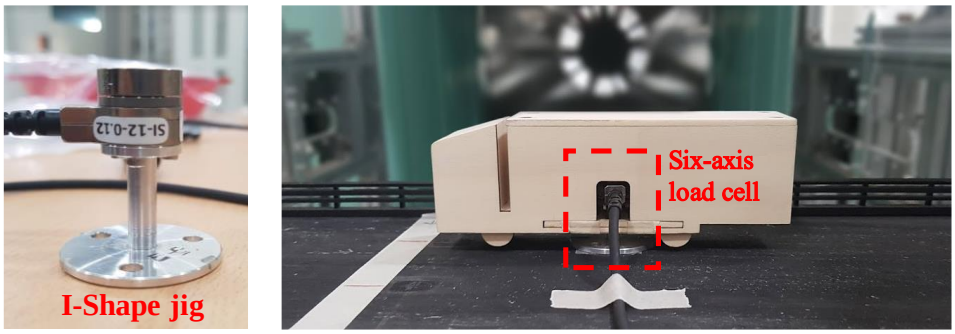

(a) (b)

Fig. 2.1. Measurement sensor and jig. (a) Six-axis load cell and I-shape jig, (b) position of the load cell inside vehicle model

The data collecting time for a single record is 60 seconds at a sampling frequency of 1 kHz, and the averaged value was taken to estimate aerodynamic coefficients. Six aerodynamic coefficients were calculated according to Equations (2.1) and (2.2).

$$C_D = \frac{2F_D}{A\rho V^2} \qquad C_S = \frac{2F_S}{A\rho V^2} \qquad C_L = \frac{2F_L}{A\rho V^2} \tag{2.1}$$

$$C_R = \frac{2M_R}{A\rho h_c V^2} \qquad C_P = \frac{2M_P}{A\rho h_c V^2} \qquad C_Y = \frac{2M_Y}{A\rho h_c V^2} \tag{2.2}$$

In Equation (2.1) and (2.2), C_D, C_S, C_L, C_R, C_P, and C_Y are the aerodynamic coefficients for drag force, side force, lift force, rolling moment, pitching moment, and yawing moment where F_D, F_S, F_L, M_R, M_P, and M_Y are the corresponding averaged forces and moment acting on the center of gravity of a vehicle model. ρ is the air density (=1.225 kg/m^3), V is the upcoming wind speed, and A is the front area of the vehicle model. Fig. 2.2 shows the sign convention of all the forces and moments acting on a vehicle model. In the figure, ψ is the wind incident angle that vehicle experiences.

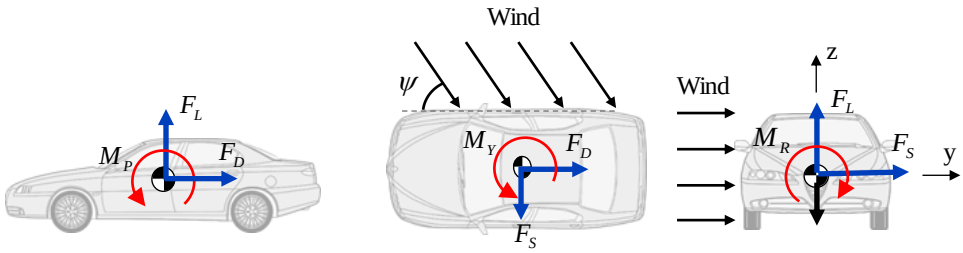

Fig. 2.2. Sign convention of aerodynamic forces and moments

2.1.2 Investigated vehicle models

Three different vehicle models were investigated: a sedan, a truck and a tractor-trailer which are the common vehicle types in South Korea. Detail dimensions provided by Zhu et al. (2012) were utilized to manufacture the models, and the shape and dimensions of each vehicle model are shown in Fig. 2.3 and Table 2.1. When upcoming wind speed is 10 m/s, the corresponding Reynolds numbers of the three models which are estimated by $Re = Uh_c/\nu$ (where U is upcoming wind speed, h_c is height of center of gravity of scaled vehicle model, and ν is the kinematic viscosity of air 1.42×10^5) are 0.5×10^4, 1.1×10^4, and 1.6×10^4, respectively. These numbers are quite small compared to the value of several literatures (Zhu et al.,2012; Dorigatti et al., 2012). Therefore, in order to evaluate the adequacy of the experiment set-up, test results were compared with that of the literatures under uniform wind condition.

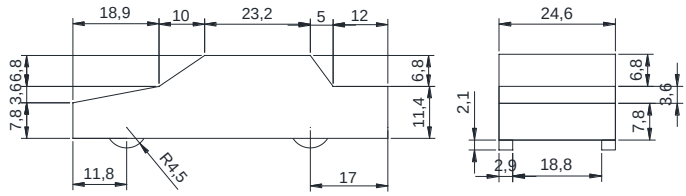

(a)

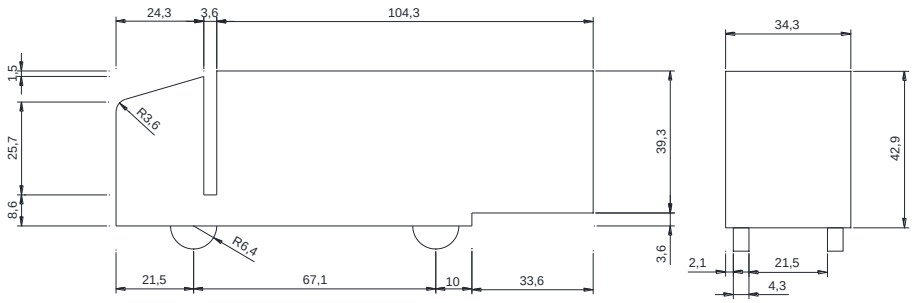

(b)

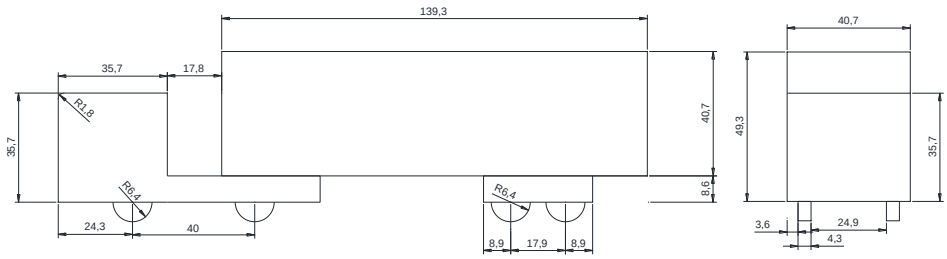

(c)

Fig. 2.3. Investigated vehicle models of 1:70 scale. (a) Sedan, (b) truck, (c) tractor-trailer

Table 2.1. Model-scale dimensions of investigated vehicle models

Vehicle type	Width (mm)	Length (mm)	Height (mm)	Height of center of gravity (mm)	Frontal area (mm^2)
Sedan	24.6	69.1	20.3	6.7	447.7
Truck	34.3	132.2	49.3	16.8	1469.4
Tractor-trailer	40.7	192.8	55.7	23.0	2006.6

2.2 Aerodynamic coefficients of vehicles under uniform wind condition

2.2.1 Examination of adequacy of the current experiment set-up

Before measuring the aerodynamic coefficients of vehicle models, the adequacy of the experiment set-up was examined by comparing measured aerodynamic coefficients of the tractor-trailer model under uniform wind to the results provided by Zhu et al. (2012) and Baker (1991a). These two research works were conducted using 1/25 scale of vehicle model under low turbulent condition with higher Reynolds number of 4.0×10^4 and 2.4×10^5, respectively.

The uniform wind condition was created using a flat round plate of which the radius is 0.5 m. The plate was established vertically in the middle of tunnel, and the vehicle model were installed on the center of the plate as shown in Fig. 2.4. The profile of wind speed and turbulence intensity according to the distance from the center of the plate was measured using hot wire anemometer at 500 Hz sampling frequency for 10 m/s of upcoming wind speed. Data was collected at the eight measurement points from 17 mm to 150 mm. Fig. 2.5 (a) shows the vertical profile of wind speed over the plate presenting by the ratio between wind speed at each point and upcoming wind speed. According to the graph, wind speed at each measurement point was almost identical to the upcoming wind speed. Also turbulence intensity was lower than 1% at all

the points as shown in Fig. 2.5 (b). According to these results, it can be concluded that the round plate can successfully reproduce uniform wind condition at a height above 17 mm. Although it is expected that wind speed dramatically reduces near the ground surface and turbulent intensity increases due to the surface roughness, this was not taken as an issue because the boundary layer is actually a natural phenomenon induced by ground surface.

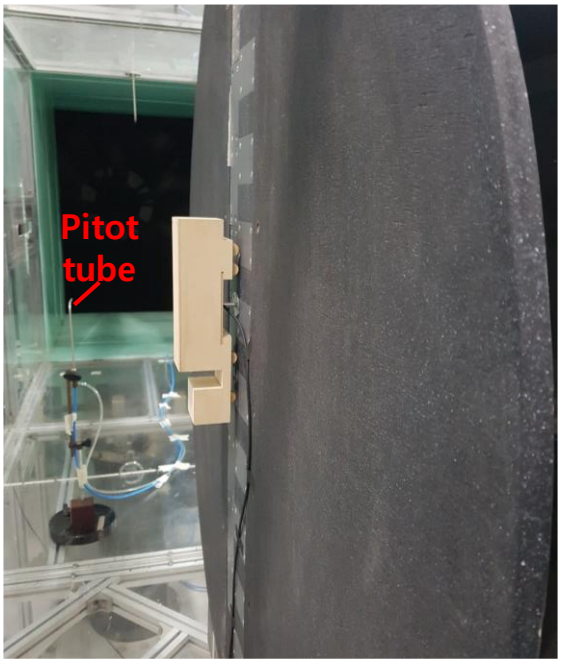

Fig. 2.4. Set-up for producing uniform wind condition

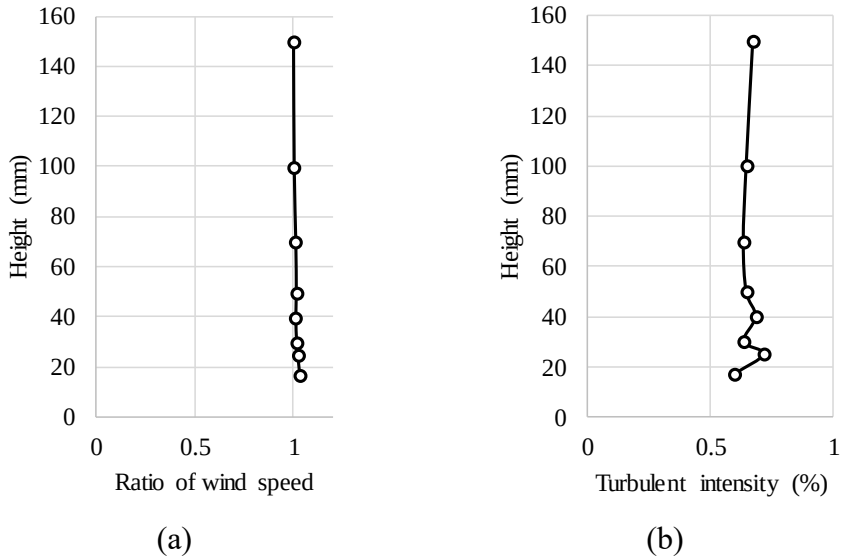

Fig. 2.5. Wind profile over the round plate. (a) Ratio of wind speed, (b) turbulence intensity

The aerodynamic coefficients of tractor-trailer were measured from 0° to 180° with 15° intervals, and the test was performed under two different upcoming wind speed, 10 m/s and 15 m/s which are corresponding to Reynolds number 1.6×10^4 and 2.4×10^4, respectively. Fig. 2.6 and Fig. 2.7 show the measurement results of three forces and three moments, and the results obtained from Zhu et al. (2012) and Baker (1991a) are also plotted together. According to these figures, the two results obtained from the 10 m/s and 15 m/s wind speeds were almost identical which means Reynolds effect is negligible for the current experiment set-up.

However, quite differences can be observed for several coefficients between the three studies. According to Fig. 2.6, drag and side forces shows very similar trend and amplitude which means that Reynolds number and test

set-up method barely effect on the overall flow pattern around the vehicle model which determines drag and side forces.

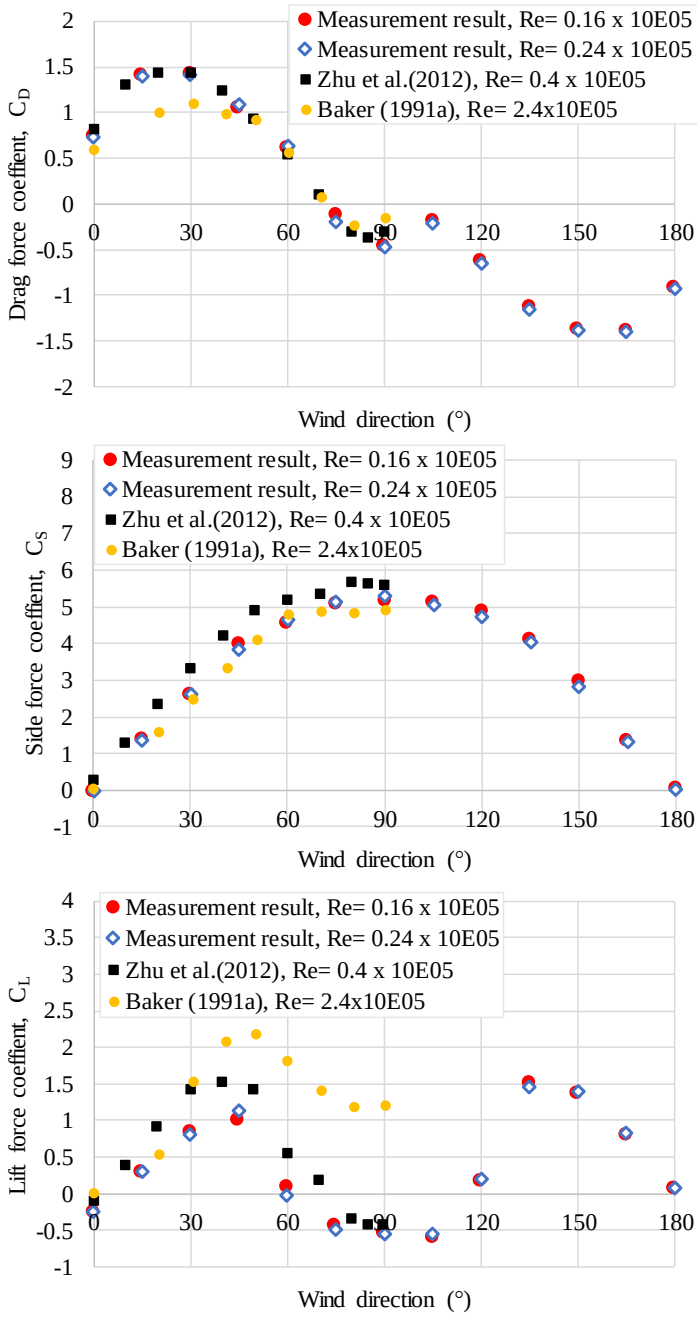

Fig. 2.6. Comparison of aerodynamic coefficients of drag, side, and lift forces

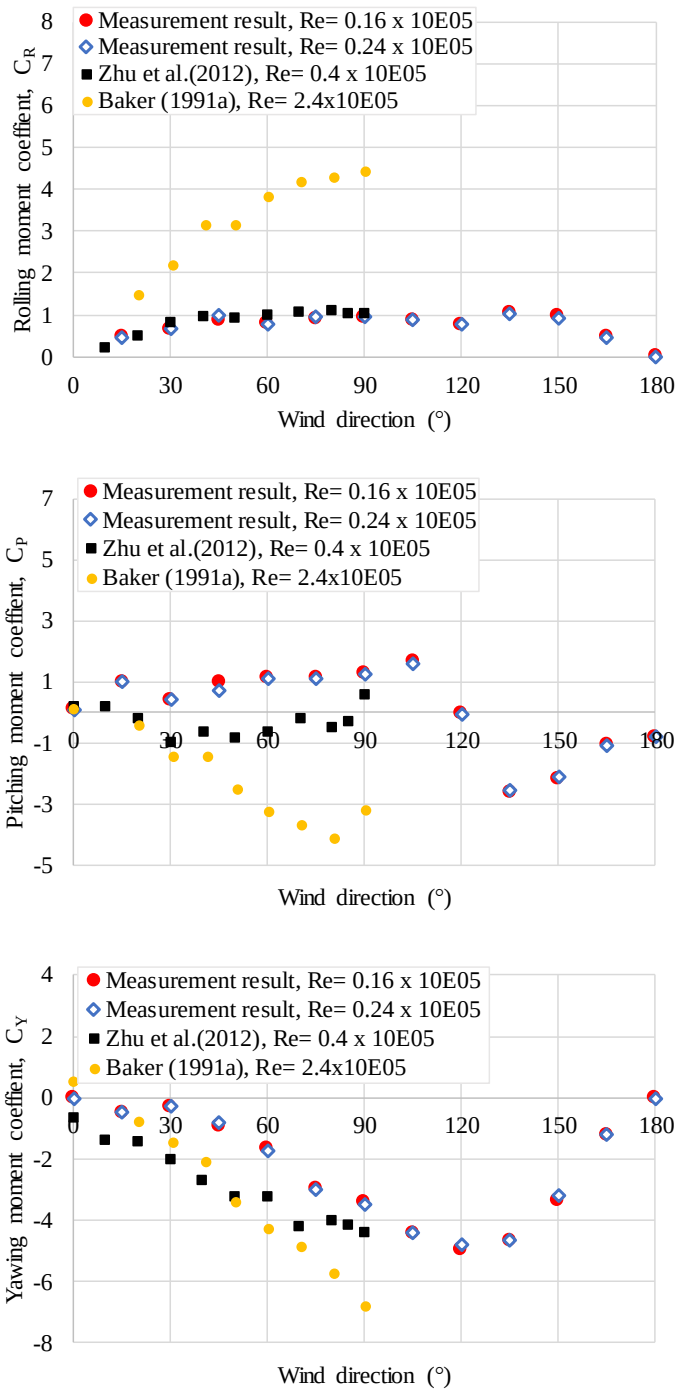

Fig. 2.7. Comparison of aerodynamic coefficients of rolling, pitching, and yawing moments

On the other hands, the lift force coefficient showed quite different results according to experiment especially when wind direction exceeds 45°. Reynolds effect is the one of probable reasons of this difference which changes flow pattern between vehicle and floor. Detail shape of the vehicle or the test set-up also could be influential factors which induces different roof vortex and underbody flow pattern. For example, distance between vehicle model and floor could effect on the results, and I-shape jig which supported load cell also possibly disturbed wind flow beneath vehicle body. Same explanation can be applied to the pitching moment shown in Fig. 2.7 which is governed by the horizontal moment arm of lift force. This divergence of lift force and pitching moment over 45° wind direction was also observed by previous researches (Baker and Humphrey, 1996; Zhu et al., 2012).

Large differences are also observed in the amplitude of rolling moment and yawing moment coefficients although the tendency of them are similar as shown in Fig. 2.7. This differences were unexpected because rolling moment and yawing moments are governed by vertical and horizontal moment arm of side and drag forces. As Baker (1991a) mentioned, the difference in the point of action of the force according to Reynolds number and vehicle shape seems to be the most probable cause since slight variation of moment arm can induce large difference of moment coefficients. Also, since the length of the moment arm depends on the position of the measurement points, the moment coefficients can be sensitively changes according to the details of test set-up. Although there were differences in the results between the three experiments

due to the influences of test set-up and Reynolds number, the authors concluded that the current experiment set-up provides reliable results because the trend of the overall results was consistent and the results of drag and side force were almost the same with the results of the literatures.

2.2.2 Variation of the aerodynamic coefficients of the three vehicles under uniform wind condition

Aerodynamic coefficients of the three vehicle types are demonstrated in Fig. 2.8, and it could be found that tendencies of all vehicles are quite similar including lift and pitching moments. First, drag force coefficient shows linear decrement for overall wind directions, but local maximum and minimum values appear around 30° and 150° rather than 0° and 180° because wind exposed area becomes minimum when vehicle and wind direction are exactly aligned. In the case of side force and rolling moment, the variation of coefficients has similar shape to haft-cycle sinewave of which maximum value appears under perpendicular wind. Variation of lift force coefficient also likes sinewave which has two local maximums at around 30~45° and 135~150° and one local minimum at 90°. The results of these four coefficients are consistent to the results provided by previous research works (Baker and Humphrey., 1996; Dorrigati et al.,2012).

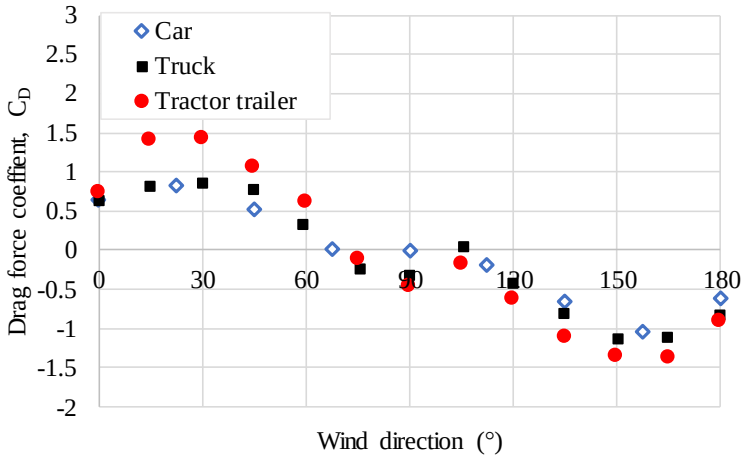
Car
Truck
Tractor trailer
Drag force coeffient, C_D
Wind direction (°)
3
2.5
2
1.5
1
0.5
0
-0.5
-1
-1.5
-2
0
30
60
90
120
150
180

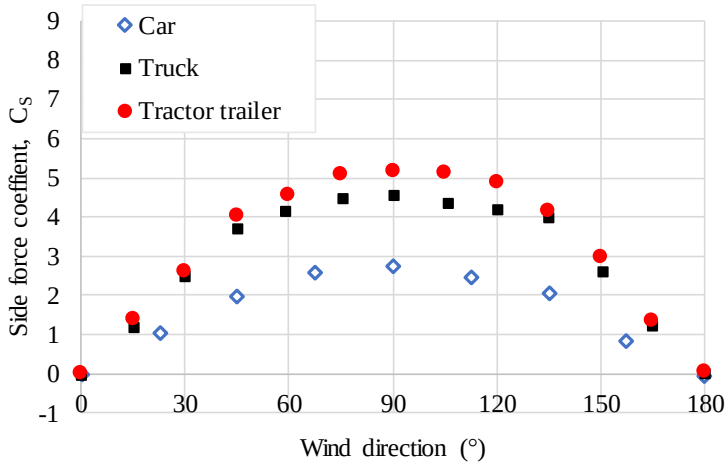
Car
Truck
Tractor trailer
Side force coeffient, C_S
Wind direction (°)
9
8
7
6
5
4
3
2
1
0
-1
0
30
60
90
120
150
180

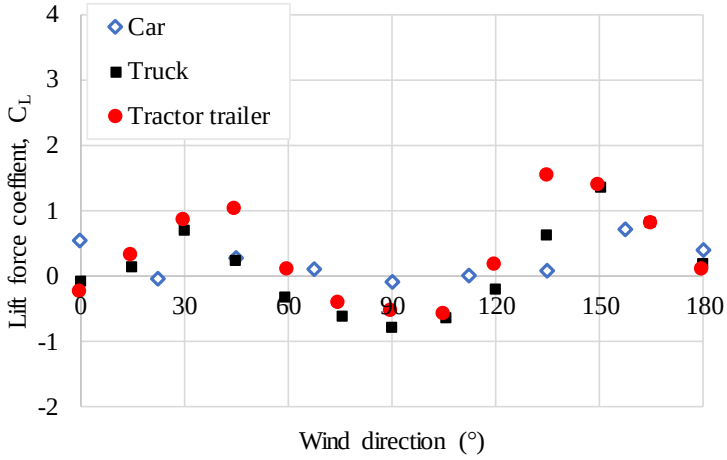
Car
Truck
Tractor trailer
Lift force coeffient, C_L
Wind direction (°)
4
3
2
1
0
-1
-2
0
30
60
90
120
150
180

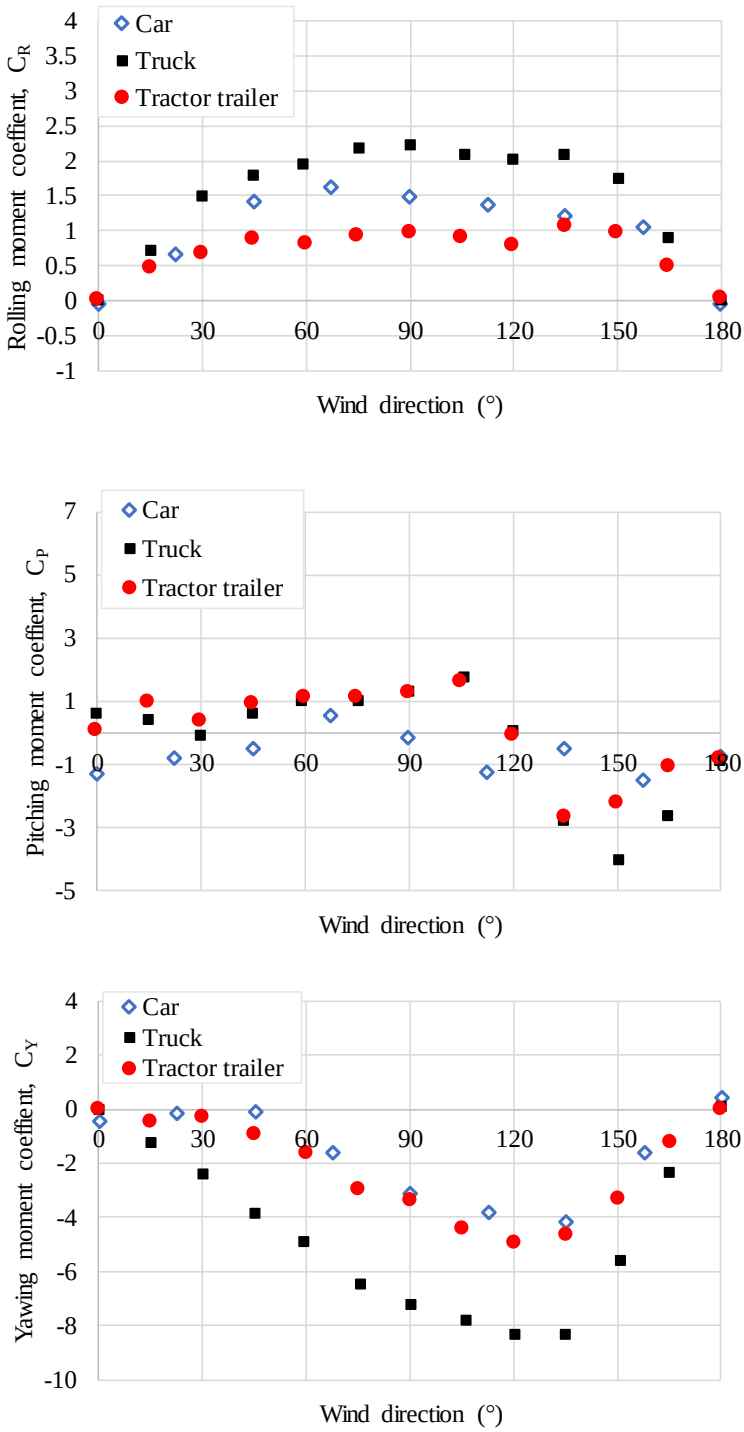

Fig. 2.8. Aerodynamic coefficients of all vehicle types: sedan, truck, and tractor-trailer

In the case of pitching and yawing moment coefficients, two interesting features could be observed. First, the tendency of pitching moment coefficient in the wind direction below 90° is very different from the distribution above 90°. If the wind incident angle is less than 90 degrees, the pitching moment coefficient does not change significantly because the two pitching moments induced by lift and drag forces balance each other. On the other hand, when the wind incident angle exceeds 90°, the sign of the pitching moment induced by the drag force becomes the same as the moment caused by the lift force, which consequently causes great change in the amplitude of the pitching moment coefficient. This unusual tendency can be changed according to the location of the measurement point.

Yawing moment coefficient shows very similar variation with side force and rolling moment coefficients, but location of maximum wind speed at 120~135° wind incident angle rather than 90°. This difference can be inferred that even though the magnitude of the side force itself becomes smaller when wind direction exceeds 90°, the yawing moment can increase as an action point of the side force moving toward the rear part of the vehicle.

In the case of tractor-trailer, it is required to consider tractor and trailer individually since they behave separately. Therefore, each of their aerodynamic coefficients were additionally measured which are demonstrated in Fig. 2.9. According to this figure, all the coefficients behave similarly with previous results, but small differences exist in the side force, rolling and yawing moment coefficients of tractor model. These coefficients

are suppressed from 60° to 180° wind direction, resulting in maximum value at 60°. This suppress is due to the wind disturbance effect of the trailer model under the high wind incident angle. On the other hand, the variation of the coefficients of trailer model does not changed significantly, which means that the tractor does not meaningfully effect on the aerodynamic loads acting on the trailer model due to its small size. Also, it could be found that side force, rolling and yawing moment coefficients of the trailer model are much larger than those of the tractor model which means that trailer portion can be the governing part in terms of vehicle stability rather than tractor potion during strong wind especially when it is empty.

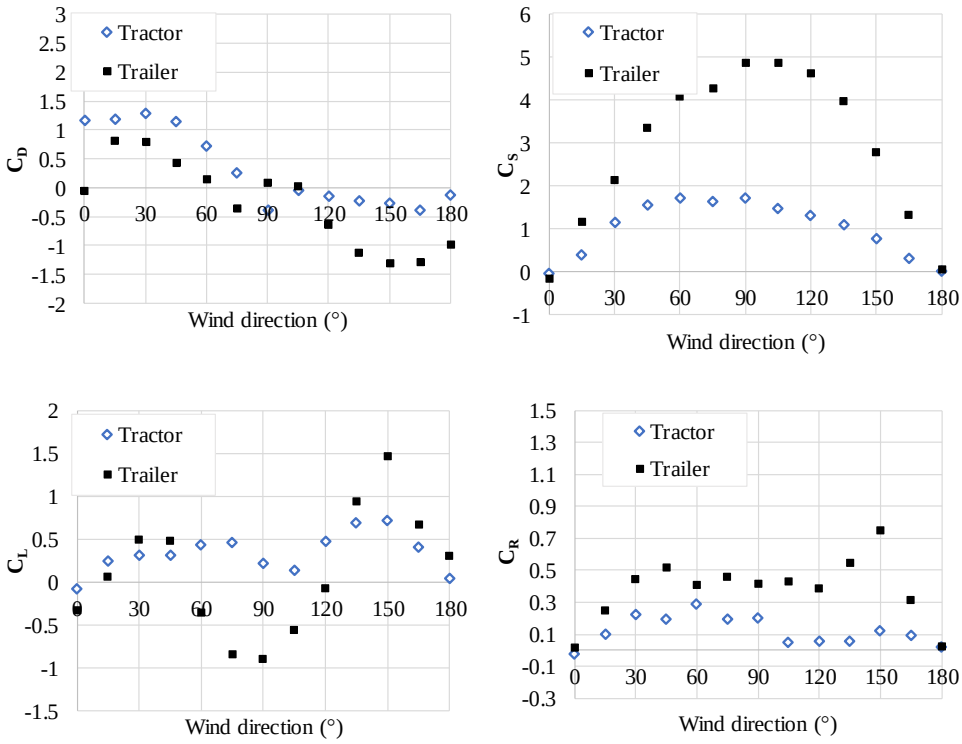

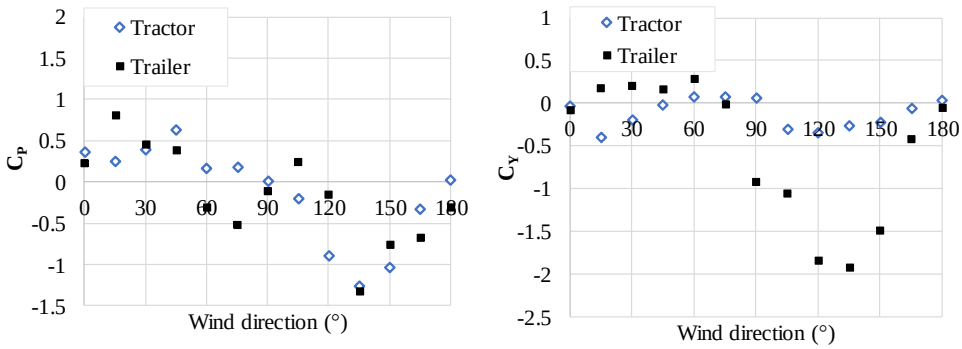

Fig. 2.9. Aerodynamic coefficients of tractor and trailer models

2.3 Variation of aerodynamic coefficients on a bridge: Gwangan Bridge

In order to measure the aerodynamic coefficients of a vehicle on a bridge girder for the various wind directions, new jig system was developed which allowed us to rotate the sectional model as shown in the picture of Fig. 2.10. The available range of the incident wind angle to vehicle and bridge model is from 50° to 130°. Lengths of the tested models were 1,600 mm in model scale which is much longer than width of wind tunnel section. Consequently, both ends of the model were located outside of wind tunnel sections as shown in Fig. 2.10, so the disturbance effect on wind flow due the both girder edges were minimized even the model was rotated with large angle.

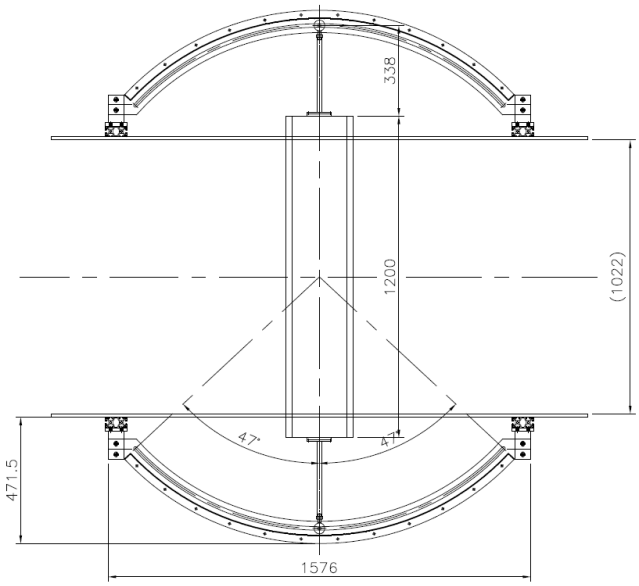

(a)

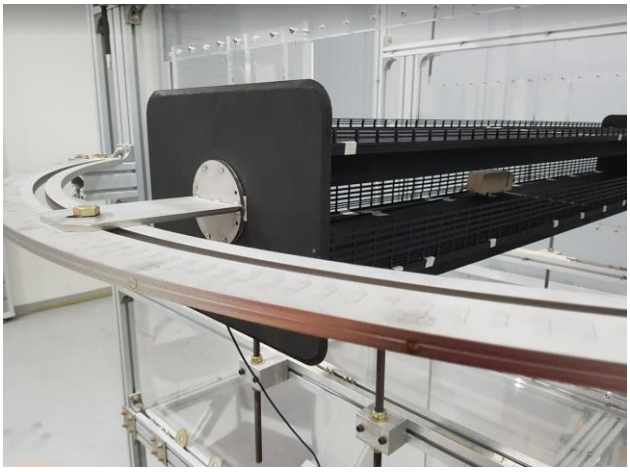

(b)

Fig. 2.10. New developed jig system. (a) Sketch of the developed system, (b) joint part connecting sectional model and jig system

2.3.1 2-D sectional models to be examined

Two girder sections of Gwangan Bridge were chosen for the wind tunnel test. The first section of which the sketch and picture are shown in Fig. 2.11

(a) belongs to the approaching span of Gwangan Bridge where the two consecutive accidents occurred at on April 3rd, 2012. The width of the section is 257 mm (18 m in full scale) and the distance between top of the upper deck and bottom of the lower deck is 179mm (12.5 m in full scale). This section has two geometric characteristics. First, there is no structures which connect upper and lower deck, so wind flow can go through between them without any disturbance. The other characteristics is the existence of two box girders below each deck. Since these two boxes decrease total flow area, it is expected that wind speed between two decks increases for constant flow rate. These two characteristics are the factors which the authors consider as main causes of the two vehicle accidents. Wind tunnel tests were conducted to investigate the effects of these factors on the vehicle stability.

The second sectional model which belongs to main span of Gwangan Bridge are shown in Fig. 2.11 (b). Since this model has truss members which connect upper and lower deck, the effect of these members on wind loads of vehicles was investigated. Experiment for the second section was only performed for perpendicular wind direction, and the length of the section was 900 mm which is smaller than the width of the wind tunnel section. The width and height of the section were 314 mm and 160 mm, respectively. The thickness of truss member was 10 mm, and the length and slope of diagonal member were 200 mm and 45°, respectively. The aerodynamic coefficients of the three vehicle models were measured on total eight traffic lanes, four lanes on each upper and lower deck.

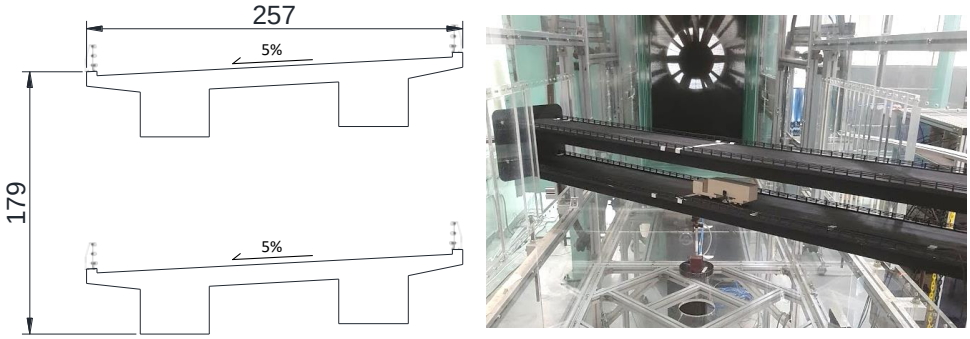

(a)

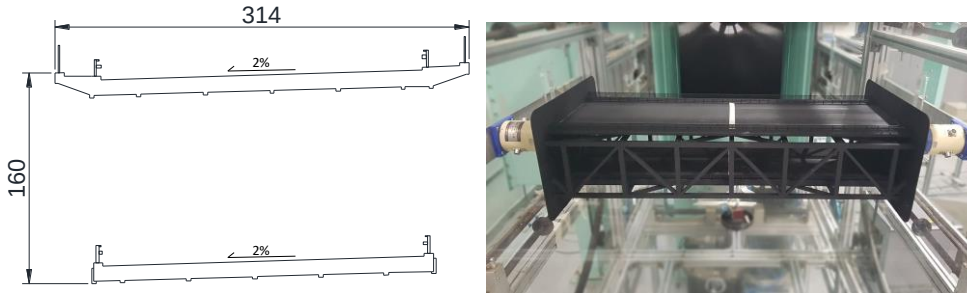

(b)

Fig. 2.11. Cross section and manufactured model of investigated girder sections (unit: mm). (a) Approaching span, (b) main span

2.3.2 Measurement results on the approaching span

In order to evaluate the effect of shape of double deck on vehicle stability for side-wind, distribution of aerodynamic coefficients of vehicles were measured on each traffic lane and girder section. First, the coefficients of three vehicle types were measured on the approaching span model, and Fig. 2.12 and Fig. 2.13 show the results obtained from the upper and lower decks, respectively, where Lane 1 indicates windward traffic lane whereas Lane 4

means leeward traffic lane. Among the six coefficients, the two most important aerodynamic coefficients, side force and rolling moment coefficients, were mainly discussed in this section.

Additionally, for in-depth investigation, the wind speed profiles on the upper and lower deck of approaching span were measured using hot wire anemometer as shown in Fig. 2.14 (a). Wind speeds were measured at five points over each traffic lane at 1 m intervals in real-scale. Fig. 2.14 (b) shows the profiles of wind speed ratio which denotes the ratio between upcoming wind speed and wind speed at each measurement point. Vertical black solid line in this figure means the wind speed profile which is the same as upcoming wind speed. Mean values of wind speed ratio on each traffic lanes are presented in Table 2.2.

First, in the case of upper deck, the rapid increments of wind speed around 2~4 m height were observed especially on the Lane 1 and 2. This change was due to the disturbance effect of guardrail which blocked the wind flow and dispersed them into the open space. As a result, wind speed below the 3 m height became almost negligible on every traffic lanes as shown in Fig. 2.14 (b) whereas wind speed was larger than upcoming wind speed above 3 m height. This disturbance effect of guardrail induced several interesting features in the distribution of aerodynamic coefficients of the vehicles. In the case of sedan, according to Fig. 2.12, all coefficients were almost zero on the every traffic lane of the upper deck. This large reduction was due to the small height of the sedan that the whole vehicle body submerged in the wake region.

Therefore, it can be expected that the sedan will be much safer on the upper deck of approaching span than on a flat ground.

In the case of the two high-sided vehicles, truck and tractor-trailer, the variation of coefficients had very similar shape with the uniform wind case, but their amplitude were quite different. First, the side force coefficients were smaller than that of uniform wind case except Lane 1, and the amplitude decreased as the vehicle location moved to the leeward side lane. This tendency is well-agreed with averaged wind speed ratio as shown in Table 2.2 which decreased from 0.86 to 0.71 according to the traffic lane. On the contrary, rolling moment coefficients showed quite different tendencies that the results were larger than that of uniform wind case even the averaged wind speed was smaller. This opposite tendency was due to the shape of boundary layer. Unlike the uniform wind condition, wind speed on the upper deck dramatically increased along the height which consequently induced large unbalanced wind pressure between top and bottom of the vehicle bodies. As a result, quite large rolling moment was induced on the high-sided vehicle bodies despite of the disturbance effect of the guardrail.

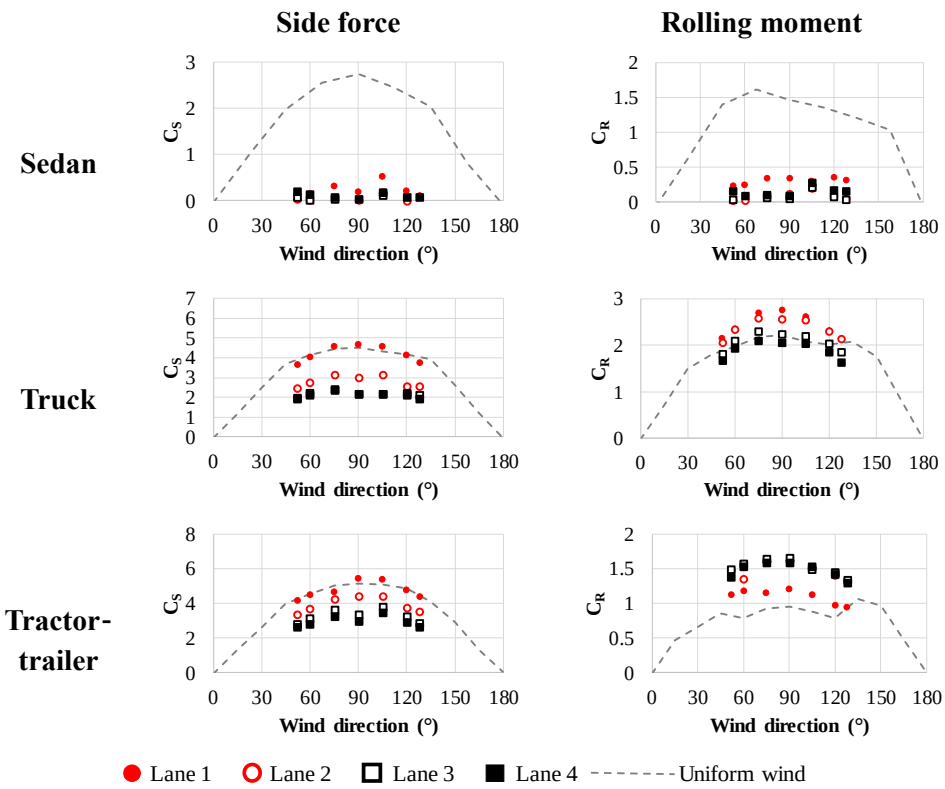

Fig. 2.12. Variation of side force and rolling moment coefficients of the three vehicle types on upper deck of approaching span

In the case of lower deck, all of the aerodynamic coefficients of the three vehicle types highly increased compared to the case of upper deck as shown in Fig. 2.13. First, the side force and rolling moment coefficients of the sedan became almost similar level with the case of uniform wind. Also, large increment in the side force and rolling moment coefficients of the two high-sided vehicle models were observed that all the coefficients exceeded that of the uniform wind case. The main reason of these large increments is the acceleration of wind flow between the upper and lower decks which is called wind tunneling effect. As shown in Fig. 2.14 (b), wind speed ratio exceeded

1.0 at the most of the measurement points which means wind speed over the lower deck is larger than upcoming wind speed. This acceleration was induced by the decrement of the wind flow area due to the two box girders below the upper deck. According to Table 2.2, wind speed increased about 10% to 20% on average, and this acceleration caused the increment of wind loads acting on the vehicle bodies. Therefore, it could be concluded that a vehicle running on the lower deck of the approaching span can be easily exposed to a wind hazard due to the wind tunneling effect which is induced by the geometric shape of the double deck. This must be the one of main causes of the two vehicle accidents which occurred on April. 3rd, 2012.

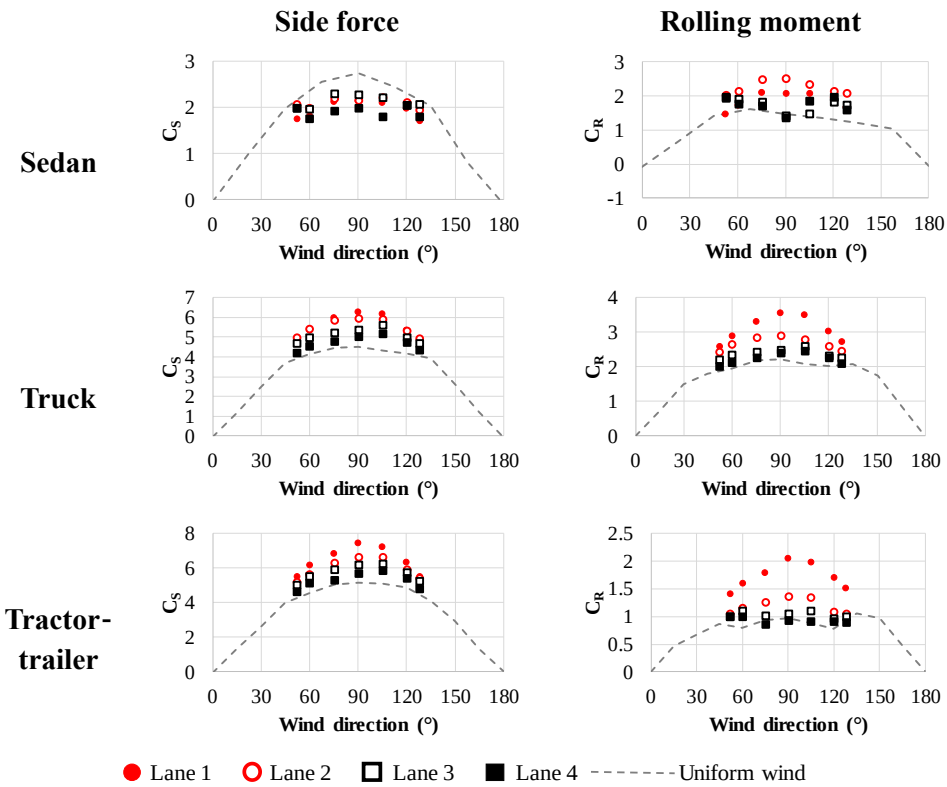

Fig. 2.13. Variation of side force and rolling moment coefficients of the three vehicle types on lower deck of approaching span

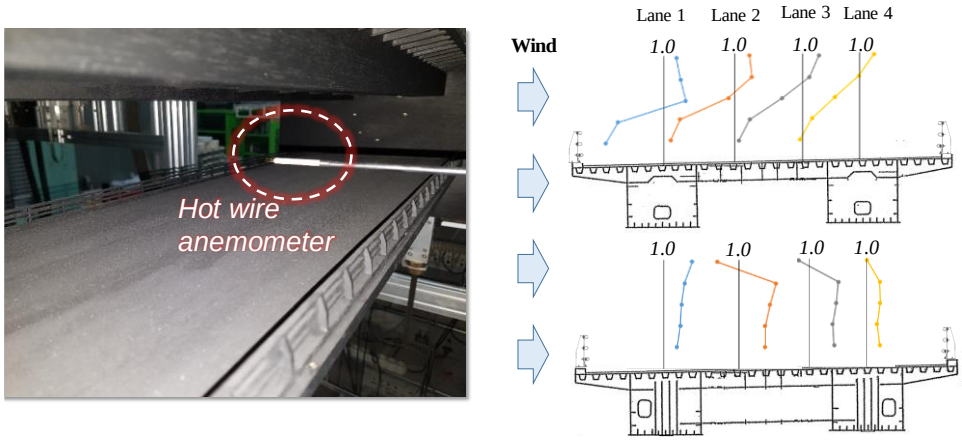

(a) (b)

Fig. 2.14. Measurement of profiles of longitudinal wind speed over each traffic lane of approaching span. (a) Hot wire anemometer, (b) profiles of ratio of wind speed

Table 2.2. Mean value of wind speed ratio of each traffic lane

	Lane 1	**Lane 2**	**Lane 3**	**Lane 4**
Upper deck	0.86	0.77	0.72	0.71
Lower deck	1.21	1.22	1.22	1.10

2.3.3 Effect of truss members on aerodynamic coefficients

In order to estimate the effect of the truss member on aerodynamic coefficients, additional experiment was performed using deck model shown in Fig. 2.11 (b). Test was conducted under the perpendicular wind, and side force and rolling moment coefficients are also discussed in this section which have maximum value under this wind incident angle. Fig. 2.15 and Fig. 2.16 shows the comparison results of the two coefficients between approaching and main spans.

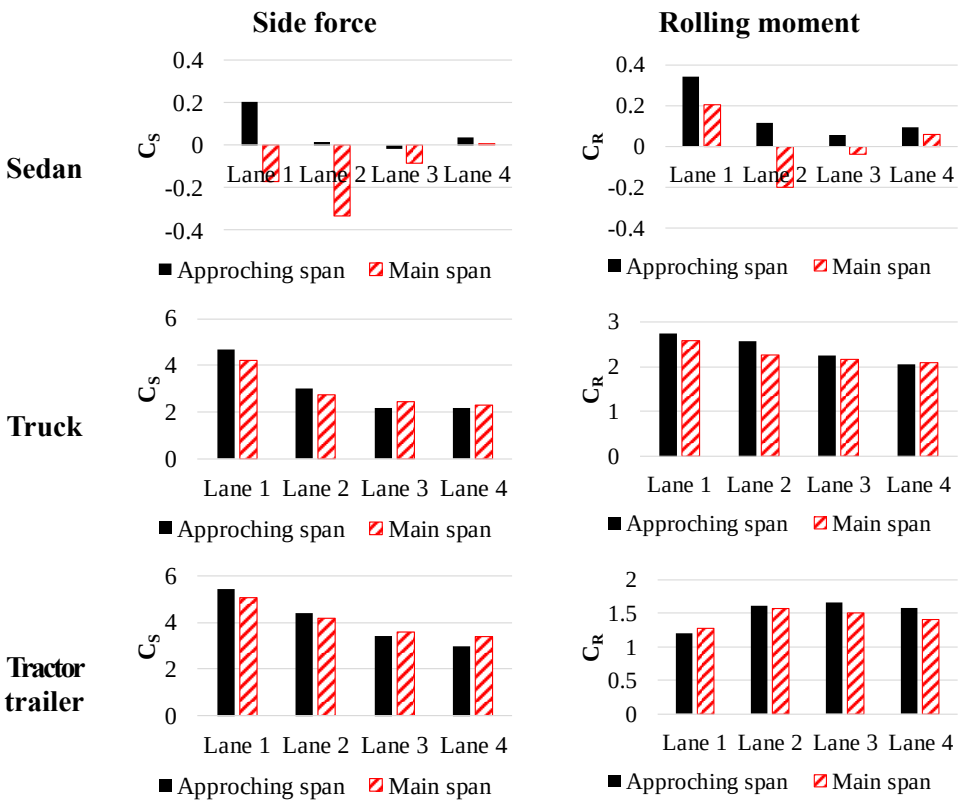

Fig. 2.15. Side force and rolling moment coefficients for perpendicular wind on the upper deck of approaching and main span

In the case of upper deck, there was no noticeable difference between the both spans. The sign of the coefficients of sedan were reversed on several traffic lanes due to the wake induced by guardrail, but the amplitudes were still negligible comparing to the results of lower deck. In the case of the two high-sided vehicles, there was only maximum 10% difference in the two coefficients, which means that the truss members effects on vehicle stability but not so significantly.

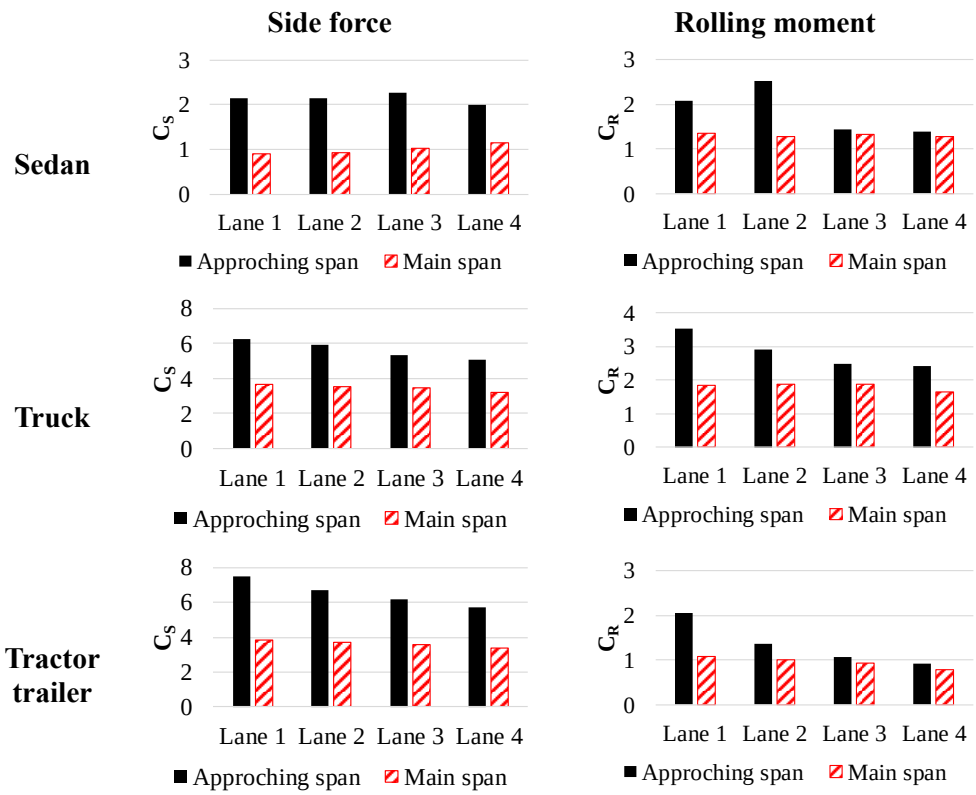

Fig. 2.16. Side force and rolling moment coefficients for perpendicular wind on the lower deck of approaching and main spans

On the other hand, large decrements of coefficients were observed on the lower deck for all vehicle types as shown in Fig. 2.16. This reduction was due to the disturbance effect of truss members on wind flow on the lower lanes. The reduction rate was greatest at the Lane 1 which is closest to the truss member and lowest at the Lane 4. As a result, all coefficients on the four lanes became similar level. Based on these results, it could be concluded that the truss members between the two decks blocks the wind flow like a wind barrier which protect the running vehicle from a wind hazard by reducing the wind speed over the decks.

2.4 Parameterization of aerodynamic coefficients

Since wind incident angle can be any value between 0 to 360°, all the aerodynamic coefficients should be defined for continuous range of the wind angle (Baker, 1986; Kim and Kim, 2019). Therefore, parameterization of aerodynamic coefficients was proceeded using a specific form of formula to obtain the coefficients under any given combination of vehicle speed and wind condition.

First, aerodynamic coefficients measured under uniform wind condition were parameterized using sine wave curve-fitting method. Curve fitting was performed using two sinusoidal functions as shown in Equation (2.3).

$$\arg\min \sum_{i=1}^{n} \left(C_{F,i} - [A_1 \sin(\omega_1 \psi_i + \phi_1) + A_2 \sin(\omega_2 \psi_i + \phi_2)]\right)^2 \qquad (2.3)$$

where C_F is the measured six aerodynamic coefficients, A_i (i=1 or 2) is the amplitude parameter, ω_i (i=1 or 2) is the angular frequency and ϕ_i (i=1 or 2) is the phase parameter of each sinusoidal function. Curve fitting algorithm provided by MATLAB (R2019a) was utilized for the parameterization, and nonlinear least square method was adopted as a fitting method. Six parameters were obtained for six aerodynamic coefficients and for five vehicle models including separated tractor and trailer model. The results of parameterization are shown in Table 2.3.

Table 2.3. Estimated parameters of coefficients under uniform wind

		C_D	C_S	C_L	C_R	C_P	C_Y
Sedan	A_1	4.86	2.76	4.91	1.62	5.04	2.82
	ω_1	2.39	1.02	1.19	0.95	0.01	0.94
	ϕ_1	-0.52	0.02	-0.17	0.09	-0.13	3.14
	A_2	4.49	-0.08	4.97	0.24	0.71	1.64
	ω_2	2.55	5.91	1.25	3.66	2.27	2.31
	ϕ_2	2.38	0.64	2.89	-1.79	-1.17	-0.31
Truck	A_1	1.10	4.69	0.45	3.61	2.53	8.19
	ω_1	0.77	0.97	2.19	1.27	2.30	1.07
	ϕ_1	2.05	0.04	2.24	-0.44	-0.72	2.95
	A_2	0.30	0.30	0.69	1.47	2.16	1.68
	ω_2	4.82	4.18	3.16	1.96	3.19	2.36
	ϕ_2	-1.63	-1.98	-0.65	1.68	1.88	5.24
Tractor-trailer	A_1	1.17	5.34	0.99	5.10	1.58	3.86
	ω_1	1.40	0.98	3.20	1.55	1.83	1.01
	ϕ_1	1.11	0.02	-0.31	-0.87	-0.44	2.93
	A_2	0.34	0.18	0.43	4.23	0.89	1.28
	ω_2	4.19	4.33	0.53	1.74	4.08	2.47
	ϕ_2	-0.68	-2.10	-0.28	1.99	0.89	5.52
Tractor only	A_1	3.77	1.79	2.12	0.20	0.90	0.39
	ω_1	1.76	1.05	1.69	0.98	1.84	0.16
	ϕ_1	2.33	-0.02	-1.18	0.29	0.95	3.18
	A_2	4.05	0.21	1.85	0.09	0.56	0.23
	ω_2	1.62	2.60	2.01	2.94	2.63	3.42
	ϕ_2	-0.42	-0.25	1.50	-0.92	3.83	3.59
Trailer only	A_1	24.38	4.94	0.85	3.72	0.88	1.12
	ω_1	2.66	1.01	3.16	1.67	0.56	1.11
	ϕ_1	-1.11	-0.07	-0.37	-1.07	2.51	2.41
	A_2	24.01	0.23	0.40	3.34	0.47	0.74
	ω_2	2.70	3.20	1.64	1.84	4.72	2.67
	ϕ_2	1.97	0.67	3.30	1.81	-0.72	4.91

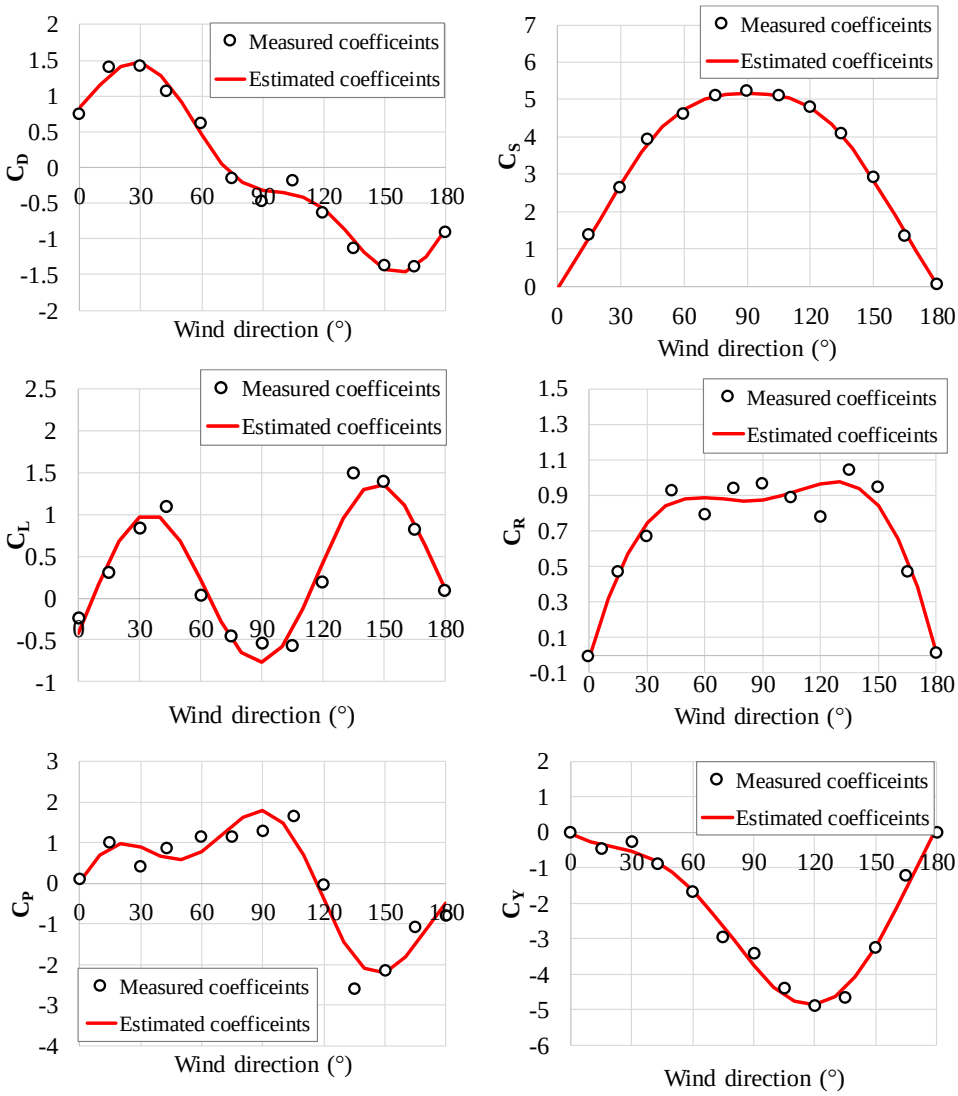

Fig. 2.17. Parameterization results of the tractor-trailer under uniform wind

Fig. 2.17 is the parameterization results of tractor-trailer model which demonstrates the measurement results (plotted in black dot) and the parameterized results (plotted in red line) together. According to the figure, the parameterized results follow the measurement coefficients with high accuracy even at the local maximum and minimum points. Similar level of accuracy also could be observed in the other vehicle types.

Next, parameterization was also performed for the measurement results of the bridge girders. Unlike uniform wind condition, however, aerodynamic coefficients were not obtained for wind direction under 50° and over 130° during the experiment in the case approaching span, and the coefficients were obtained only for perpendicular wind in the case of main span. Due to the lack of the information, direct application of the curve-fitting method is not appropriate. Therefore, another parameterization method was utilized based on the parameters obtained under the uniform wind condition which is shown in Table 2.3. The applied assumption here is that the variation of the coefficients on a bridge girder is similar to that of the uniform wind case.

Equation (2.4) is the proposed formula for the parameterization of the measurement results on the traffic lanes of the approaching span.

$$\arg\min \sum_{i=1}^{n} \left(C_{F,i} - [M_1(A_1 \sin(\omega_1 \psi_i + \phi_1)) + M_2(A_2 \sin(\omega_2 \psi_i + \phi_2)) + Z] \right)^2 \quad (2.4)$$

where M_1 and M_2 are the multiplication parameters for each sine function, and Z is the offset parameter. A_i, ω_i, and ϕ_i are the parameters of the uniform wind case obtained from Table 2.3. The method of least square was applied for the optimization.

Parameterization was performed for sedan, truck and tractor-trailer except separated tractor and trailer. All estimated parameters are demonstrated in the Appendix, and Fig. 2.18 show the parameterization result of tractor-trailer on the lower deck of approaching span as an example. According to the figure,

estimated formulas follow experiment result very well having a similar shape of coefficients to the uniform wind case.

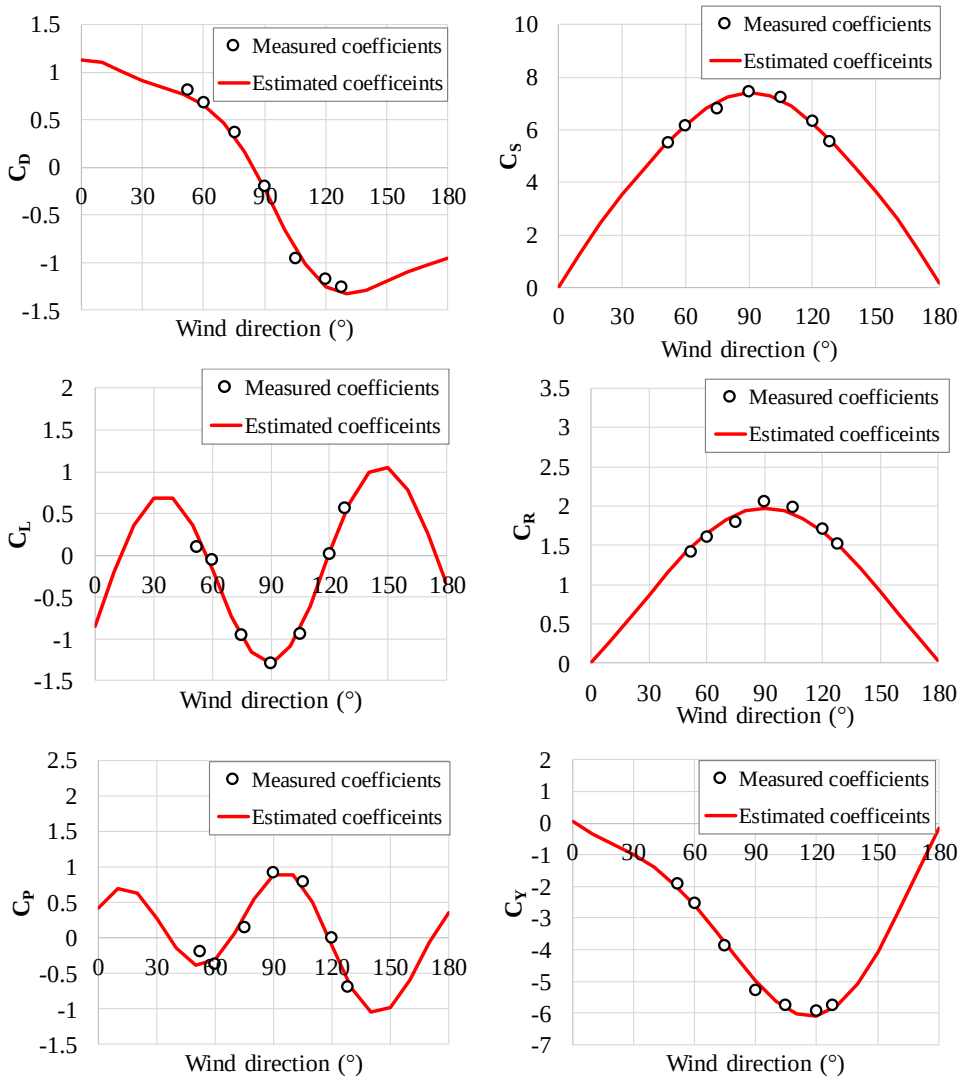

Fig. 2.18. Parameterization results of the tractor-trailer on Lane 1 of the lower deck of approaching span of Gwangan Bridge

Since aerodynamic coefficients of vehicles on the main span of Gwangan Bridge were measured only for the perpendicular wind, it is difficult to parameterize the formulas. Especially drag, lift forces and pitching moment

coefficients are the problem since they have no meaningful information at 90° wind direction. Drag force generally has minimum value at 90° wind direction which is useless information. In the case of lift force and pitching moment coefficients, the variation changes very sensitively according to the location of vehicle and wind condition. Due to this lack of the information and irregular patter, it is nearly impossible to perform parameterization.

On the other hand, in the case of side force and rolling moment coefficients, there is an expectable pattern that the maximum values normally appears at 90° wind direction. Yawing moment coefficient also has half-cycle variation of sinusoidal waveform which shows extreme value around 120° wind direction. Based on this pattern, parameterization can be performed for these three coefficients according to Equation (2.5).

$$M' = \frac{C_F(90°)}{[(A_1 \sin(\omega_1 \pi/2 + \phi_1)) + (A_2 \sin(\omega_2 \pi/2 + \phi_2))]} \tag{2.5}$$

where M' is the ratio of the measured coefficients on the girder and the coefficients under the uniform wind condition at 90° wind direction. All estimated parameters are demonstrated in the Table 2.4, and the parameters of drag, lift force, and pitching moment were assumed as 1.0 based on the assumption that contributions of these coefficients on the vehicle stability is negligible compared to side force, rolling and yawing moment coefficients. By multiplying parameter M' to the variation of the coefficients of the uniform wind case, it was able to define all the coefficients of main span for all wind directions.

Table 2.4. Estimated parameters of all vehicles on the main span of Gwangan Bridge

			C_S	C_R	C_Y
Sedan	**Upper deck**	Lane 1	-0.06	0.14	-0.03
		Lane 2	-0.12	-0.14	-0.11
		Lane 3	-0.03	-0.03	0.00
		Lane 4	0.00	0.04	0.03
	Lower deck	Lane 1	0.33	0.94	0.36
		Lane 2	0.34	0.89	0.34
		Lane 3	0.38	0.92	0.35
		Lane 4	0.42	0.88	0.49
Truck	**Upper deck**	Lane 1	0.95	1.21	0.97
		Lane 2	0.62	1.06	0.74
		Lane 3	0.56	1.01	0.63
		Lane 4	0.52	0.98	0.59
	Lower deck	Lane 1	0.83	0.87	0.72
		Lane 2	0.81	0.88	0.73
		Lane 3	0.80	0.88	0.77
		Lane 4	0.73	0.77	0.71
Tractor-trailer	**Upper deck**	Lane 1	0.98	1.45	1.07
		Lane 2	0.81	1.79	1.18
		Lane 3	0.70	1.71	1.13
		Lane 4	0.66	1.62	1.10
	Lower deck	Lane 1	0.75	1.25	0.67
		Lane 2	0.72	1.16	0.59
		Lane 3	0.69	1.07	0.54
		Lane 4	0.65	0.91	0.53

CHAPTER 3

DYNAMIC AND QUASI-STATIC APPROACHES FOR SIMULATION OF VEHICLE SYSTEM

Using the measurement results of the wind tunnel test, vehicle simulation was performed to estimate critical wind speed or to determine wind speed for traffic control. Two approaches were used for the vehicle simulation: dynamic and quasi-static approaches. Both methods have their own advantages and disadvantages.

The merit of the dynamic approach is that it can simulate more realistic vehicle system by considering various interactions among the vehicle components based on vehicle dynamics. CarSim and TruckSim are the examples of the commercial software that is available to support the dynamic approach. The construction of a reliable dynamic model, however, requires tremendous effort and detailed data, which are usually not available to general researchers. Furthermore, vehicles consist of many parts with different characteristics depending on the vehicle. These differing parts include tires, suspension springs, shock absorbers, and brake systems. Therefore, if there is a small error in the modeling of these components, the complexity of the dynamic model can cause a large propagation error (Baker, 2013).

The quasi-static vehicle model, on the other hand, is convenient to use, because it requires only a few basic dimensional and aerodynamic configurations of vehicle information. The quasi-static model is also very

intuitive and shows much faster performance compared to dynamic approach because it focuses on the equilibrium condition of static forces acting on vehicles. For these reasons, the quasi-static model has also been utilized for simulation of vehicle system in this study, even though it is less realistic than the dynamic approach.

In section 3.1, brief introduction of the commercial software CarSim and TruckSim which is for the dynamic approach was provided. In section 3.2, a quasi-static approach developed by the author was introduced. In section 3.3, feasibility of quasi-static approach was examined by comparing obtained tire reaction forces with the results of CarSim and TruckSim.

3.1 Dynamic approach using CarSim and TruckSim

The commercial soft CarSim and TruckSim, which was developed by Mechanical Simulation Corporation was adopted as a dynamic approach to simulate dynamic vehicle system. The program provides various vehicle types, such as vans, busses, and trucks, with sophisticated modeling capacity for optional suspension types, steering conditions, powertrain modeling, systems, and interaction mechanism with a driver. Also the programs have module to edit the road geometry such as cant, curvature, and roughness profile. Total six math models are available in these programs, and Adams-Moulton 2nd Order Method was chosen for current research which shows best performance among them (Mechanical Simulation Corporation, 2016).

One of the most powerful advantage of these programs is the connection module which makes possible to communicate with external program such as Matlab by Simulink program as shown in Fig. 3.1. Utilizing this module, it is able to control the two commercial program by Matlab which let us possible to perform numerous simulation cases with high efficiencies. Fig. 3.1 shows the brief introduction of Simulink algorithm. In first step, pre-defined wind speed and direction information is sent from Matlab program to the commercial software modules based on the Simulink algorithm. Then, the modules perform vehicle simulation using provided wind information and return simulation results like tire reaction forces and displacements of vehicle body to the Matlab. This is quite simple algorithm, but it was able to reduce total simulation time remarkably by defining all the simulation cases in advance. This algorithm was also utilized to perform an iteration loop in order to estimate critical wind speed, and this will be introduced in Chapter 4.

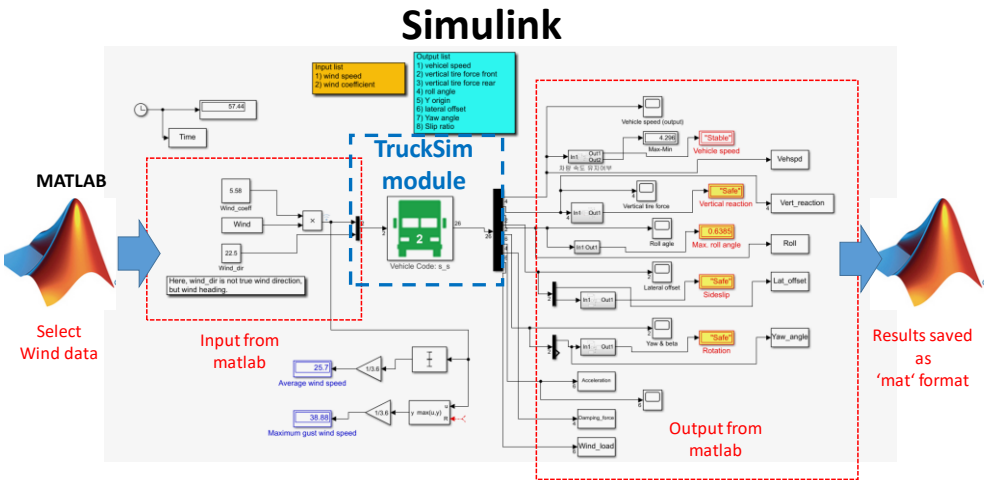

Fig. 3.1. Simulation of CarSim and TruckSim using Simulink-Matlab

3.2 Quasi-static approach for evaluation of tire forces

Six equilibrium equations and additional assumptions were utilized for the evaluation of unknowns that include tire forces. This so-called quasi-static approach has been applied only to the two-axle types of vehicles tested in previous studies (Baker, 1986; Kim et al., 2016). The present study, however, extended the procedure to tractor-trailers, which are also vulnerable to strong side winds (Kim et al., 2016)

3.2.1 Vehicle models with two axles and four wheels

In order to establish a two-axle, quasi-static vehicle model, the basic concept proposed by Baker (1986) and Batista and Perkovič (2014) was adopted. Six equilibrium equations for x, y, and z axes were derived to consider the longitudinal, lateral, and vertical tire forces, as shown in Fig. 3.2. After adding the weights of the wheel, we obtained six equilibrium equations as follows.

$$i_1 q(F_{z1} + F_{z3}) + i_2 q(F_{z2} + F_{z4}) - f_R \sum_{i=1}^{4} F_{zi} = F_D \tag{3.1}$$

$$\sum_{i=1}^{4} F_{zi} = (m_s + m_f + m_r)g - F_L \tag{3.2}$$

$$F_{yf} + F_{yr} = F_S \tag{3.3}$$

$$\frac{c}{2}(F_{z3} + F_{z4} - F_{z1} - F_{z2}) = M_R + h_c \cdot F_S \tag{3.4}$$

$$aF_{yf} - bF_{yr} + \frac{c}{2} f_R (F_{z1} + F_{z2} - F_{z3} - F_{z4}) = M_Y \tag{3.5}$$

$$\begin{aligned} b(F_{z2} + F_{z4}) - a(F_{z1} + F_{z3}) \\ = (-m_f \cdot a + m_r \cdot b)g + M_P + h_c \cdot F_D \end{aligned} \tag{3.6}$$

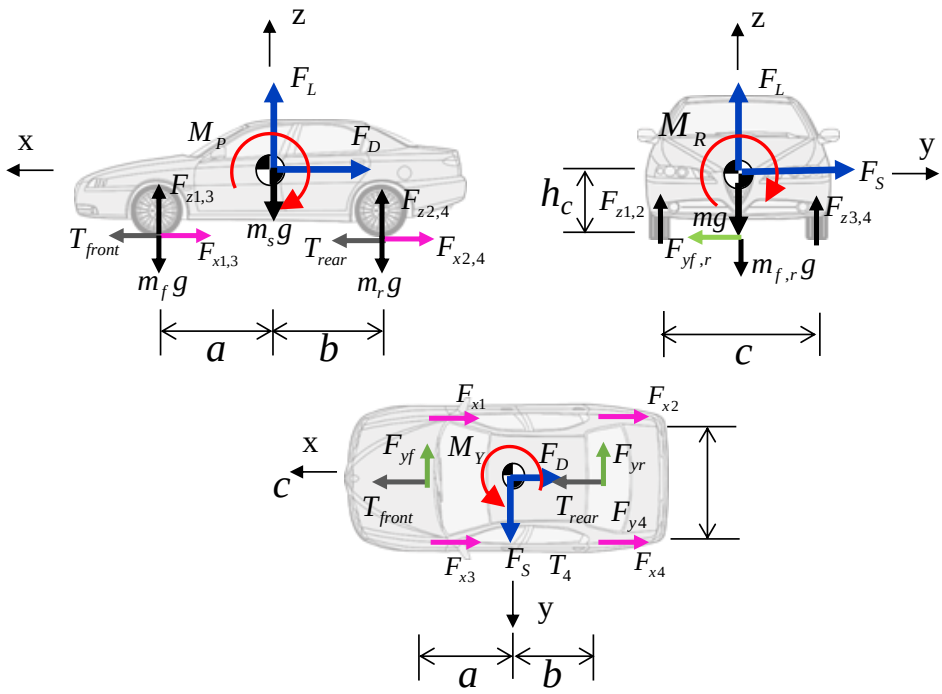

Fig. 3.2. Applied actions and corresponding tire forces of two-axle vehicles

Equations (3.1)–(3.6) use the following designations: a and b are the distance of the front and rear axles from the center of gravity; c is the track width; h_c is the vertical distance between the ground and the center of gravity; g is the acceleration of gravity (=9.81 m/s^2); and, m_s, m_f, and m_r are the masses of the sprung vehicle body, the front axle, and the rear axle, respectively. There are six wind-induced forces and moments: Drag force, F_D;

lift force, F_L; side force, F_S; rolling moment, M_R; yawing moment, M_Y; and, pitching moment, M_P. F_{zi} (i = 1, 2, 3, 4) are the vertical reaction forces of tires, and F_{yi} (i = f and r) are the lateral friction force of front and rear axles. The symbols i_1 and i_2 are variables that can only be 0 or 1 according to whether the corresponding axle is driven or not. (Baker, 1986). Traction parameter q is the ratio of vertical reaction forces to traction forces of front T_{front} and rear axles T_{rear} based on the assumption that traction forces acting on left and right tires are equal on same axle. This parameter is unknown value, so that it is required to estimate from Equations (3.1)–(3.6). Rolling resistance coefficient f_R are the ratio of vertical reaction forces to rolling resistance forces F_{xi} (i = 1, 2, 3, 4) which is a constant value determined by vehicle speed v (unit: km/h) according to Equation (3.7) (Mechanical Simulation Corporation, 2016).

$$f_R = 0.0041 - 0.0000256 \times v \tag{3.7}$$

A constraint condition whereby all wheel centers constantly lie on a plane was also introduced to solve the above seven unknowns. When the stiffness of all suspension was assumed to be equal, the constraint condition was represented as shown by Equation (3.8) (Baker, 1986).

$$F_{z1} - F_{z3} + F_{z4} - F_{z2} = 0 \tag{3.8}$$

Since the number of unknowns in the equations were equal, the tire forces of a vehicle could be determined for given levels of wind-induced forces and moments. The quasi-static approach suggested by Baker (1986) and Batista

and Perkovič (2014), however, provided a negative contact force for the tires when one of the wheels had lost contact with the ground, which is unrealistic. Therefore, we established two modifications in order to calculate the tire forces under situations where any wheel loses contact with the ground. First, the vertical tire force, F_{zi}, of the wheel being lifted up was fixed at 0 during the calculation. Second, the compatibility condition illustrated by Equation (3.8) was no longer effective. The tire forces could then be evaluated by considering the remaining three tires.

When the vehicle is running on a curved section of a bridge deck, the vehicle is subjected to additional centrifugal forces. Furthermore, the deck in a curved section inclines from the horizontal plane due to the cant by an angle α, which changes the direction of external forces, as shown in Fig. 3.3. Those factors are taken into consideration, as shown by Equations (3.9)–(3.13).

$$F_S' = \left(F_S + \frac{m_{tot}v^2}{R}\right)\cos\alpha + (F_L - m_{tot}g)\sin\alpha \tag{3.9}$$

$$F_L' = F_L\cos\alpha - \left(F_S + \frac{m_{tot}v^2}{R}\right)\sin\alpha + m_{tot}g(1-\cos\alpha) \tag{3.10}$$

$$M_R' = M_R - (m_f + m_r)\left(\frac{v^2}{R}\cos\alpha - g\sin\alpha\right)\cdot d \tag{3.11}$$

$$M_Y' = M_Y + (m_f \cdot a - m_r \cdot b)\left(\frac{v^2}{R}\cos\alpha - g\sin\alpha\right) \tag{3.12}$$

$$M_P' = M_P + (-m_f \cdot a + m_r \cdot b)\left(\frac{v^2}{R}\sin\alpha - g(1-\cos\alpha)\right) \tag{3.13}$$

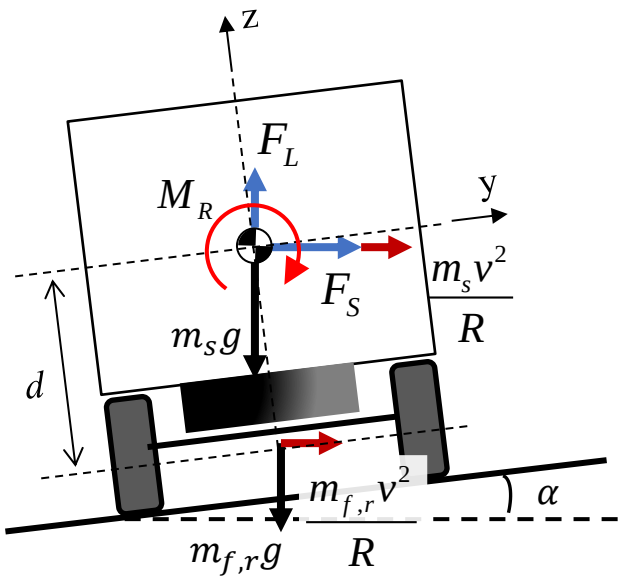

Fig. 3.3. External forces acting on the vehicle on a curved road with a cant

In Equations (3.9)–(3.13), R is the radius of the curvature for the curved section, and $m_{tot} = m_s + m_f + m_r$. d is the vertical distance between the sprung mass and the center of the wheel. F_S', F_L', M_R', M_Y', and M_P' are the updated side, lift forces, and the rolling, yawing, and pitching moments along the tilted x, y, and z axes, respectively, as shown in Fig. 3.3. For simplicity, the aerodynamic coefficients of the vehicle were assumed to have not changed due to the angle of the cant.

Furthermore, an additional rolling moment which is induced by lateral displacement of sprung mass was considered as shown in Fig. 3.4. In general, this rolling moment is not an influential factor comparing to aerodynamic loads. However, large lateral displacement can occur in high-sided vehicles like large vans and trucks which leads considerable additional rolling moments on the vehicle body. Therefore, a modification of the equilibrium

equation was proposed for an enhanced quasi-static approach that could consider the additional rolling moment.

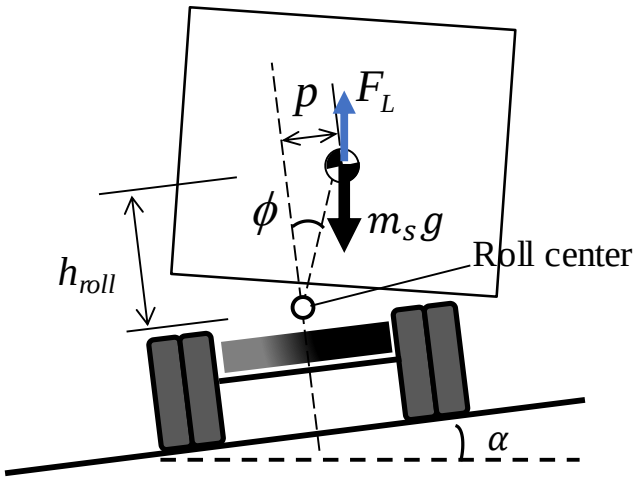

Fig. 3.4. Additional rolling moment induced by lateral displacement of sprung mass

According to Fig. 3.4, the additional rolling moment can be calculated as shown by Equation (3.14).

$$M_a = (m_s g - F_L) p \cos \alpha \tag{3.14}$$

In Equation (3.14), M_a is the additional rolling moment induced by the lateral displacement, p, of the sprung mass, m_s. The vehicle body rotates relative to the roll center of the sprung mass, as shown in Fig. 3.4, and the lateral displacement, p, is proportional to the roll angle, ϕ, which results in Equation (3.15).

$$M_a = (m_s g - F_L) \phi h_{roll} \cos \alpha \tag{3.15}$$

In Equation (3.15), h_{roll} is the distance of the roll center from the center of gravity along the local vertical axis. If the roll stiffness of the vehicle, K_ϕ, is given, Equation (3.16) is the equilibrium.

$$K_\phi \phi = M_R + \left(\left(F_S + \frac{m_s v^2}{R} \right) \cos\alpha + (F_L - m_s g) \sin\alpha \right) \cdot h_{roll} + M_a \tag{3.16}$$

From Equations (3.15) and (3.16), the roll angle ϕ can be derived as follows, which is similar to an equation proposed by Gillespie (1992).

$$\phi = \frac{M_R + \left(\left(F_S + \frac{m_s v^2}{R} \right) \cos\alpha + (F_L - m_s g) \sin\alpha \right) \cdot h_{roll}}{K_\phi - (m_s g - F_L) h_{roll} \cos\alpha} \tag{3.17}$$

From Equations (3.15) and (3.17), the additional rolling moment, M_a, could be calculated. The additional moment, M_a, should be added to the right-hand side of Equation (3.4), as shown in Equation (3.18), which results in an enhanced quasi-static approach.

$$\frac{c}{2}(F_{z3} + F_{z4} - F_{z1} - F_{z2}) = M_R' + M_a + h_c \cdot F_S' \tag{3.18}$$

Road roughness and a driver model were not reflected in the quasi-static approach. Baker (2013) has shown that the degree of the surface roughness effect on the vehicle behavior is negligible compared with wind turbulence. The impact of roughness on vehicle stability could also be further mitigated by the vehicle's suspension and dampers. Therefore, leaving these minor factors as a future task, the next section focuses on an overall behavioral assessment. On the other hand, a driver behavior model is one of the influential factors that can induce large lateral and yaw displacement. Side-

slip accidents can occur due to this large movement even though the friction forces of the tires have not reached a friction-limited state. As Chen and Chen (2009) pointed out, however, since no driver model has been well established, it would be difficult to consider this complex factor during the risk assessment procedure. Therefore, in the following sections, the driver behavior model was not taken into consideration for the evaluation of tire forces.

3.2.2 Tractor-trailer model with three axles and six wheels

Tractor-trailers are very vulnerable to side winds. The trailer portion, in particular, is vulnerable to side winds due to its large surface area, and it only has one rear axle to resist overturning. The present study simulated the quasi-static approach for both tractor and trailer portion separately. The tractor portion was simulated using the vehicle model introduced in section 3.2.1 while it was required to simulate trailer portion with different quasi-static model due to its unique structure.

Trailer with one hitch point and one axle was modeled in this section as shown in Fig. 3.5. Tractor and trailer were connected at the hitch point using 5th wheel which is the hitch model generally adopted to connect a trailer to a tractor. The hitch model produces rolling moment which resists the relative rolling movement between tractor and trailer.

First, six equilibrium equations were developed as shown in Equations (3.19)–(3.24).

$$T - f_R \sum_{i=2}^{3} F_{zi} = F_D \tag{3.19}$$

$$\sum_{i=1}^{3} F_{zi} = (m_s + m_r)g - F_L' \tag{3.20}$$

$$F_{yf} + F_{yr} = F_S' \tag{3.21}$$

$$\frac{c}{2}(F_{z3} - F_{z2}) + h_T \cdot F_{yf} = M_R' + h_c \cdot F_S' + M_a + M_{hitch} \tag{3.22}$$

$$aF_{yf} - bF_{yr} + \frac{c}{2} f_R (F_{z2} - F_{z3}) = M_Y' \tag{3.23}$$

$$b(F_{z2} + F_{z3}) - a(F_{z1}) + h_T \cdot T = m_r \cdot b \cdot g + M_P' + h_c \cdot F_D \tag{3.24}$$

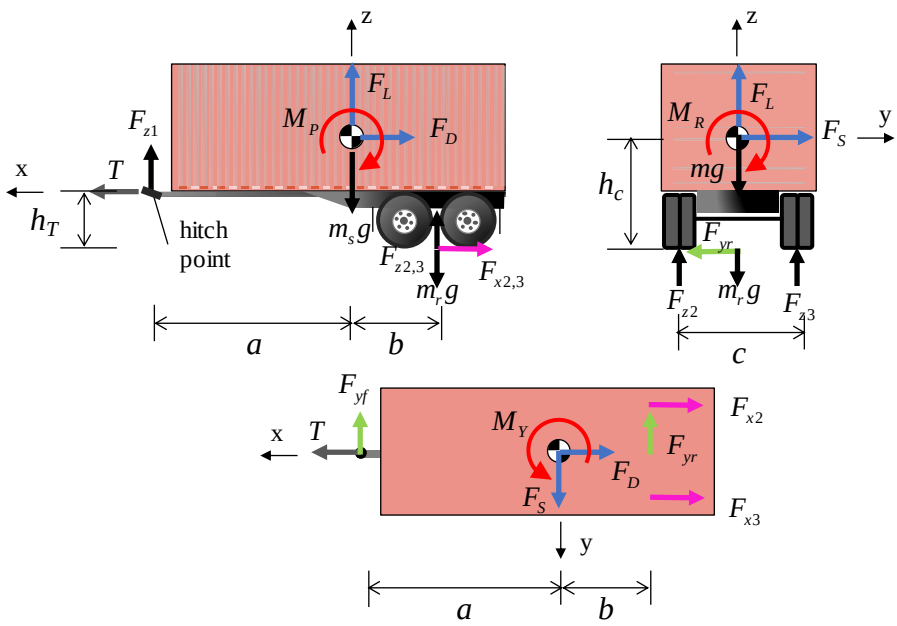

Fig. 3.5. Applied actions and corresponding tire forces of trailers

In Equations (3.19)–(3.24), T is the traction force by the tractor, and M_{hitch} is rolling moment induced by 5th wheel hitch model. h_c and h_T are the height of the center of gravity and the hitch point, respectively.

The rolling moment at the hitch point can be calculated according to relative rolling movement between two bodies following linear model as shown in Equation (3.25).

$$M_{hitch} = K_{\phi}^{hitch} \cdot (\phi_{tractor} - \phi_{trailer}) \tag{3.25}$$

where K_{ϕ}^{hitch} is the roll stiffness of the hitch model, and ϕ_i (i=tractor and trailer) is roll angle of the sprung mass of tractor and trailer models. Since the rolling moment at the hitch point acts not only on the trailer but also on the tractor, two equilibrium equations for rolling moment are obtained as shown in Equations (3.26) and (3.27).

$$\begin{aligned} K_{\phi}^{hitch}(\phi_{tractor} - \phi_{trailer}) + K_{\phi}^{tractor} \cdot \phi_{tractor} \\ = M_R^{tractor} + \{(m_s g - F_L)\phi h_{roll} \cos\alpha\}^{tractor} \end{aligned} \tag{3.26}$$

$$\begin{aligned} K_{\phi}^{hitch}(-\phi_{tractor} + \phi_{trailer}) + K_{\phi,trailer} \cdot \phi_{trailer} \\ = M_R^{trailer} + \{(m_s g - F_L)\phi h_{roll} \cos\alpha\}^{trailer} \end{aligned} \tag{3.27}$$

M_R^i (i=tractor and trailer) is the rolling moment acting on the sprung mass induced by aerodynamic loads and road geometry. Since lateral reaction force at the hitch point also induces rolling moment, M_R^i can be calculated according to Equation (3.28).

$$M_R^i = \left[M_R + \left(\left(F_S + \frac{m_s v^2}{R} \right) \cos\alpha + (F_L - m_s g) \sin\alpha \right) \cdot h_{roll} \right]_i \pm F_{yf}^{trailer} (h_c + h_T - h_{roll}) \tag{3.28}$$

Applying the assumption that contribution of rolling resistance force at the tires of trailer model is negligible compared to the aerodynamic side force and yawing moment, lateral reaction force $F_{yf}^{trailer}$ can be estimated as Equation (3.29).

$$F_{yf}^{trailer} = \frac{F_S^{trailer} \cdot b + M_Y^{trailer}}{a + b} \tag{3.29}$$

As a result, based on the Equations (3.26)-(3.29), following 2 by 2 matrix equation can be derived.

$$\mathbf{K_{roll}} \cdot \mathbf{\Phi} = \mathbf{F_{roll}} \tag{3.30}$$

where

$$\mathbf{K_{roll}} = \begin{bmatrix} K_{roll}^{tractor} & -K_{\phi}^{hitch} \\ -K_{\phi}^{hitch} & K_{roll}^{trailer} \end{bmatrix}$$

$$\mathbf{\Phi} = \begin{bmatrix} \phi_{tractor} \\ \phi_{tractor} \end{bmatrix}$$

$$\mathbf{F_{roll}} = \begin{bmatrix} M_R^{tractor} \\ M_R^{trailer} \end{bmatrix} \tag{3.31}$$

$$K_{roll}^{tractor} = K_{\phi}^{hitch} + K_{\phi}^{tractor} - \{(m_s g - F_L) h_{roll} \cos\alpha\}^{tractor}$$

$$K_{roll}^{trailer} = K_{\phi}^{hitch} + K_{\phi}^{trailer} - \{(m_s g - F_L) h_{roll} \cos\alpha\}^{trailer}$$

In Equation (3.30) and (3.31), $\mathbf{K_{roll}}$ is the roll stiffness matrix of tractor-trailer, $\mathbf{\Phi}$ is the vector of roll angles of sprung masses, and $\mathbf{F_{roll}}$ is the matrix of rolling moment induced by aerodynamic loads and road geometry. Since $\mathbf{K_{roll}}$ and $\mathbf{F_{roll}}$ can be obtained based on the information obtained from vehicle models provided by CarSim and TruckSim software and Equations (3.28)-(3.29), roll angle can be calculated under any given wind condition. After calculating roll angle of each sprung mass, two rolling moment M_a and M_{hitch} are determined according to Equations (3.15) and (3.25) for each vehicle bodies.

Since M_a and M_{hitch} can be estimated according to the above procedure, Equations (3.19)-(3.24) include only six unknowns (one traction force, two lateral friction forces, and three vertical reaction forces) which means that all the tire forces can be determined from the equilibrium equations.

3.2.3 Simulation of aerodynamic forces and moments

Based on the quasi-steady theory, aerodynamic forces and moments induced by side winds can be expressed as shown in Equations (3.32) and (3.33).

$$F_D = C_D A \frac{\rho V^2}{2} \qquad F_S = C_S A \frac{\rho V^2}{2} \qquad F_L = C_L A \frac{\rho V^2}{2} \tag{3.32}$$

$$M_R = C_R A h_c \frac{\rho V^2}{2} \qquad M_P = C_P A h_c \frac{\rho V^2}{2} \qquad M_Y = C_Y A h_c \frac{\rho V^2}{2} \tag{3.33}$$

In Equations (3.32) and (3.33), C_D, C_S, C_L, C_R, C_P, and C_Y are the aerodynamic coefficients for drag force, side force, lift force, rolling moment,

pitching moment, and yawing moment, which can be determined from wind tunnel tests or by computational fluid dynamic analysis; ρ is the air density (=1.225 kg/m^3); V is the apparent wind speed; and A is the front area of the vehicle.

All aerodynamic coefficients are functions of the effective wind direction, ψ, which can be defined from the true wind speed vector $\boldsymbol{w}$ and the vehicle's own speed vector $\boldsymbol{v}$, as shown in Fig. 3.6. When the true wind direction is β, the apparent wind speed vector $\boldsymbol{V}$ and effective wind direction ψ can be defined as shown in Equations (3.34) and (3.35).

$$|\boldsymbol{V}|^2 = (|\boldsymbol{v}| + |\boldsymbol{w}|\cos\beta)^2 + |\boldsymbol{w}|^2 \sin^2\beta \tag{3.34}$$

$$\psi = \arctan\frac{|\boldsymbol{w}|\sin\beta}{|\boldsymbol{v}| + |\boldsymbol{w}|\cos\beta} \tag{3.35}$$

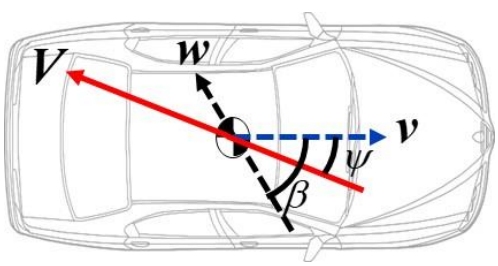

Fig. 3.6. Vehicle speed $\boldsymbol{v}$, true wind speed $\boldsymbol{w}$, and apparent wind speed $\boldsymbol{V}$

3.3 Feasibility of quasi-static approach for estimation of tire reaction forces

The feasibility of the quasi-static approach in estimating reasonable tire forces was examined under uniform and turbulent wind conditions. The

quasi-static approach was validated using the commercial software CarSim and TruckSim (v2017.1). The benchmarking responses for validation were the tire forces of two vehicle types—trucks (vehicle with two axles) and tractor-trailers—under various wind speeds. As a numerical integration method, the Adams–Moulton 2nd order method was adopted. This is an implicit linear multistep method that involves a prediction procedure at each half step. A time step of 0.002 s was selected, which was confirmed as a sufficiently small value via convergence testing.

3.3.1 Modelling options: Truck and tractor-trailer

The modeling information for the two vehicle types was obtained from the built-in models in TruckSim, as shown in Table 3.1. The roll stiffness of hitch model which connects tractor and trailer was selected as 10,000 N·m/deg according to TruckSim. However, roll stiffness of suspension of vehicle is not deterministic value due to various stiffness components such as tire and shock absorber, so numerical experiment was performed to estimate approximate value by measuring roll angle of each vehicle when rolling moment 10,000 N·m was applied on each body. The aerodynamic coefficients of the two vehicle types obtained from the wind tunnel test were adopted which were introduced in Chapter 2. In the case of tractor-trailer models, aerodynamic coefficients of the separate bodies were utilized which is demonstrated in Fig. 2.9.

Table 3.1. Dimensions and parameters of vehicle models

	Truck	Tractor	Trailer
a (m)	1.11	1.11	5.22
b (m)	3.89	2.39	4.78
c (m)	2.00	2.00	1.86
h_c (m)	1.18	1.18	1.94
h_T (m)	-	1.10	1.10
A (m^2)	7.20	7.20	8.12
m_s (kg)	4,455	4,455	6,000
m_f (kg)	570	570	-
m_r (kg)	735	735	665
K_ϕ (N·m/deg)	25,000	18,000	11,000
K_{hitch} (N·m/deg)	-	100,000	

3.3.2 Comparison of tire forces under constant wind

Vertical reaction and lateral friction forces were evaluated for two vehicle types under a driving speed of 80 km/h on a flat straight road ($R = \infty,\ \alpha = 0\%$). Since an initial vibration occurred in the dynamic approach, stabilized results were obtained by providing a sufficient simulation time of 30 s.

Uniform wind speeds were gradually increased at 10 m/s until one of the vertical tire forces reached zero. Fig. 3.7 and Fig. 3.8 show the variations in the tire forces for the truck and tractor-trailer, respectively. The quasi-static approach provided tire forces that compared to those of the dynamic approach. The vertical reaction forces showed a certain difference between the quasi-static and dynamic approaches, while the lateral friction forces were quite similar in both approaches.

The differences in vertical reaction forces for the two vehicle types were further investigated. One interesting point was a tendency for differences according to the wind speeds in the two vehicle types. In the case of the truck, the gap between the two approaches remained constant to the wind speed whereas the gap for the tractor-trailer increased with increases in the wind speed. This differing tendency implies that the main cause of the gap was from different sources for the two vehicle types.

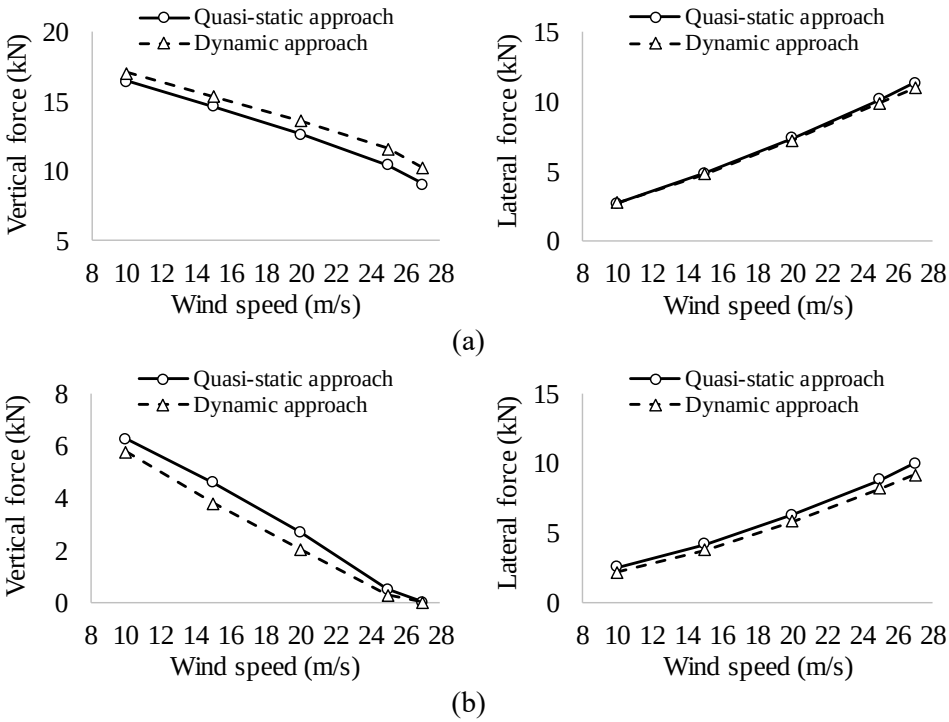

Fig. 3.7. Reaction forces of windward tries of the truck in uniform wind for: (a) front axle, (b) rear axle

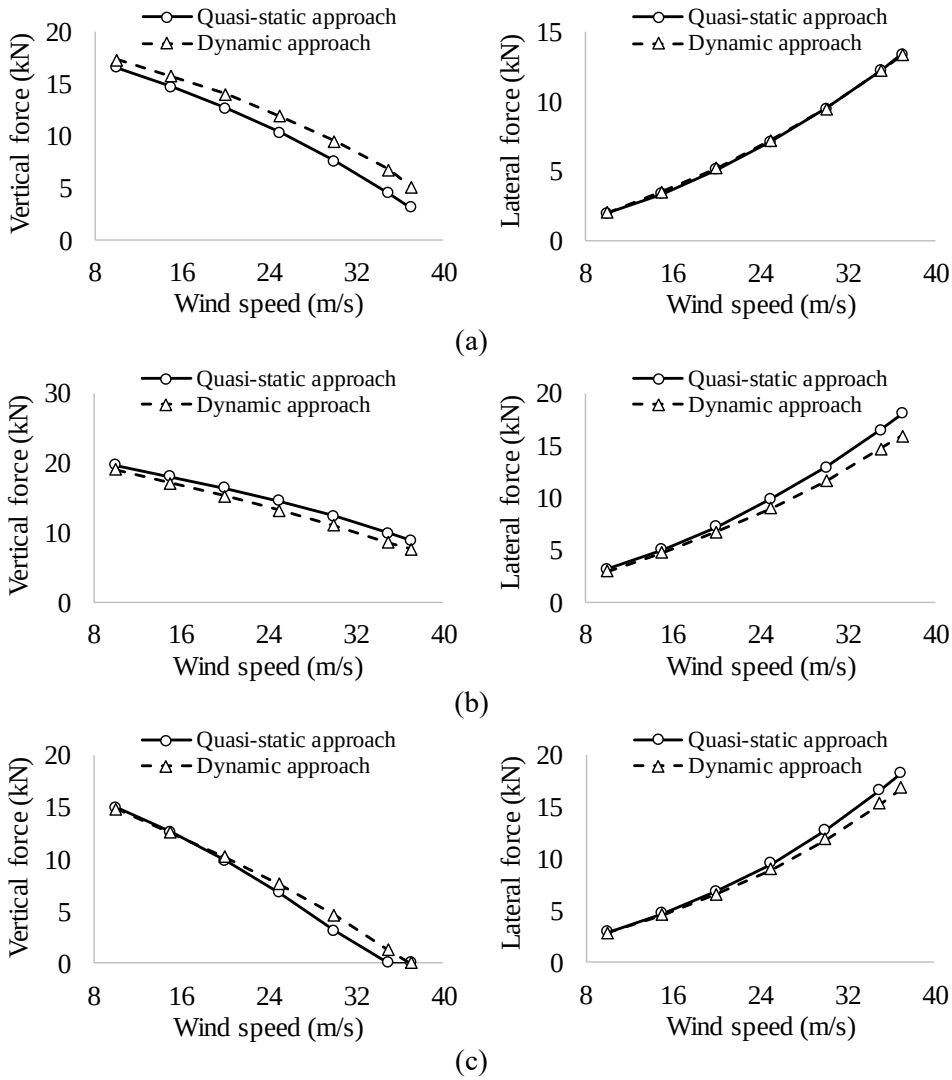

Fig. 3.8. Reaction forces of windward tires of the tractor-trailer in uniform wind for: (a) front axle, (b) rear axle of the tractor, (c) rear axle of the trailer

In the case of the truck, this gap was induced by the difference in suspension modeling between the two approaches. The dynamic approach with TruckSim analysis reflects the type of suspension (independent or solid), the differences in stiffness values for the front and rear axles, and the changeable location of the suspension for the solid type. Since the present

study utilized the default truck model provided by TruckSim, the stiffness and location of the suspensions were different in the front and rear axles. However, the quasi-static approach adopts an assumption of equal suspension stiffness and location for both the front and rear axles, which resulted in constraint condition, as shown in Equation (3.8). Accordingly, both approaches showed a difference in the vertical reaction forces for the truck, as shown in Figure 3.6. In order to support this inference, we modified the truck model for the dynamic approach so that the same stiffness values and location of suspension could be applied to both axles. Figure 3.8 shows similar vertical reaction forces in both approaches, which confirms that the difference in vertical reaction forces was induced from the suspension modeling between the two approaches, particularly for the truck.

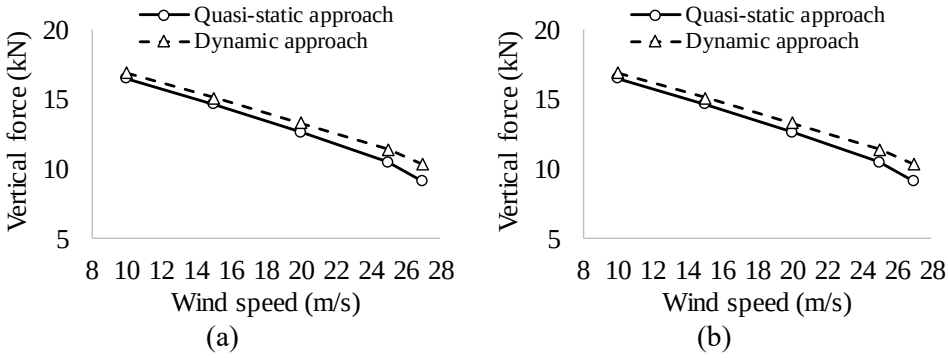

Fig. 3.9. Windward vertical reaction force of the truck with equal stiffness of suspension for: (a) front axle, (b) rear axles

On the other hand, in the case of tractor-trailer, there were the gap in the vertical reaction but also in the lateral friction forces. These gaps were due mainly to the modelling of the hitch point and roll stiffness of the suspension.

Since quasi-static model does not consider complex structure of the hitch model and suspension, it is hard to estimate accurate additional moment induced by lateral displacement. Also, there were rotational displacement of the axles in the dynamic approach which caused increment of additional rolling moment.

Also, yaw angle of the vehicle body was another cause of the difference. Unlike quasi-static approach, dynamic model could rotate along the vertical axis which results the change of the effective wind direction, and this change can quite cause the difference in the aerodynamic forces and moments.

Although there was the effect of the suspension and complex structure of the vehicle body, quasi-static approach method still can provide reasonable tire reaction forces even though there can be a certain level of error. Under the constant wind condition, those effect were not serious compared to the influence of the aerodynamic forces and moments. In the next section, quasi-static approach is examined whether it provides reasonable results under the turbulent wind condition.

3.3.3 Feasibility of the quasi-static approach under turbulent wind

Since overturning and side-slip accidents are particularly vulnerable to high wind speeds during a short period of time, the vehicle safety must be assessed under turbulent wind conditions. Both wind speed and wind direction change over time. Accordingly, the feasibility of the quasi-static

approach under time-varying wind conditions should be further examined. Gradual changes in the traveling direction of a vehicle and the cant effect for a curved road were also taken into consideration in the evaluation of tire forces. The time histories of the six components of aerodynamic forces were obtained using Equations (3.32) and (3.33) and fed into the equilibrium Equations (3.1)-(3.6) and (3.19)-(3.24) by neglecting the aerodynamic admittance effect due to turbulence.

The wind data measured at the tops of the pylons, located at 182 m from the sea level, of an actual sea-crossing cable-stayed bridge were utilized for the feasibility analysis of quasi-static and dynamic procedures for turbulent winds. The data were collected with a sampling rate of 100 Hz for a duration of 10 min during a typhoon. Since the wind speed measured at the top of the pylon was too high to investigate the triggering of vehicle instability, the magnitude of the wind speed was scaled down by half, as shown in Fig. 3.10 (a). The time history of the wind direction is also given in Fig. 3.10 (b). The 10 min. average and standard deviations in wind speeds were 10.8 m/s and 2.9 m/s, respectively. Wind data for a duration of 30 seconds were utilized in the analysis. The wind direction was measured in the direction of a running vehicle at a starting point of 1 min for analysis in the clockwise direction. A vehicle speed of 80 km/h was assumed on a curved road with a curvature radius of 450 m at a cant of 5%. The total analysis time was 70 s, which includes the stabilization time, and the wind direction was modified according to the direction of a vehicle running on a curved road. The tire forces were

evaluated at a time step of 0.01 s in the quasi-static approach and of 0.002 s in the dynamic approach.

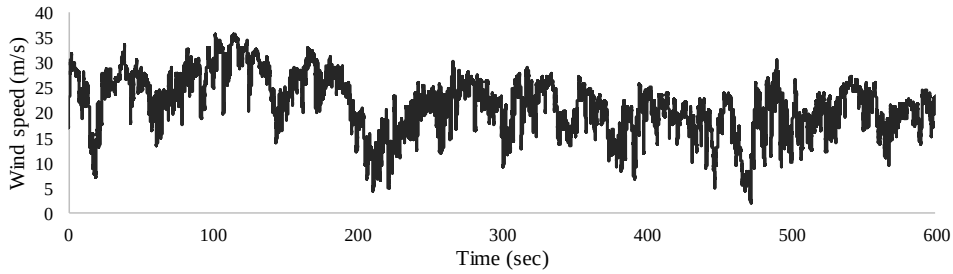

(a)

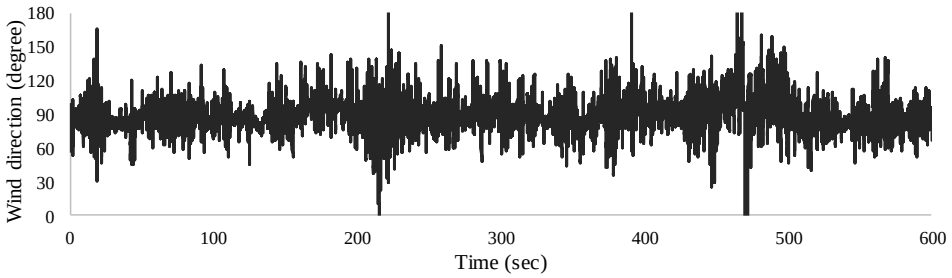

(b)

Fig. 3.10. Time history of wind data: (a) wind speed and (b) wind direction

Fig. 3.11 and Fig. 3.12 show the tire forces for the truck and the trailer, respectively, for the 30 seconds turbulent wind. According to these figures, under turbulent wind conditions, the quasi-static approach also provided results that were comparable to those of the dynamic approach. Amplitude and variation of all tire reaction forces were very similar under the high wind speed.

However, there is one noticeable difference between the two approaches that the phase and frequency for the two approaches changed within a smaller time duration due to the effect of the suspension model in the dynamic approach. However, this effect was not critical in estimating the magnitude of

the vertical reaction forces of the tire. Accordingly, the feasibility of the quasi-static approach for the safety assessment was successfully demonstrated even under turbulent wind conditions.

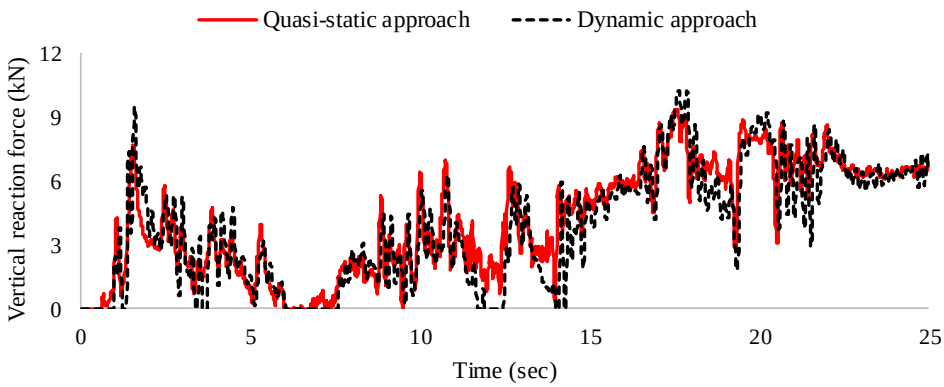

(a)

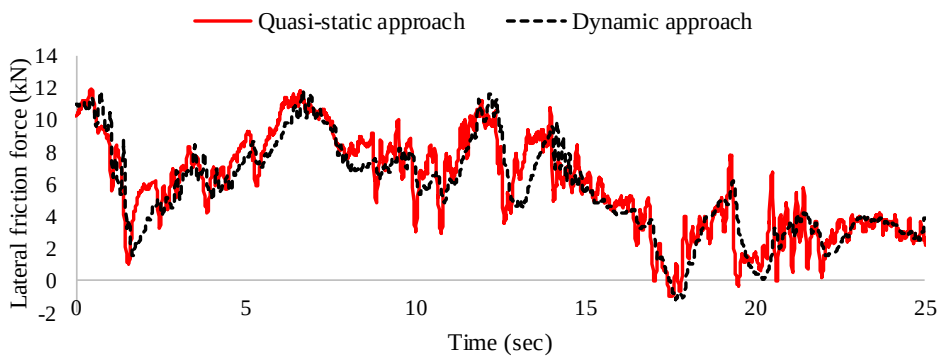

(b)

Fig. 3.11. Time histories of tire forces of rear axle of the truck: (a) vertical and (b) lateral force

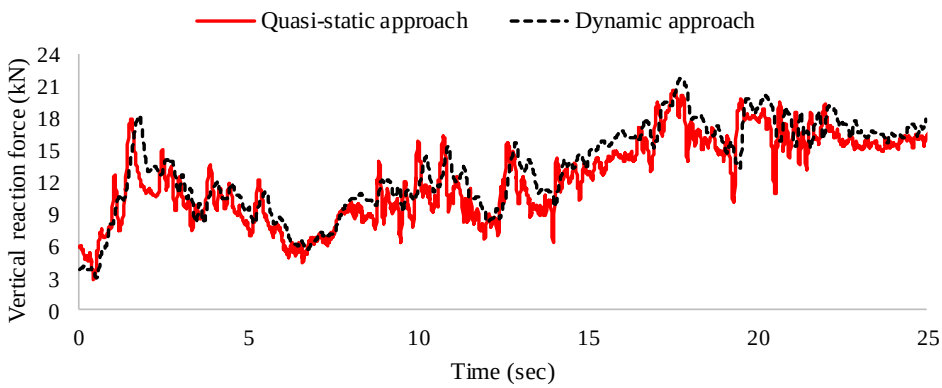

(a)

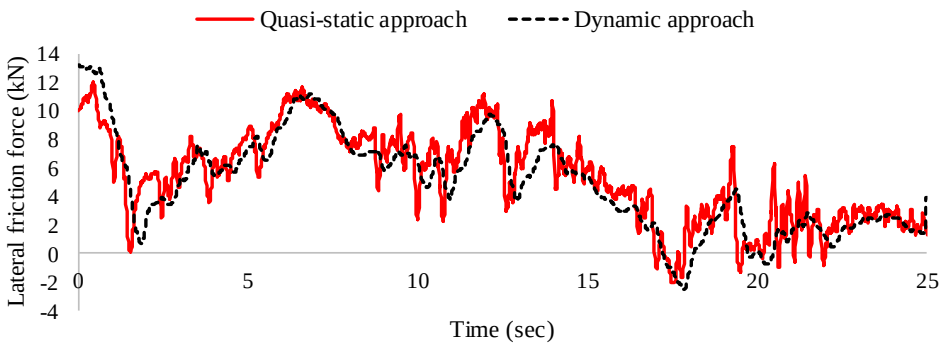

(b)

Fig. 3.12. Time histories of tire forces of rear axle of the trailer: (a) vertical and (b) lateral force

CHAPTER 4

DETERMINATION OF WIND SPEED FOR TRAFFIC CONTROL THROUGH VEHICLE SIMULATION

A method to estimate critical wind speed and to determine the wind speed for traffic control was proposed with consideration of vehicle dynamics, wind direction, and disturbance effect of girder shape on wind flow. Road geometry such as curvature, cant, and length of a road were also considered as influential factors. In section 4.1, the algorithm to estimate critical wind speed curve, in short CWC, was introduced considering the uncertainty of the wind turbulence by probabilistic approach. In section 4.2, a procedure for determining wind speed for traffic control for long-span bridges using both quasi-static and dynamic approaches was introduced. In section 4.3, wind speed for traffic control was estimated for Gwangan Bridge as a numerical application.

4.1 Estimation of critical wind speed curve considering the uncertainty of wind turbulence

Critical wind speed is the wind speed which can cause overturning or side-slip accidents, and it changes according to various factors like vehicle speed, wind direction, and road geometry. In this section, a methodology to estimate

a variation of critical wind speed according to wind direction which is called critical wind speed curve(CWC) was introduced.

Unlike several previous research works (Kwon et al., 2011; Thomas et al., 2010), the proposed method utilizes time histories of turbulence winds rather than short gust wind or constant wind in order to perform more realistic simulation. However, because of the uncertainty of the turbulence component in wind speed, critical wind speed also can change according to the wind history. Therefore, a probabilistic method was applied to determine CWC is determined considering more than 50 sets of time histories of turbulence wind.

4.1.1 Definition of accident criteria

First, accident criteria were defined for both quasi-static and dynamic approaches. In the case of quasi-static approach, tire reaction forces are the only results obtained from the vehicle simulation as shown in Chapter 3, so the critical wind speed was determined based on the tire reactions. Two accidents, side-slip and overturning accidents, were considered as shown in Fig. 4.1 and the limits for the states of the two accident types are defined as follows (Kim and Kim, 2019):

- Side-slip: when one of the axles reaches the friction limit
- Overturning: when one of the vertical reaction forces of the tires becomes zero

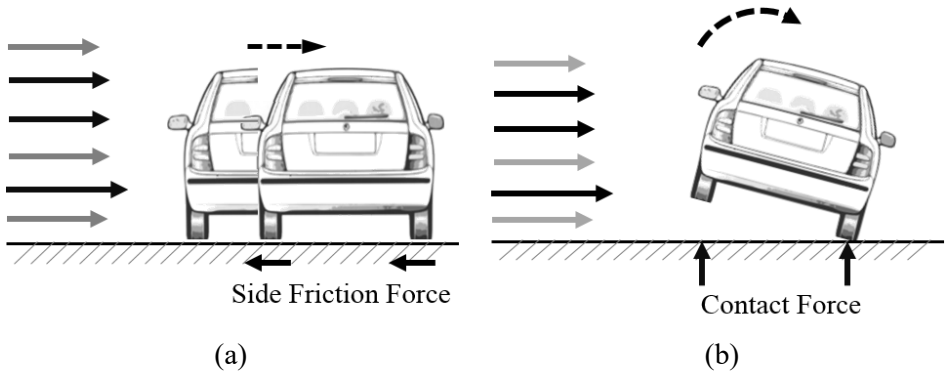

Fig. 4.1. Considered accident types for quasi-static approach. (a) side-slip accident and (b) overturning accident

In order to determine the friction limit state, the definition of the normalized friction force, $\overline{F_f}$ and $\overline{F_r}$, was introduced in Equation (4.1) and (4.2) as the friction force divided by the vertical tire forces. According to Grip et al. (2009), the friction force increased in a linear fashion until the occurrence of tire slip, at which point it was saturated and road grip was lost when the normalized friction force reached friction coefficient, μ. Therefore, the friction limit state can be defined by Equation (4.1) and Equation (4.2).

$$\overline{F_f} = \frac{\sqrt{F_{yf}^2 + q(F_{z1} + F_{z3})^2}}{F_{z1} + F_{z3}} > \mu \tag{4.1}$$

$$\overline{F_r} = \frac{\sqrt{F_{yr}^2 + q(F_{z2} + F_{z4})^2}}{F_{z2} + F_{z2}} > \mu \tag{4.2}$$

Criteria for dynamic approach is defined in different way from quasi-static approach. Three accident types, overturning, side-slip, and rotation accidents were considered, and the limit state of the overturning accident is same as that of quasi-static approach whereas criteria for the side-slip and rotation

accidents were defined based on the displacement of vehicle. The limit states of side-slip and rotation accidents are as follow.

- Side-slip: when vehicle deviates to next traffic lanes
- Rotation: when yaw angle reaches 0.2 radian (Baker, 1986)

The lateral displacement of center of gravity of the vehicle was utilized to determine whether side-slip accident occurred or not. The limit state of side-slip accident also can be expressed as Equation (4.3).

$$y > \frac{W_{lane} - W_{axle}}{2} \tag{4.3}$$

where y is the maximum lateral displacement of the center of gravity of vehicle, W_{lane} and W_{axle} are the width of traffic lane and axle of vehicle, respectively. Based on these criteria, critical wind speeds were estimated for various road and wind conditions.

4.1.2 Algorithm to estimate critical wind speed curve

When vehicle is running on a bridge under strong wind condition, there are several factors effecting on vehicle stability a lot such as wind turbulence, road roughness, and vehicle system. All of these factors have certain level of uncertainty, so it is hard to estimate critical wind speed by deterministic way. In this study, critical wind speed was determined by probabilistic approach by considering the uncertainty of turbulence of wind speed. Although there are many other uncertain factors, they were set in constant values because wind

turbulence is the most influential uncertain factor compared to other factors (Baker, 2013).

The uncertainty of turbulence was considered by estimation of critical wind speed for various sets of time histories of wind speed. Critical wind speed was estimated repeatedly under same simulation scenario but for the different set of wind history. Estimation was performed under 16 wind directions using 50 or 100 sets of wind speed variation which were generated by simple decomposition of the wind spectrum. The algorithm to estimate critical wind speeds is demonstrated in Fig. 4.2.

As shown in Fig. 4.2, the basic idea of estimation of critical wind speed is very simple. Simulation starts with generated wind speed data of which mean value k is 5 m/s under pre-defined simulation scenario, and tire reaction forces or displacement were estimated. The simulation is iterated by increasing mean wind speed with interval dk=5 m/s until accident occurs. If vehicle accident occurs, mean wind speed k decreases to the value of the previous step and increment interval of mean wind speed dk decreases to one fifth. The iteration is proceeded over and over, and stops when dk becomes less than 0.2 m/s which is the tolerance limit of the iteration. Then, critical wind speed is determined as k m/s. During an iteration, only one fixed random phase was used for generating turbulence wind. All wind histories were simulated by utilizing the Von-Karman spectrum which is given by (Simiu and Scalan, 1996) as shown in Equation (4.4) and (4.5).

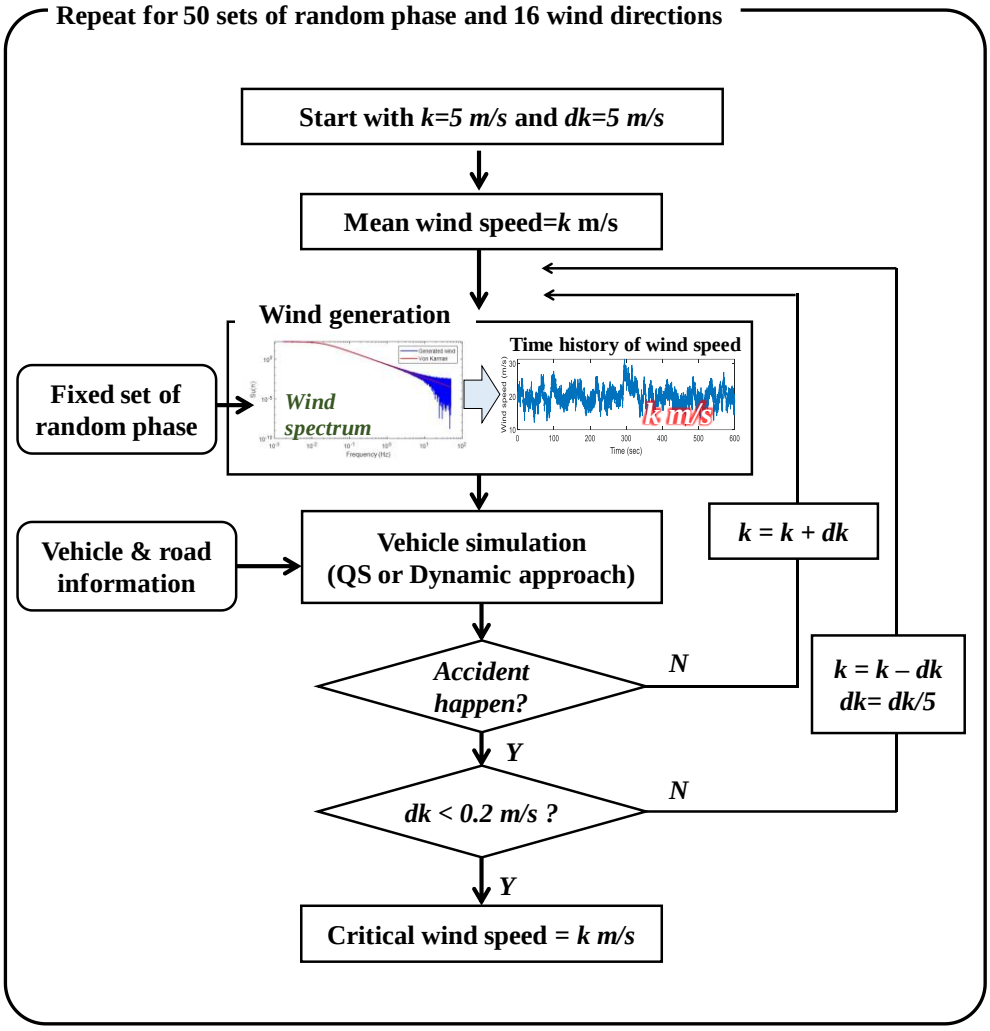

Fig. 4.2. Algorithm to estimate critical wind speeds for given set of random phase and wind direction

$$\frac{f \cdot S_u\{f\}}{\sigma_u^2} = \frac{6.4 \cdot \widehat{f_u}}{\left(1 + 10.2 \cdot \widehat{f_n}\right)} \tag{4.4}$$

where,

$$\widehat{f_u} = \frac{f \cdot L_u}{U} \tag{4.5}$$

In Equation (4.4) and (4.5), f is the frequency of longitudinal velocity fluctuation, L_u is the length scale of the fluctuation, U is the mean wind speed, and σ_u is the standard deviation of wind speed. Fig. 4.3 is an example of generated wind speed time history.

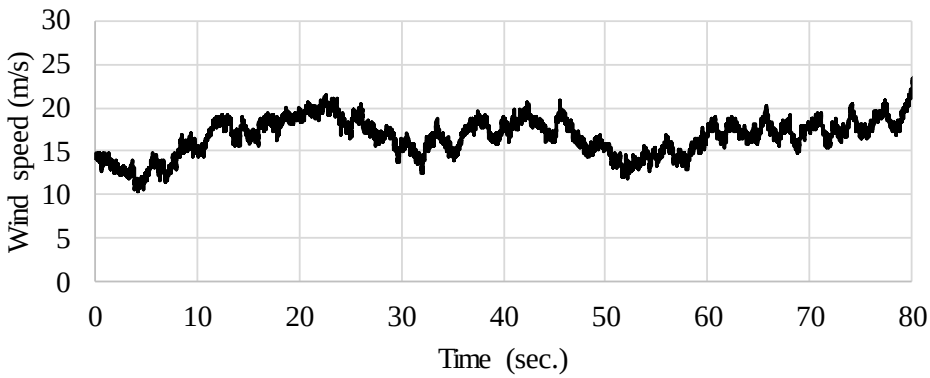

Fig. 4.3. An example of generated wind speed time history

The time step of the generated wind data is 0.01 second, and the range of considered wind frequency is from 0 to 50 Hz. In order to consider aerodynamic admittance effect due to the length and height of vehicle body, moving average filter was used for smoothing the wind speed data with 0.5 second window size. The length of the generated wind history is equal to travel time T which is calculated by road length over vehicle speed, and the critical wind speed is obtained by averaging the T seconds wind speed data. For example, if vehicle speed and road length are 72 km/h and 1,000 m respectively, the critical wind speed k m/s is then calculated by averaging 50 seconds wind histories.

Multiple critical wind speeds are obtained from the algorithm for each wind direction using various sets of random phase. 100 and 50 sets of random phase were used for quasi-static and dynamic approach, respectively. Fig. 4.4 shows an example of 50 estimated critical wind speeds (black circle marker) in the form of the cumulative distribution function which were obtained using dynamic approach. As shown in this figure, critical wind speed can have various values because maximum gust speed is different according to wind time history. This distribution of critical wind speed can be changed according to road geometry or vehicle speed.

In order to express this distribution by a probabilistic function, Generalized Extreme Value (GEV) distribution model was utilized of which equation is as follows.

$$F\left(X < U_j; \mu, \sigma, \xi\right) = \exp\left\{-\left[1 + \xi \frac{U_j - \mu}{\sigma}\right]^{-1/\xi}\right\} \tag{4.6}$$

where σ is the scale parameter, μ is the location parameter, and ξ is the shape parameter. These three parameters can be estimated for 16 wind directions by applying the maximum likelihood estimation. There are two reasons for choosing GEV function for the curve fitting. First, GEV function showed best performance among 16 distribution models (GEV, Normal, Generalized-Pareto, Uniform, Rayleigh, Exponential, Beta, Lognormal, Birnbaum-Saunders, Inverse-Gaussian, Logistic, Log-Logistic, t Location-Scale, Nakagami, Gamma, Rician), having the highest log-likelihood value. Second, GEV function is the probability distribution which is appropriate for

approximating extreme values. Since vehicle accident occurs by short and high gusty winds, it is expected that GEV function can capture the trend in the critical wind speed distribution. According to the Fig. 4.4, the GEV function, which is demonstrated as red line, actually well follows the distribution of critical wind speed with high accuracy. Estimated GEV function is also can be called fragility curve since it provides the accident probability according to mean wind speed. Therefore, total 16 fragility curves are estimated for each wind direction as the final outputs of the algorithm.

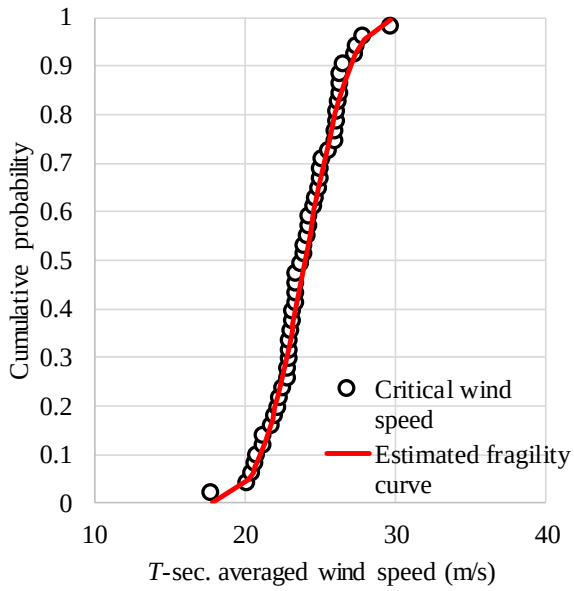

Fig. 4.4. Cumulative distribution of critical wind speed and estimated fragility curve

In order to obtain critical wind speed curve (CWC), one representative critical wind speed is selected which corresponds to certain level of accident probability α% for each fragility curve. As a result, total 16 critical wind

speeds are obtained from 16 wind directions, that is to say CWC. Too small target accident probability α% produces too conservative CWC whereas large target value can produce too high CWC. In this study, 5% probability was adopted as the target α%, so a representative critical wind speed $U_{critical}$ was estimated by equation (4.7). In the case of Fig. 4.4, the selected critical wind speed is 19.6 m/s.

$$U_{critical} = \mu + \frac{\sigma}{\xi}\left[\ln(100)^{-\xi} - 1\right] \tag{4.7}$$

Fig. 4.5 shows CWC of the truck running on a northbound flat straight road (cant= 0% and μ= 0.85). According to this figure, the critical wind speed changes dramatically according to the wind incident angle. The variation is due to the changes of the aerodynamic coefficients of the vehicle. The critical wind speed is very high at north and south direction which is quite obvious results because side force, rolling and yawing moment are almost zero at this wind direction. On the other hand, the smallest critical wind speed appears at ENE and WNW wind direction rather than perpendicular wind direction. Although side force and rolling moment coefficients become maximum when the effective wind direction is 90°, the wind load is maximum at 30~60° wind direction because relative wind speed is much higher due to the vehicle own speed as shown in Fig. 3.6. This is the reason of the necessity to consider not only the perpendicular wind but also all the diagonal winds during risk assessment.

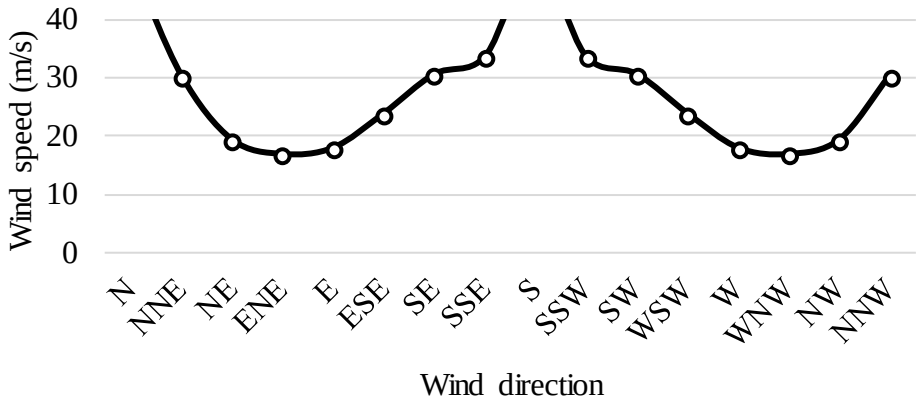

Fig. 4.5. CWC of the truck on straight road(cant= 0% and μ= 0.85)

4.2 Procedure to determine wind speed for traffic control for long-span bridges

The procedure to determine wind speeds for traffic control using estimated CWCs is introduced in this section. Both quasi-static and dynamic approaches are utilized during the estimation procedure in order to minimize total simulation time by using their pros and cons which mentioned in Chapter 3.

The run-time of the algorithm introduced in section 4.1 is very different according to the approaches. In the case of quasi-static approach, the algorithm takes maximum two hours for estimating a single CWC whereas dynamic approach requires maximum 40 hours which is 20 times higher than that the quasi-static approach takes. Since long-span bridge has many road sections and traffic lanes to be simulated, quasi-static approach is much useful in terms of the total simulation time.

However, dynamic approach also has its own advantage that realistic vehicle system can be simulated which can provide not only the tire reaction forces but also the displacements of vehicle bodies. Therefore, more reasonable critical wind speed can be expected with consideration of the complex interaction between vehicle components using the dynamic approach.

Accordingly, in order to perform all simulation cases as short as possible and also obtain reasonable results, both quasi-static and dynamic approaches are utilized. Each approach takes its own role that quasi-static approach is applied to identify the most dangerous traffic lane or road section among the whole bridge area in order to minimize simulation cases. Then, one representative CWC is estimated for the identified traffic lane using dynamic approach. The wind speed for traffic control is determined based on the obtained CWC. The detail procedure which is composed of three steps is introduced in the following sections.

4.2.1 Step 1. Identification of the most dangerous traffic lane using quasi-static approach

The aim of the first step is to minimize the simulation cases which will be tested by CarSim and TruckSim in step 2 by identifying the most dangerous traffic lane among the whole bridge. All traffic lanes and all road sections including main and approaching spans are simulated and examined. Each

traffic lane is modeled based on their geometry such as length, curvature, and cant. The coefficient of friction, μ, between the tire and the road surface is also defined according to the weather, and it was assumed to be 0.85 to simulate dry condition (Gustafsson,1997).

Tested vehicle speed is generally set as the limit of vehicle speed actually adopted in the actual bridge. Aerodynamic coefficients of vehicle on the girder section obtained from wind tunnel test are applied to simulate wind load acting on the vehicle body with consideration of vehicle own speed.

One hundred turbulent wind data generated based on Von-Karman spectrum are utilized to estimate CWCs of all tested traffic lanes of the all road sections. By comparing all the estimated CWCs, the most dangerous traffic lane and road section which provides the smallest critical wind speed value is selected as the most dangerous case. In the case of double deck bridge like Gwangan Bridge, two traffic lanes are selected for upper and lower deck, respectively.

The one thing to be solved is that the CWCs obtained by the vehicle simulation provide T-averaged wind speed as the critical wind speed. Since travel time T is different between road sections according to their length such as main and approaching spans, direct comparison between the CWCs of each road section may not be appropriate. Therefore, it is necessary to convert all the critical wind speeds to the equal time averaged value. In this study, 10 minute is utilized as the reference time duration. In order to convert T-averaged wind speed to 10-min. averaged wind speed, a ratio of probable

maximum speed averaged over travel time T to that averaged over 10 minutes is obtained using the methodology provided by Simiu and Scalan (1996). According their method, the ratio γ can be estimated as Equation (4.8).

$$\gamma = \frac{\overline{U_T(z)}}{\overline{U_{10\min}(z)}} = \frac{2.5\ln(z/z_0) + \beta^{1/2} c(T\,\text{sec.})}{2.5\ln(z/z_0) + \beta^{1/2} c(10\,\text{min.})} \tag{4.8}$$

where $\overline{U_T(z)}$ and $\overline{U_{10\min}(z)}$ are maximum T seconds and 10 minutes averaged wind speed at height z. β is the coefficient which changes according the surface roughness length z_0 as shown in Table 4.1. c(t) is the coefficient which depends on time t as shown in Table 4.2. According to these two tables, all the variables in the Equation (4.8) are determined, and the ratio γ can be estimated which is to convert $\overline{U_T(z)}$ to $\overline{U_{10\min}(z)}$. By converting all the CWCs of the investigated road sections in to 10-min. averaged wind speed, the most dangerous traffic lane can be determined.

Table 4.1. Values of β corresponding to various roughness lengths (Simiu and Scalan, 1996)

Z_0 (m)	0.005	0.07	0.30	1.00	2.50
β	6.5	6.0	5.25	4.85	4.00

Table 4.2. Coefficients c(t) (Simiu and Scalan, 1996)

t (sec.)	1	10	20	30	50	100	200	300	600	1000	3600
c(t)	3.00	2.32	2.00	1.73	1.35	1.02	0.72	0.54	0.36	0.16	0.00

4.2.2 Step 2. Estimation of critical wind speed curve of selected traffic lane using dynamic approach

In step 2, CWCs of the selected traffic lane are re-estimated using dynamic approach. In this study, CarSim and TruckSim were used to estimate CWCs of the three vehicles, and total 50 different wind speed data were generated to simulate wind loads. As same as step1, all critical wind speeds are obtained as 10-min. averaged value.

Only one or two traffic lanes are examined in step 2, but various CWCs are obtained by considering two influential factors, vehicle speed and tire-road friction coefficient. Many test scenarios can be simulated by changing the combination of these factors. In this study, two vehicle speed and three friction coefficients were considered. For the first parameter, the vehicle speed which was utilized in step 1 and half of that were adopted. In the case of second parameter, three friction coefficient were adopted for three different road condition; 0.85 for dry road, 0.5 for wet road, and 0.2 for snowy road (Ghandour et al., 2010). As a results, total six CWCs were estimated for each selected traffic lane. The combination of the parameters can be changed according to the desired complex level of traffic control.

The two commercial programs provide realistic vehicle system which was great advantages for reasonable estimation, but due to the complexity of the vehicle system it was hard to realize the simulation which the author desired. For example, vehicles could not keep their speed constant when wind

direction is aligned with the driving direction. When vehicle faces the strong headwind, it lost its own speed a lot whereas tailwind largely raised the speed of vehicle. This was undesirable situation but also inevitable, so it was required to consider this fluctuation of vehicle speed during estimation of critical wind speed. In this study, 70% of target vehicle speed was selected as allowable fluctuation in vehicle speed. Therefore, critical wind speed was determined when deviation of vehicle speed becomes larger than 70% of its target value.

4.2.3 Step 3. Determination of wind speed for traffic control

As a final step, wind speed for traffic control is determined based on CWCs obtained in step 2. There are several ways to determine wind speed for traffic control. For example, Imai et al. (2002) established traffic control strategy for train according to the wind direction by applying different wind speed for traffic control to west wind (240°~300°) and rest wind directions. In this study, however, the minimum critical wind speed was applied to all wind direction equally for the traffic control for the simplicity of bridge operation. Since six CWCs are obtained from step 2, total six wind speeds for traffic control according to vehicle speed and road condition are determined as final outputs.

4.3 Application to Gwangan Bridge

4.3.1 Modelling options: road, wind, and vehicle

Road modelling

The developed procedure was applied to determine wind speed for traffic control of Gwangan Bridge. Total three road sections, one main span and both side of approaching spans of Gwangan Bridge, were selected for the case study as shown in Fig. 4.6. The main span is the straight road which has truss members between upper and lower deck, and both side of the approaching spans are composed of the straight and curved roads which do not include truss member. The total covered length is 4.45 km and, the specific geometry information of each span are demonstrated in Table 4.3. The vehicles move toward south on the upper deck whereas northward on the lower deck. The lane numbers were assigned from the land-side (West) to the sea-side (East) as shown in Fig. 4.6, and all the deck sections tilts toward land-side.

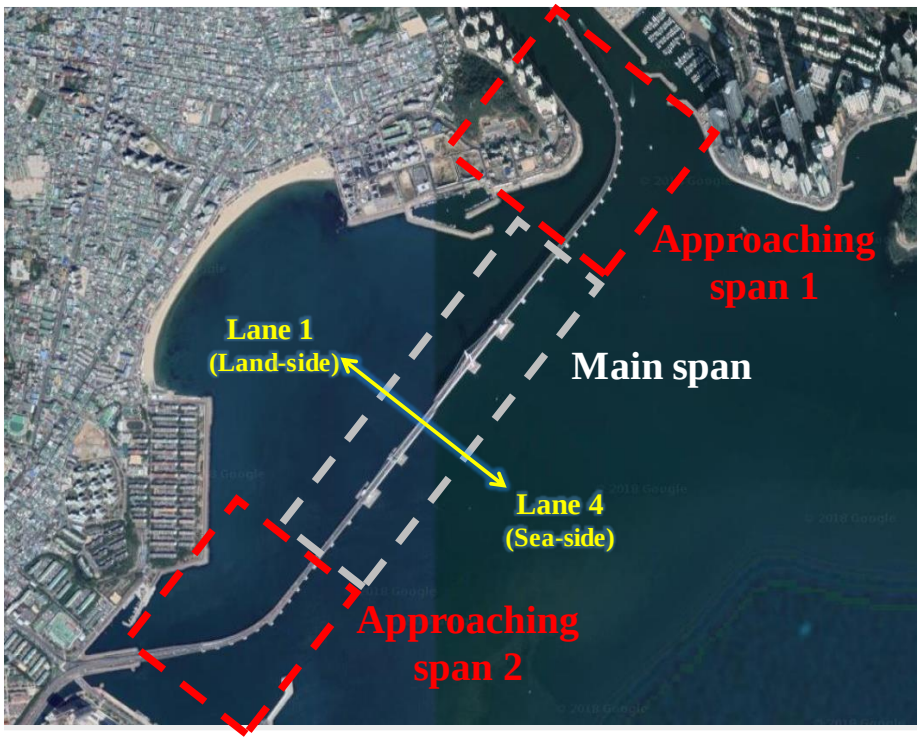

Fig. 4.6. Three investigated sections of Gwangan Bridge

Table 4.3. Geometry information of the three road sections

		Approaching span 1	Main span	Approaching span 2
Total span length (curved section)		1,563 m (480 m)	1,680 m	1,204 m (384 m)
Radius of curved section		450 m	-	500 m
Cant (curved section)		2% (5%)	2% (-)	2% (5%)
Reference Height	**Upper deck**	32.0 m	50.3 m	33.6 m
	Lower deck	21.8 m	40.8 m	23.3 m

Wind modelling

Since wind properties are dependent on the height of road sections, different sets of wind data were generated for each section. Two wind

properties, turbulence intensity and length scale, were considered to generate various time histories of wind speed assuming that the terrain category of the bridge site is open sea (Category I). The turbulence intensity was determined by Equation (4.9) according to KSCE (2006), and the length scale was calculated by Equation (4.10) which is provided by Strommen (2010). The estimated wind properties are shown in Table 4.4.

$$I_u = \frac{1}{\ln(30/0.01)} \cdot \left(\frac{30}{z}\right)^{0.12} \tag{4.9}$$

$$L_u = 100m \cdot \left(\frac{30}{10m}\right)^{0.3} \tag{4.10}$$

Table 4.4. Target wind properties of the three road sections

	Approaching span 1		**Main span**		**Approaching span 2**	
	Upper	Lower	Upper	Lower	Upper	Lower
Turbulence intensity	12.3 %	12.9%	11.7%	12.0%	12.4%	13.0%
Length scale	143 m	129 m	162 m	152 m	142 m	126 m

Vehicle modelling

Three vehicle types, sedan, truck, and tractor-trailer, were simulated. The dimension and parameter shown in Table 3.1 were adopted for the two high-sided vehicle, and the information of sedan was provided in Table 4.5. Aerodynamic coefficients of vehicles on Gwangan Bridge which were obtained from the experiment mentioned in Chapter 2 were utilized.

Table 4.5. Dimensions of sedan

a (m)	b (m)	c (m)	h_c (m)	A (m^2)	m_s (kg)	m_f (kg)	m_r (kg)	K_ϕ (N·m/deg)
1.11	1.67	1.55	0.54	2.64	1,370	80	80	10,000

4.3.2 Application results

Step 1. Identification of the most dangerous traffic lane

As the first step, CWCs of all traffic lanes on the three road sections were estimated in order to identify the most dangerous traffic lane for each traffic lane. Fig. 4.7, Fig. 4.8 and Fig. 4.9 shows the all estimated CWCs of sedan, truck, and tractor-trailer, respectively, when vehicle travels on each traffic lane by 80 km/h. According to these figures, many similarities and differences could be found between the simulation cases.

First, the results of the sedan is discussed based on the Fig. 4.7. According to the figure, big differences in the results could be found between the upper and lower decks. Most of the critical wind speeds on the upper deck are much larger than those of the lower deck. This difference was due to the large reduction of wind speed below 3 m height on upper deck where the sedan submerged in as shown in Fig. 2.14. Nevertheless, on main span, the critical wind speed was calculated as about 32 m/s from south to west-south-west direction.

In the case of lower deck, variations of all CWCs were very similar that smallest value was obtained from north to east wind directions whereas

largest value was obtained from south to west direction. This can be explained by the summation of vehicle speed and wind speed vector which is shown in Fig. 3.6. Due to the vehicle own speed, wind speed that vehicle actually experiences becomes extremely large when the angle between wind speed and vehicle speed vector is small enough. On the other hands, the wind speed dramatically decreases when the angle between two vectors increases which leads large reduction in wind load acting on the vehicle body. Since vehicle travels northward on the lower deck, north-east wind would be the most vulnerable compared to other directions. Even though the variation of the all CWCs were similar on the approaching spans, one noticeable difference could be observed between the CWCs of approaching span 1 and 2. The wind direction where maximum critical wind speed appears was south on approaching span 1 whereas it was west-south-west on approaching span 2. The driving direction was the main reason of this difference that the direction of the vehicles changes from north-north-east to north-west on approaching span 1 whereas it changed from east to north-north-east on approaching 2.

Comparing the results between main span and approaching spans, the smallest critical wind speed was obtained as 24 m/s which was obtained from approaching span 1. This result shows the negative effect of wind tunneling effects on vehicle stability which is induced by the shape of the girder shape. On the other hands, the largest value was 32 m/s obtained from the main span due to the wind mitigation effect by truss members.

Results of the two high-sided vehicles were very similar to each other. Unlike sedan, quite small critical wind speeds were also obtained on upper deck since the heights of the two vehicle are higher than 3 m. Another interesting point in the results of upper deck is that Lane 4 which was the most sea-side traffic lane had much lower critical wind speed for south-east wind direction compared to the other traffic lanes whereas land-side lanes, Lane 1 and 2, had slightly lower critical wind speed for west winds. There are several reasons for this difference. First, according to the results obtained from the wind tunnel test, side force, rolling and yawing moment coefficients generally have largest value on windward lanes and smallest value on leeward lane. Second, the cant of the sections is another reason of the difference. Since all deck sections tilt toward land-side, wind flow disperses upward much quickly by the disturbance effects of guard-rail when wind blows from the sea to the land. This phenomenon was especially noticeable on the curved road of approaching spans due to the large cant that critical wind speeds of Lane 1, 2 and 3 were much higher than that of Lane 4 for south-east direction. Due to this dispersion of wind flow, the shape of CWC was very dependent on traffic lanes that windward traffic lanes was generally much vulnerable than leeward lanes on the upper deck.

On the other hand, in the case of the lower deck, the variance of CWC was small compared to the upper deck. This uniformity was due to the wind tunneling effect which makes wind load almost constant for all traffic lanes. Unlike upper deck, the effect of cant or guardrail of the girder was also not

significant because wind flow could not disperse in the open space due to the existence of the upper deck.

Another noticeable characteristic in all CWCs of approaching span is that minimum critical wind speed was observed at multiple wind directions whereas minimum value was obtained at only one or two particular directions on main span. For example, in the case of truck on Lane 1 of upper deck of approaching span 1, nearly constant value was obtained as critical wind speed from south-south-west to west-north-west directions while minimum value was obtained only from west and west-north-west directions on main span. This phenomenon was due to the characteristic of curved road of approaching spans that driving direction keep change according to vehicle location which raises the possibility to encounter dangerous wind incident angle. This was the reason of the flat variation of critical wind speed in the CWCs of approaching spans.

Based on the obtained CWCs, the most dangerous traffic lanes for each decks were selected for each vehicle types which were to be examined by dynamic approach. Table 4.6 shows the selected traffic lanes and corresponding minimum critical wind speed for each case. On upper deck, main span is more dangerous than two approaching spans whereas approaching span 1 is the most vulnerable section on lower deck.

According to the table, the truck is more vulnerable than tractor-trailer especially on the upper deck even though wind load acting on the body is much smaller. This is due to the light weight of the truck which is more than

twice lighter than that of the tractor-trailer which causes truck model more vulnerable especially for overturning.

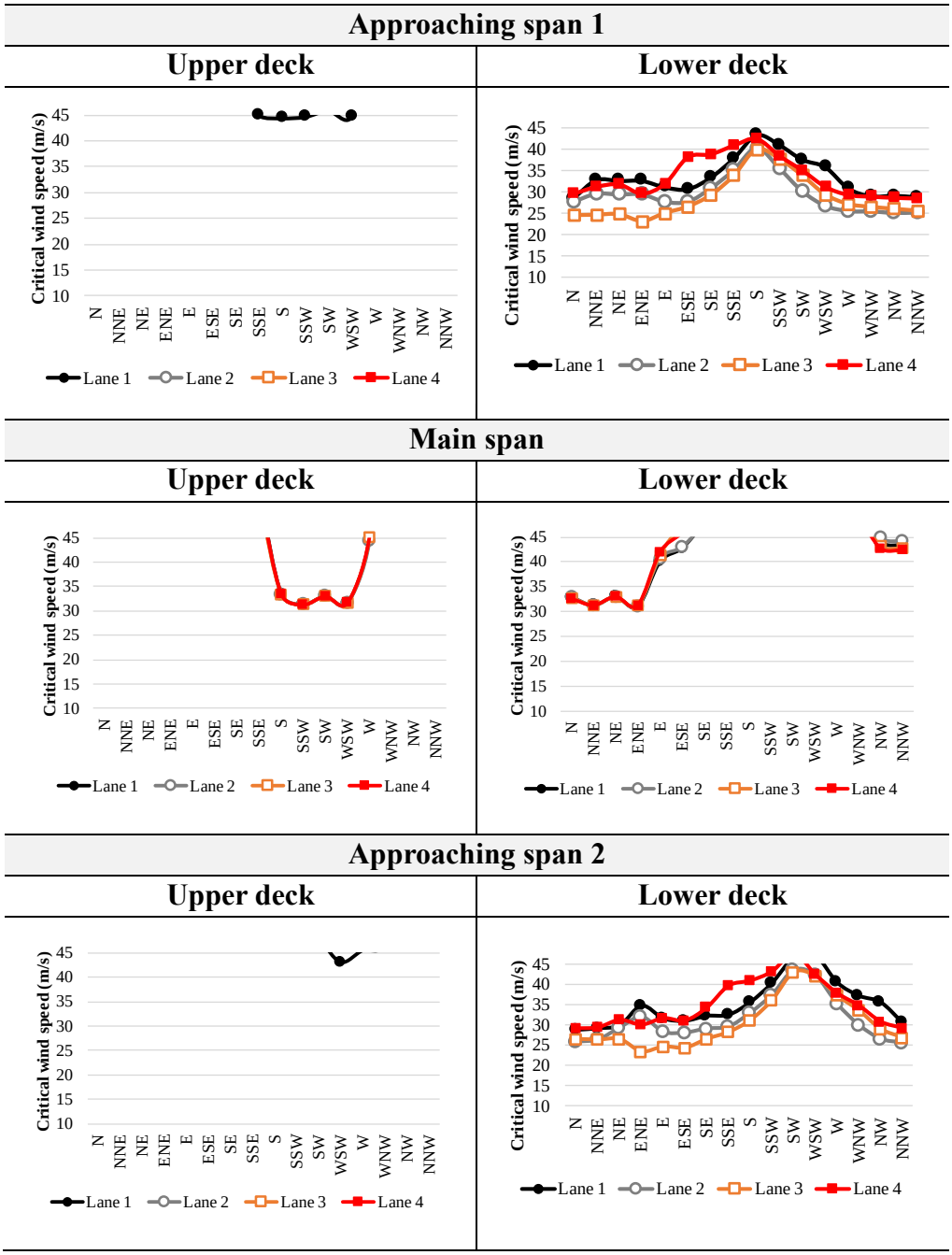

Fig. 4.7. Estimated CWCs of sedan on the three road sections

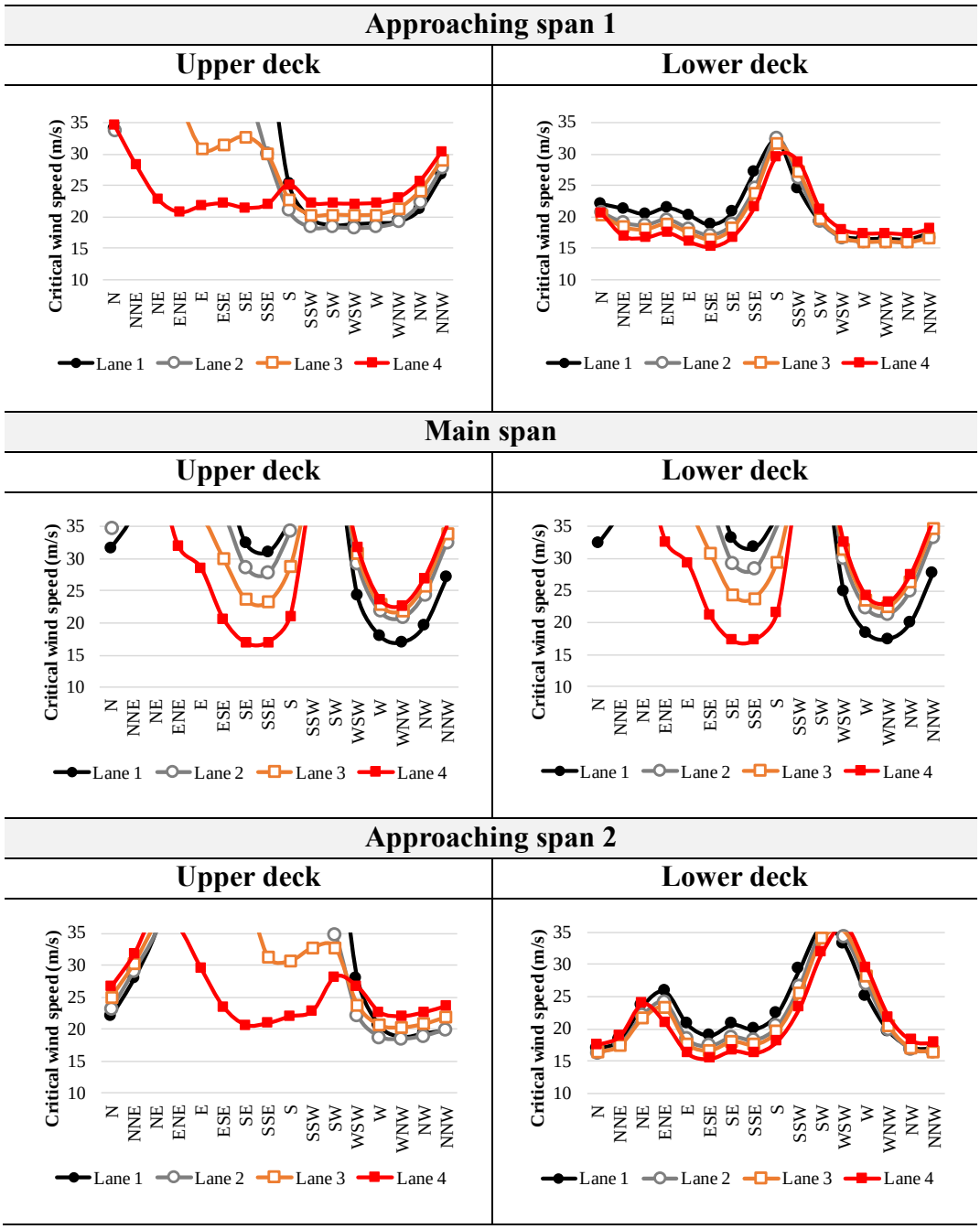

Fig. 4.8. Estimated CWCs of truck on the three road sections

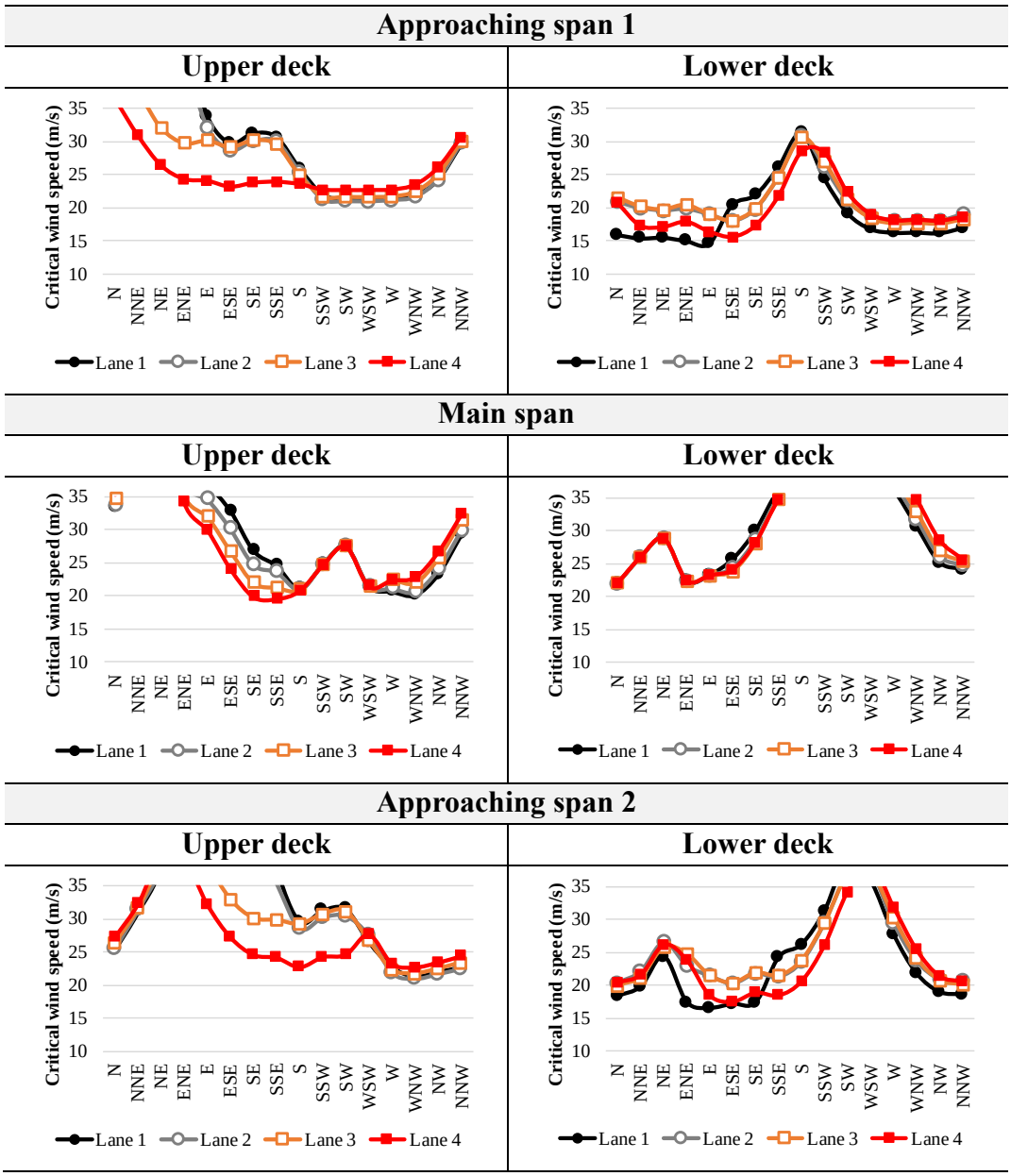

Fig. 4.9. Estimated CWCs of tractor-trailer on the three road sections

Table 4.6. Selected road section and traffic lane for each case

	Sedan	**Truck**	**Tractor-trailer**
Upper deck	Main span (Lane 3, 31 m/s)	Main span (Lane 4, 17 m/s)	Main span (Lane 4, 20 m/s)
Lower deck	Approaching span1 (Lane 3, 24 m/s)	Approaching span1 (Lane 4, 15 m/s)	Approaching span1 (Lane1, 16 m/s)

Step 2. Estimation of CWCs of selected traffic lanes according to road conditions and vehicle speeds

As a next step, CWCs were re-estimated using CarSim and TruckSim for the selected traffic lanes which are shown in Table 4.6. CWCs were estimated for three different road condition, dry, wet, and snowy road, and for two vehicle speeds 80 km/h and 40 km/h. All estimated CWCs of each vehicle are demonstrated in Fig. 4.10, Fig. 4.11 and Fig. 4.12. Interestingly, the shape and the level of CWCs are very similar with that of the quasi-static approach which shows the feasibility of the quasi-static approach for CWC estimation.

According to the three figures, both two parameters, vehicle speed and road condition, had obvious influence on the level of critical wind speed. In the most cases, critical wind speed decreased when vehicle speed increased. This is quite obvious results since wind load generally increases as vehicle speed increases especially when wind incident angle is smaller than 90°. When wind direction and vehicle speed was almost parallel, increment of vehicle speed rather caused increment of critical wind speed by balancing each other. This phenomenon was observed at north-east direction on upper deck which make almost 180° incident angle with driving direction.

The large variations of CWC were also observed according to the road condition. The critical wind speed reduced remarkably as road friction coefficient decreased due to the increment of the probability of side-slip and rotation accidents. In the case of truck and tractor-trailer, the difference between dry and wet road condition was not significant since overturning

accident is the major accident type due to the large capability of tires for the lateral resistance. However, the capability of tires became not enough to hold the vehicle body laterally when road friction coefficient further decreased to 0.2 (snowy road condition) which resulted in large decrement of CWCs. Most of vehicle accident type on snowy road were side-slip and rotation even in the cases of truck and tractor-trailer. Since the gap between the wet and snowy road condition is too large, special care is required in winter so that snow or ice does not accumulate on the traffic lanes.

Step 3. Determination of wind speed for traffic control

Before suggesting traffic control guideline, the minimum critical wind speeds were extracted from each CWC. All extracted critical wind speed values were rounded off to the nearest integer. Table 4.7, Table 4.8, and Table 4.9 shows the results of the extraction. According to the tables, truck and tractor-trailer had similar level of minimum critical wind speed in most cases whereas sedan had much higher critical wind speed especially for dry and wet road. Therefore, traffic control guideline was proposed for two vehicle types, sedan and high-sided vehicle. Also, since there was large difference in critical wind speed between upper and lower decks, different wind speed for traffic control was applied for each deck. In the case of sedan, traffic restriction was applied simultaneously for the simplicity of the guideline. Consequently, below four levels were adopted in order to develop traffic control guideline.

- Level 1: Limit the speed of all vehicles by 40 km/h
- Level 2: Close lower deck to high-sided vehicles
- Level 3: Close all lanes to high-sided vehicles
- Level 4: Close all lanes

Because critical wind speed is too low in the case of snowy road when vehicle speed is 80 km/h, traffic control Level 1 was applied since 0 m/s wind speed. The final traffic guideline for each road condition was demonstrated in Table 4.10. Since the wind speeds for traffic control provided by the guideline were determined conservatively, high safety is expected if it is able to control the traffic on the bridge at the right moment. The values in the guideline can be modified according to desirable target safety level by changing target α% or accident criteria during estimation of CWC.

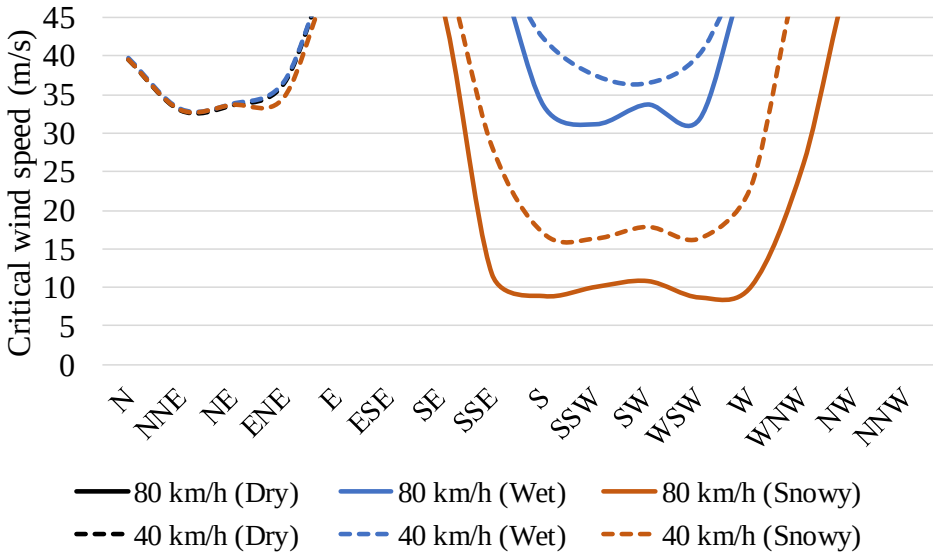

(a)

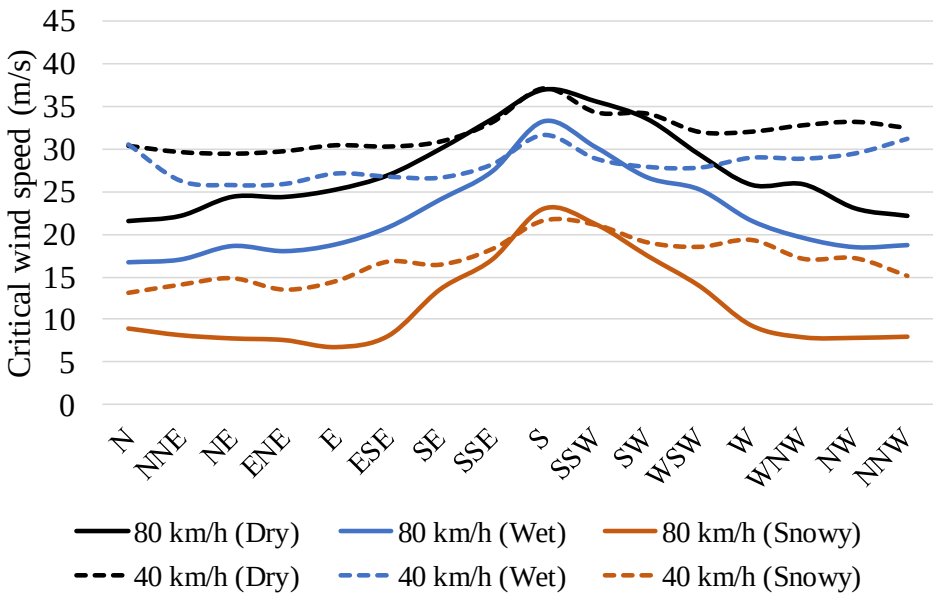

(b)

Fig. 4.10. CWCs of sedan for three road conditions and two vehicle speeds on (a) upper deck (Lane 3) and (b) lower deck (Lane 3)

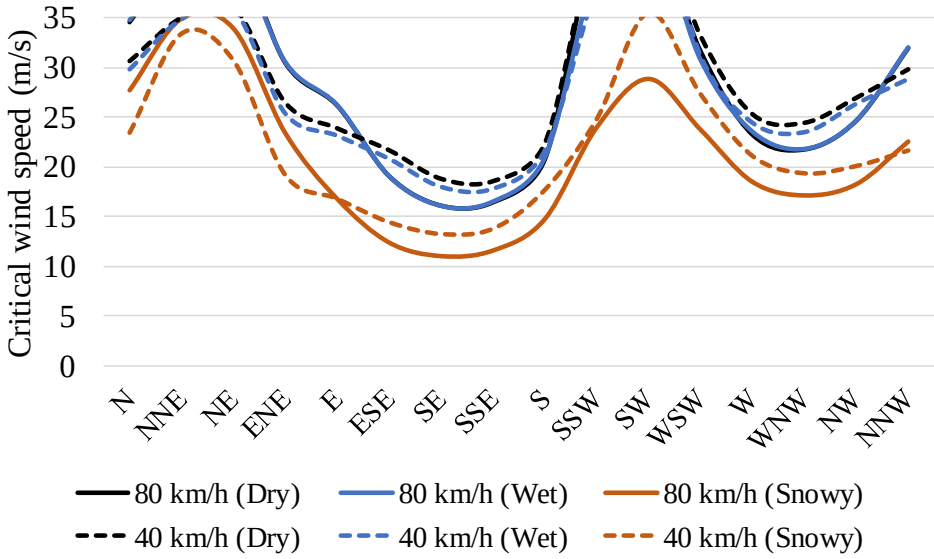

(a)

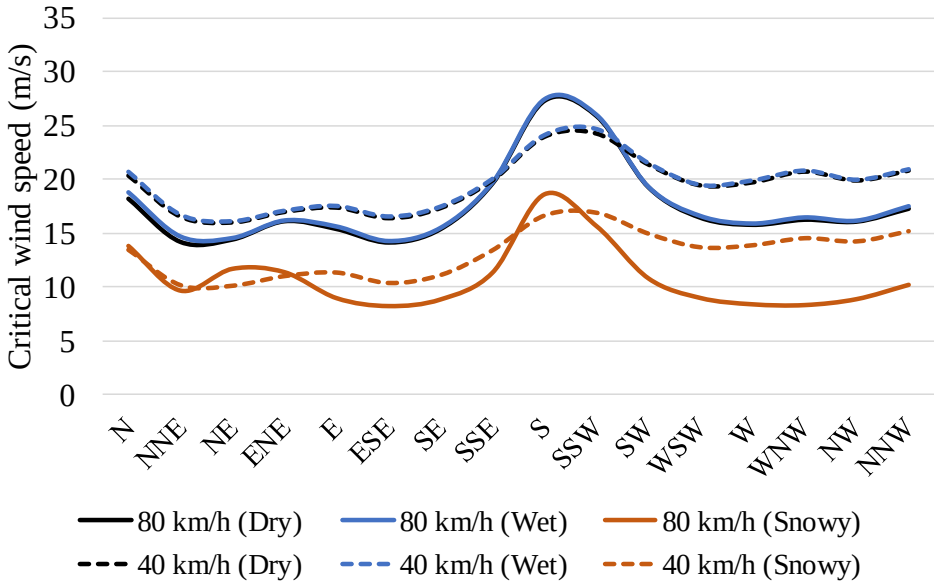

(b)

Fig. 4.11. CWCs of truck for three road conditions and two vehicle speeds on (a) upper deck (Lane 4) and (b) lower deck (Lane 4)

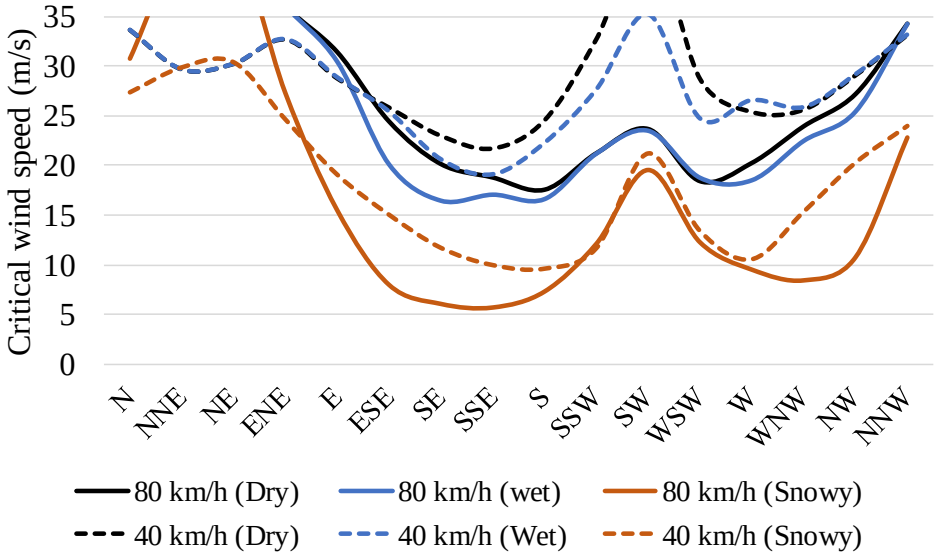

(a)

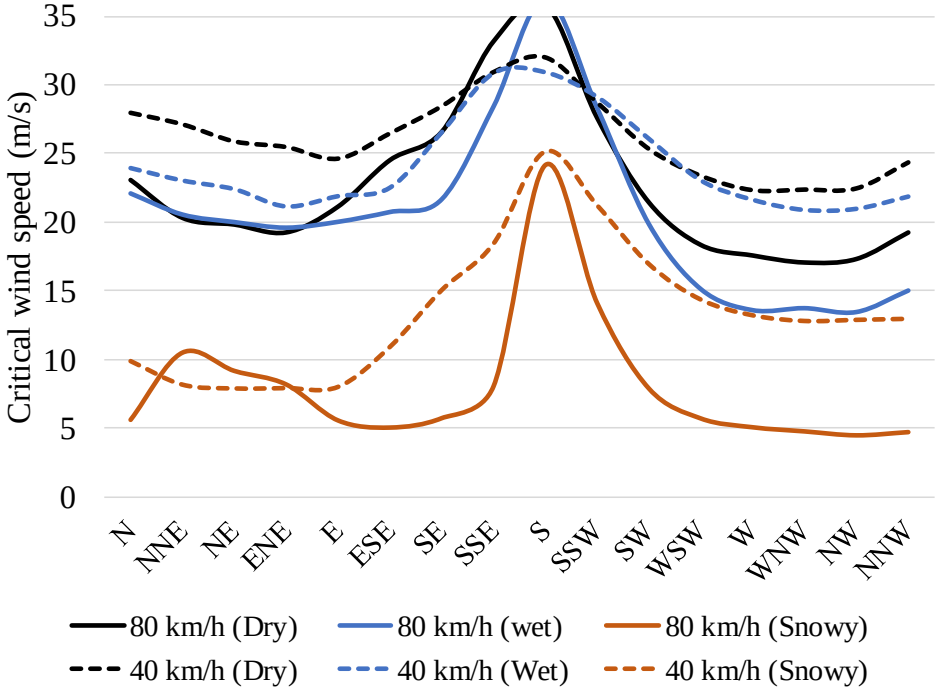

(b)

Fig. 4.12. CWCs of tractor-trailer for three road conditions and two vehicle speeds on (a) upper deck (Lane 4) and (b) lower deck (Lane 1)

Table 4.7. Minimum critical wind speeds for dry road condition

Dry road (μ= 0.85)	80 km/h			40 km/h		
	Sedan	Truck	Tractor-trailer	Sedan	Truck	Tractor-trailer
Upper deck	33 m/s	16 m/s	19 m/s	33 m/s	19 m/s	24 m/s
Lower deck	22 m/s	14 m/s	17 m/s	29 m/s	16 m/s	22 m/s

Table 4.8. Minimum critical wind speeds for wet road condition

Wet road (μ= 0.5)	80 km/h			40 km/h		
	Sedan	Truck	Tractor-trailer	Sedan	Truck	Tractor-trailer
Upper deck	31 m/s	16 m/s	18 m/s	33 m/s	18 m/s	21 m/s
Lower deck	17 m/s	14 m/s	13 m/s	26 m/s	16 m/s	21 m/s

Table 4.9. Minimum critical wind speeds for snowy road condition

Snowy road (μ= 0.2)	80 km/h			40 km/h		
	Sedan	Truck	Tractor-trailer	Sedan	Truck	Tractor-trailer
Upper deck	9 m/s	10 m/s	6 m/s	16 m/s	13 m/s	11 m/s
Lower deck	7 m/s	8 m/s	5 m/s	13 m/s	10 m/s	8 m/s

Table 4.10. Suggested traffic control guideline according to road condition

Road condition	**Level 1**	**Level 2**	**Level 3**	**Level 4**
	Speed limit of 40 km/h	**Close lower deck to high-sided vehicle**	**Close all lanes to high-sided vehicle**	**Close all lanes**
Dry	14 ~ 16 m/s	16 ~ 19 m/s	19 ~ 29 m/s	Over 29 m/s
Wet	13 ~ 16 m/s	16 ~ 18 m/s	18 ~ 26 m/s	Over 26 m/s
Snowy	0 ~ 8 m/s	8 ~ 11 m/s	11 ~ 13 m/s	Over 13 m/s

CHAPTER 5

VULNERABILITY EVALUATION USING LONG-TERM MEASURED WIND DATA

Since it is not easy to restrict traffic on a bridge at the perfect timing due to the various factors such as human or mechanical errors, possibility of wind-induced accident always exists even though traffic control guideline is applied. Therefore, it is necessary to evaluate the exposure frequency of dangerous situation during normal operational state and to decide whether another additional countermeasure like construction of wind barrier is required or not.

Therefore, in this chapter, a probabilistic method for evaluation of vulnerability level for crosswind is proposed. The final output obtained from this method is expected number exceeding critical level per year N_E. In order to estimate this index, the fragility curves of vehicles obtained through the vehicle simulation and long-term wind data are utilized. Based on the estimated N_E as the target index, the vulnerability level of a bridge for vehicle safety can be evaluated with consideration of wind environment at the bridge site. This index provides intuitive information on the degree of vehicle safety.

In section 5.1, the methodology to estimate the vulnerability index using long-term measured wind data was introduced. In section 5.2, the proposed procedure was applied to Gwangan bridge and parameter studies were conducted to estimate the effect of several factors on the vulnerability level. In section 5.3, the effectiveness of wind barrier for reducing vulnerability

level of the bridge was examined through the additional wind tunnel test and vehicle simulation.

5.1 Vulnerability evaluation method

The proposed vulnerability assessment method consists of two steps: 1) estimation of probability density functions of wind speed, and, 2) estimation of the vulnerability index N_E using the fragility curves which can be obtained by Equation (4.6)

5.1.1 Estimation of probability density functions of wind speed

First, probability density functions are obtained using long-term wind speed data collected from the bridge site or nearby weather station. Because wind speed at the position of anemometer and each traffic lane is normally different, it is necessary to modify the measured wind data by applying correction factors which is to convert wind data from measurement location to the target area. The correction factor is the ratio between wind speeds at the measurement point and at the target traffic lane which considers the differences of terrain roughness and elevation. KSCE (2006) proposes an equation for estimating correction factor as follow:

$$C = (\frac{z_{G1}}{z_1})^{\alpha 1} \times (\frac{z_2}{z_{G2}})^{\alpha 2}, \quad z_2 \geq z_b$$
$$= (\frac{z_{G1}}{z_1})^{\alpha 1} \times (\frac{z_b}{z_{G2}})^{\alpha 2}, \quad z_2 < z_b \tag{5.1}$$

where subscript 1 refers to the weather station and subscript 2 refers to the bridge site or interested traffic lane; α is the exponent that governs the shape of the wind profile; z is the height of the measurement point; z_G is the gradient height of the wind profile, and z_b is the minimum height. By multiplying this correction factor, wind data can be transferred from measurement location to the interested location.

If wind data obtained at bridge site is too short, Measure-Correlate-Predict (MCP) method is the useful method which converts the long-term wind data of weather station to the bridge site with consideration of properties of wind distribution at the bridge site. Linear regression equation is derived from long term wind data of weather station and short field-monitored data as shown in Equation (5.2)

$$U_T = \frac{\sigma_T}{\sigma_W} U_W + m_T - \frac{\sigma_T}{\sigma_W} U_W \tag{5.2}$$

where *U, σ, and m* are wind speed, standard deviation and average of wind data, and subscript *T* and *W* mean target area and weather station. According to the equation, long-term wind data obtained from weather station can be transferred to the bridge site based on the relation between wind properties of two areas.

Next, probability density functions of wind speed are obtained for various wind directions. Because critical wind speed is highly dependent on the wind direction, the probability function of wind speed is also obtained for 16 wind directions. As mentioned in Chapter 4, the most vulnerable wind direction is not generally 90° due to the vehicle own speed, so consideration of the effect of wind direction is desirable during risk assessment.

In general, Weibull or GEV functions are utilized in order to estimate probability density function of wind speed, (Kim et al., 2011; Baker, 2015; Kim et al., 2016). These functions have quite high goodness of fit for overall wind distribution, but accuracy for high wind speed is not enough due to the lack of information compared to low wind speed. Unfortunately, critical wind speeds of vehicles are generally high, so accurate evaluation of vulnerability index is difficult using these distribution function. Therefore, in this study, histogram was adopted to obtain probability density function as shown in Fig. 5.1. Since histogram can show probability distribution based on the frequency of each class of wind speed, there is no loss of information of high wind speed. Therefore, total 16 histograms were obtained from each wind direction.

In the case of Korea, the form of the long-term measured wind data is generally statistical value which is obtained by averaging raw data for 10 minutes. Since the critical wind speed obtained during vehicle simulation is T-sec. averaged value, so it is required to convert the type of the long-term wind data to T-sec. averaged value in order to estimate vulnerability index and it is performed by multiplying the ratio estimated by Equation (4.8). As a

results, maximum *T*-sec. averaged wind data which corresponds to original long-term 10-min averaged data is obtained. Since all the converted wind speed is larger than the original data, probability density function is also changed as shown in Fig. 5.1 of which higher probability is observed at high wind speed.

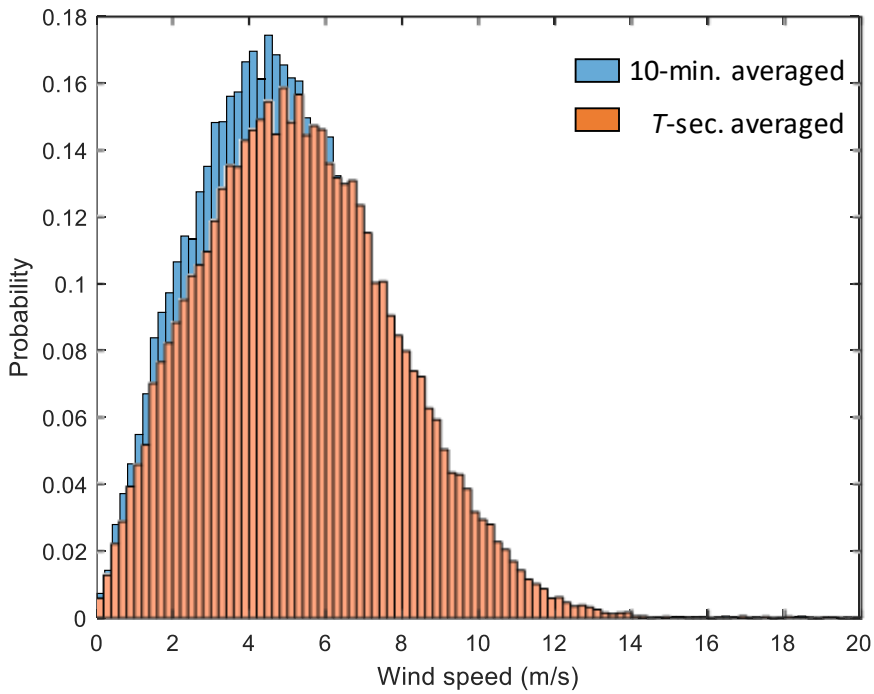

Fig. 5.1. An example of probability density function of wind speed

5.1.2 Estimation of vulnerability index

The vulnerability index N_E is estimated through probability assessment using the fragility curves and the probability density functions of wind speed. First, the probability of exceeding critical level for i^{th} wind direction according to Equation (5.3).

$$P_{E|dir=i} = \sum_{j=1}^{N} P(\overline{U}_{cri,i} \leq \overline{U}_{j,i}) \cdot f(\overline{U}_i = \overline{U}_{j,i}) \Delta \overline{U} \tag{5.3}$$

where subscript i means i^{th} direction among 16 wind directions, and $\overline{U}_i$ is the maximum T-sec. averaged wind speed during 10 minutes, and $\overline{U}_{j,i}$ is the representative wind speed of jth class of the histogram of ith wind direction. Therefore, $f(\overline{U}_i = \overline{U}_{j,i})$ means the probability that a maximum T-sec. averaged wind speed during 10 minutes is classified in j^{th} class which can be obtained from the corresponding histogram. $P(\overline{U}_{cri,i} \leq \overline{U}_{j,i})$ is the probability that $\overline{U}_{j,i}$ exceeds critical wind speed $\overline{U}_{cri,i}$, and this probability is estimated based on the fragility curves obtained from vehicle simulation. $P_{E|dir=i}$ is the probability that a maximum T-sec. averaged wind speed during 10 minutes exceeds critical level for i^{th} wind direction.

By considering all 16 wind directions, the probability of exceeding critical level during 10 minutes P_E can be estimated as follows:

$$P_E = \sum_{i=1}^{16} P_i \cdot P_{E|dir=i} \tag{5.4}$$

where P_i is the probability that the direction of the wind is i which can be obtained from the frequency analysis of wind data. Based on the assumption that all wind data is independent and has exceedance probability P_E equally, the exceedance event of critical level can be defined as Bernoulli trial process. Therefore, the expected number of exceeding critical level per year N_E can be calculated by multiplying P_E by 365 days, 24 hours, and 6 times as shown

in Equation (5.5). This equation can be modified according to the data form of the obtained long-term wind data. If the data form is 1-min. averaged value, 60 should be utilized rather than 6. In this study, 10-min. averaged wind data was utilized, so vulnerability index N_E also means expected number of 10-min. wind data which exceeds critical level per year.

$$N_E = P_E \cdot 365 \cdot 24 \cdot 6 \tag{5.5}$$

5.2 Application to Gwangan Bridge

The proposed method was applied to the example bridge, Gwangan Bridge. Wind environment analysis was performed using the long-term wind data, and the vulnerability index N_E was calculated for the three road sections and three vehicle type. Quasi-static approach was adopted to estimate CWCs of all the investigated traffic lanes to reduce whole simulation time. In order to consider normal operational state, 80 km/h vehicle speed was selected without any traffic restriction, and dry road condition(μ=0.85) was simulated. Other road conditions were not considered in this application case because it was difficult to consider the correlation between wind speed and precipitation precisely. However, this factor should be considered in the futher study since several natural events such as typhoon bring strong wind and heavy rainfall simultaneously which can be a critical factor for the evaluation of vulnerability level.

5.2.1 Wind data and wind characteristics of the bridge site

The long-term wind data were obtained from a nearby weather station. The type of the wind data is 10 min. averaged wind speeds and measurement period is about 20 years from 2000 to 2018. The total number of wind data measurement used for the estimation was 1004,835, and all data were classified into 16 wind directions. The anemometer at the weather station was located 10 m above the ground.

Since only one-year field-monitored wind data was available which was measured at the top of the tower of Gwangan Bridge, MCP method was applied in order to reflect the properties of wind environment at the bridge site. Measurement period was from 2012.01.01 to 2012.12.31, and wind data was collected in the form of 10 min. averaged value.

The maximum daily 10 min. averaged wind speed was extracted from long-term wind data set and field-monitored data set, and Fig. 5.2 shows the one-year daily maximum wind data obtained from the weather station and the top of the tower. Both of the wind set had almost linear relation as shown in Fig. 5.3 of which the correlation coefficient was estimated as 0.78. The parameters in Equation (5.2) were estimated, and Equation (5.6) shows the derived first-order regression model which was utilized to convert long-term data from the weather station to the top of the tower with consideration of mean and standard deviation of wind speed. The red line in Fig. 5.3 is the estimated regression model.

$$U_T = \frac{\sigma_T}{\sigma_W} U_W + m_T - \frac{\sigma_T}{\sigma_W} U_W \\ = 2.77 U_W - 2.82 \tag{5.6}$$

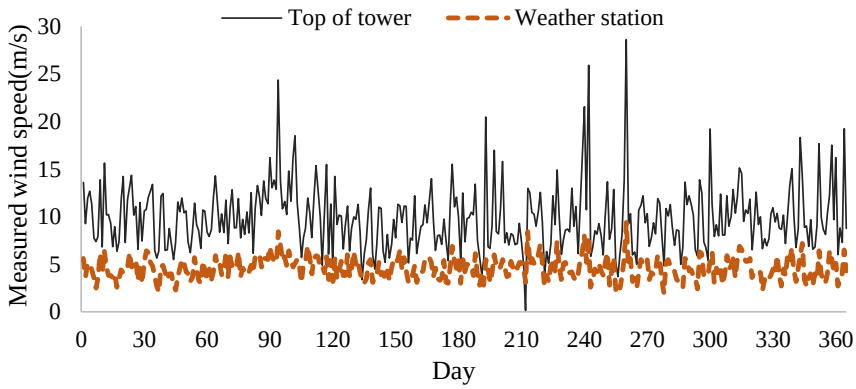

Fig. 5.2. Wind data measured at bridge site and weather station

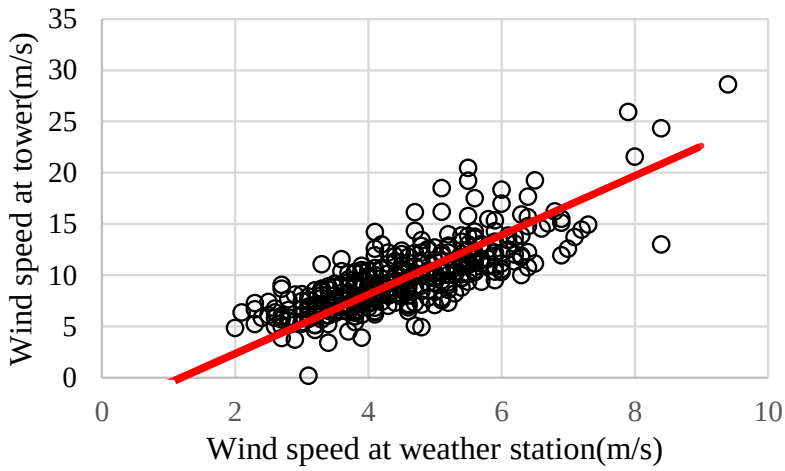

Fig. 5.3. Correlation between two wind data sets (R=0.78)

By applying Equation (5.6), it was able to convert the long-term wind data to the top of the tower, but still one more transfer process was required to obtain the wind data at the level of the road sections. Therefore, in order to transfer the wind speed data at the top of the tower to the level of each road

section, the correction factors were estimated based on Equation (5.1). Assuming the terrain category I, the exponent α and the gradient height z_G were determined as 0.12 and 500 m, respectively, according to KSCE (2006). Using the height of the each section mentioned in Table 4.3, the correction factors were estimated. Table 5.1 demonstrates the estimated factors corresponding to each deck level. According to the table, wind speed decrease to the level of 80 to 90% of the wind speed at the top of the tower according to the height of the deck section.

Table 5.1. Wind speed correction factors at each road section

	Approaching span 1	**Main span**	**Approaching span 2**
Upper deck	0.85	0.90	0.86
Lower deck	0.81	0.88	0.82

Fig. 5.4 shows a wind rose diagram for the 10 min. averaged wind data transferred from weather station to the top of the tower, and the percentage of frequencies for each direction are shown in Table 5.2. According to Fig. 5.4 and Table 5.2, west-south-west is the dominant wind directions which is nearly parallel to the longitudinal direction of the main span. These frequencies correspond to P_i in Equation (5.4).

The occurrence rate of high wind speed is also important factor during the assessment. Fig. 5.5 shows the distribution of occurrence rate of the wind speed higher than 15 m/s for 16 wind directions. According to the figure, more

than 40% of strong wind speed data were measured from north-east direction whereas only 9% of data were obtained from west-south-west direction. By comparing the contribution of each wind direction on the vulnerability indexes, the effect of the wind distribution will be discussed in the following section.

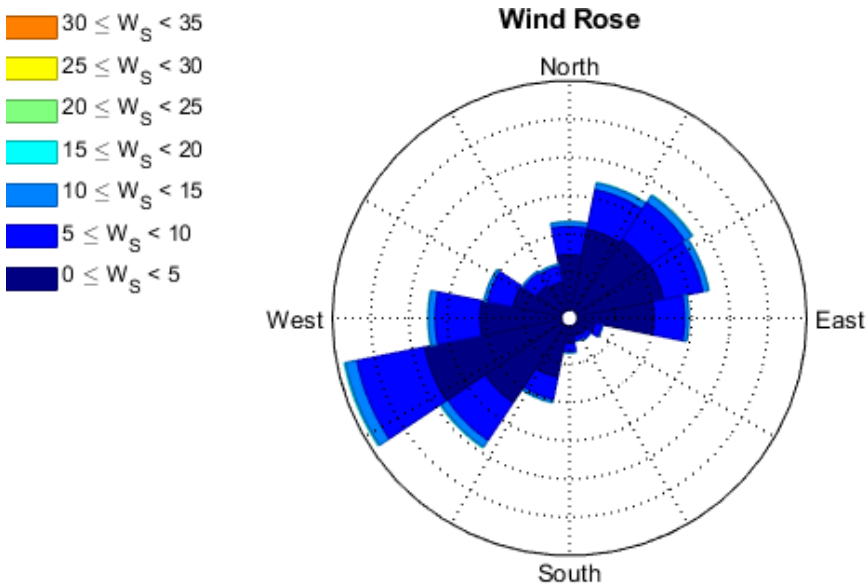

Fig. 5.4. Wind rose at the bridge site

Table 5.2. Frequencies for each direction

Direction	Frequency (%)	Direction	Frequency (%)
N	5.8	S	1.8
NNE	8.8	SSW	5.5
NE	9.1	SW	9.8
ENE	9.6	**WSW**	**14.7**
E	8.8	W	9.6
ESE	2.0	WNW	5.6

SE	1.3	NW	3.4
SSE	1.1	NNW	3.1

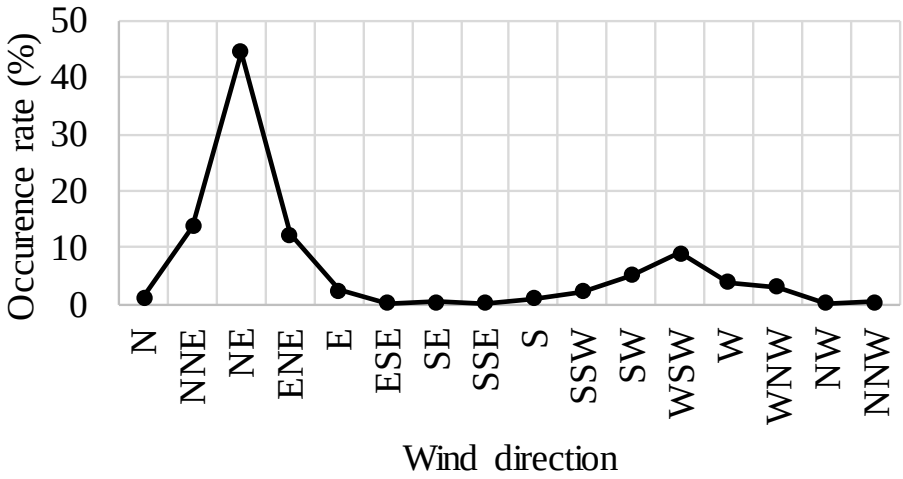

Fig. 5.5. Occurrence rate of strong wind speed over 15 m/s according to wind direction

5.2.2 Assessment results

The expected number of exceeding critical level N_E was estimated for each vehicle type and traffic lane using the fragility curves and the probability density functions of wind speed. Fig. 5.6 shows the estimated N_E for each case when a vehicle is running at 80 km/h.

According the figure, there were very distinct differences between the simulation cases. First, the vulnerability level of sedan was negligible compared to other vehicle types. This was expectable according the CWCs of the sedan that its critical wind speed was generally much higher than that of the high-sided vehicles.

The index was also highly dependent on the vehicle location. In the case of approaching spans, lower deck was much vulnerable than upper deck due to the wind tunneling effect while the index on lower deck of main span was small due to the mitigation effect of truss member.

The most conspicuous point in the figures is that the index on lower deck of approaching span 1 was much higher than those of other road sections. This was unexpected result because the minimum critical wind speed of upper deck of main span and lower deck of approaching span 2 were also very small with that of lower deck of approaching span 1. The reason of this large difference could be found by considering the wind environment at bridge site and the variation of critical wind speed for 16 wind directions.

Fig. 5.7 and Fig. 5.8 shows the distribution of estimated N_E of truck and tractor-trailer on lower deck of approaching span 1 according to wind direction. According to these figures, north-east was the most vulnerable wind direction of which the occurrence rate of strong wind speed was extremely high compared to other directions as shown in Fig. 5.5. Also, according to Fig. 4.8 and Fig. 4.9, north-east was the most vulnerable wind direction for truck and tractor-trailer on lower deck of approaching span 1. This agreement was the reason that caused the large vulnerability level on truck and tractor-trailer at this road section. On the other hands, in the case of other five road sections, the critical wind speed of the three vehicles at north-east direction was not low enough to induce high vulnerability. These results draw very important conclusion that vulnerability for strong wind is not the only matter of vehicle

dynamics but also wind environment surround the bridge site. Especially, occurrence rate of high wind speed is the important factor and the frequency of low wind speed has almost no influence on the result. Therefore, not only wind speed but also direction is very influential information during the evaluation procedure.

Road geometry was another very important factor because the variation of critical wind speed is normally determined by driving direction. As mentioned in section 4.3, it is hazardless when wind blows along the road because relative wind direction to vehicle is almost zero which produces very low side force, rolling and yawing moment. Large incident wind angle over 90° is also not so dangerous when considering summation of vehicle speed and wind speed vectors. This was the reason of the small vulnerability index on the upper deck of main span that the angle between driving direction and north-east direction was too large to induce large wind loads on running vehicle. In the case of lower deck of approaching span 1, the driving direction was almost parallel with north-east wind at the beginning of the road section. However, the driving direction changed at every single moment on the road due to the curvature, so the possibility of forming the vulnerable angle between vehicle and north-east direction remarkably increased. This phenomenon also could be observed on the lower deck of approaching span 2, but the angle between north-east wind and driving direction was still too small to induce large vulnerability level. According to the results, it could be concluded that the relative direction between bridges or roads and the most vulnerable wind

direction should be considered during vulnerability evaluation with consideration of road geometries, such as curvature.

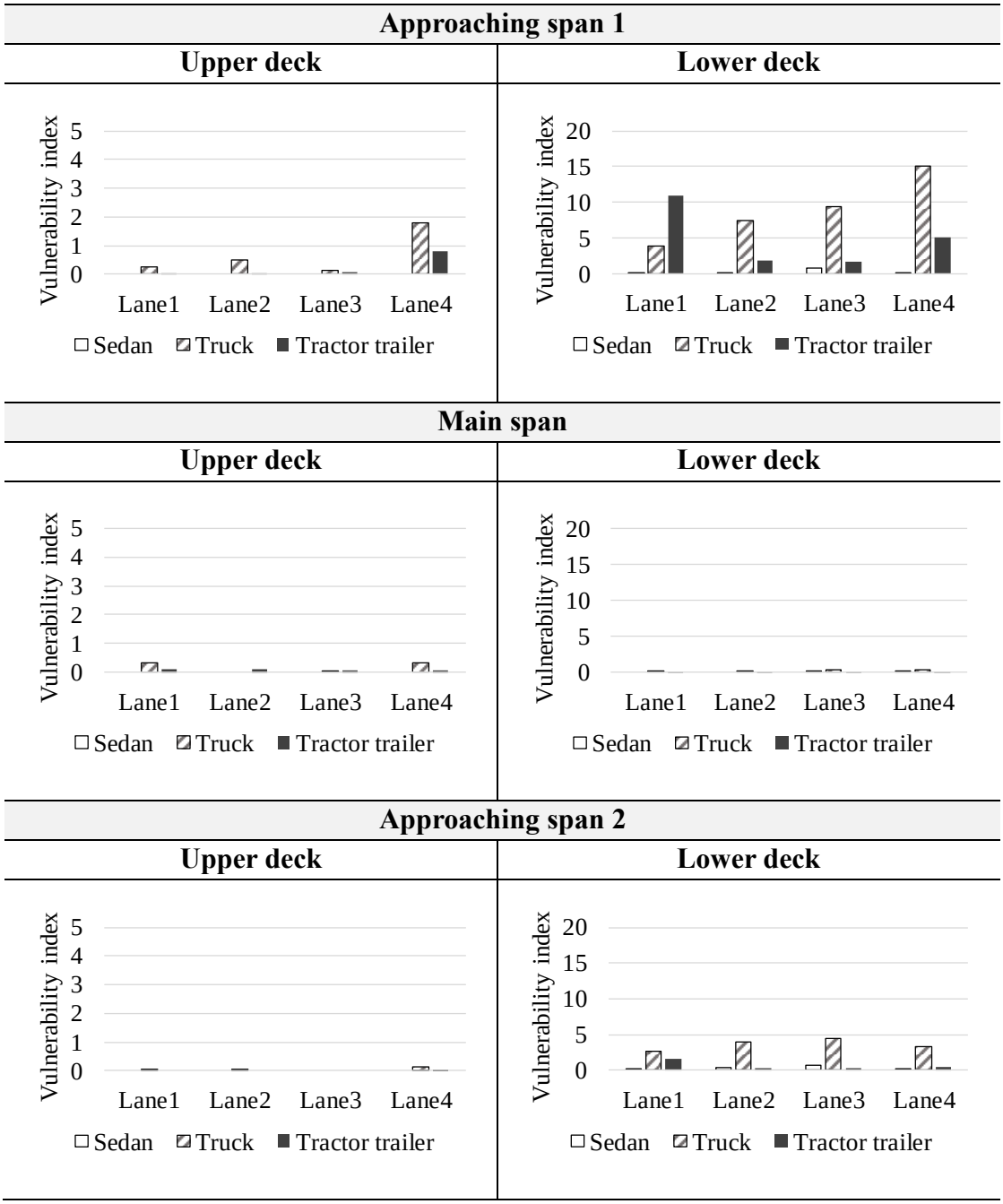

Fig. 5.6. Distribution of vulnerability index N_E according to vehicle type and traffic lane (vehicle speed= 80 km/h)

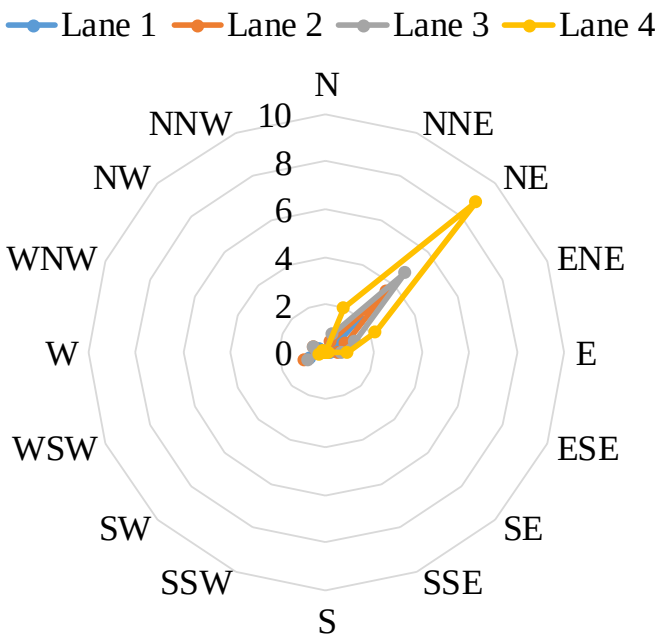

Fig. 5.7. Distribution of vulnerability index N_E of the truck for 16 directions on lower deck of approaching span 1

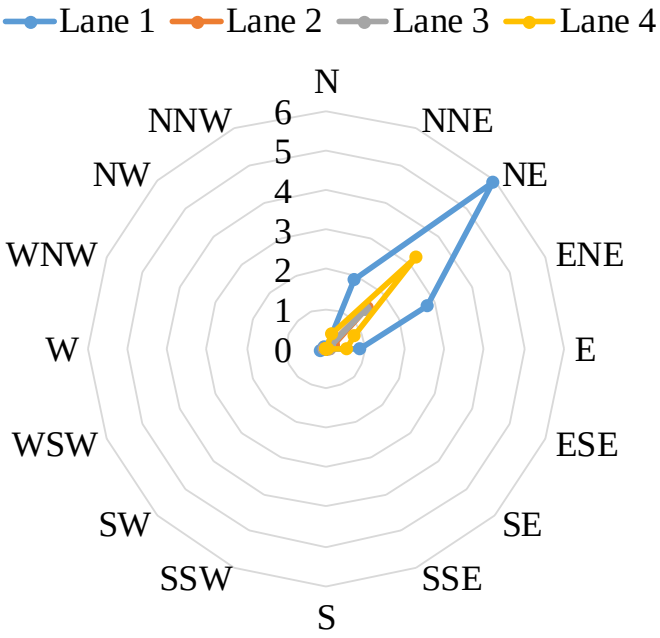

Fig. 5.8. Distribution of vulnerability index N_E of the tractor-trailer for 16 directions on lower deck of approaching span 1

5.3 Countermeasure: installation of wind barrier

Since vulnerability level of the lower deck of approaching span 1 was much higher than other road sections, the overall vulnerability level of Gwangan Bridge can be efficiently reduced by applying a countermeasure only for this section.

Construction of wind barrier was considered as a countermeasure to reduce vulnerability of lower deck of approaching span 1, and the truck was chosen for the parameter study. The effect of the wind barrier was evaluated through wind tunnel test and vulnerability assessment.

5.3.1 Effect of wind barrier on aerodynamic coefficients

Configuration of the test wind barrier is shown in Fig. 5.9. The height of the barrier is about 4 m in real scale which covers the height of the truck. The ventilation ratio of this model is 47.3 %.

The wind barrier model was attached on the both sides of the lower deck of approaching span model during wind tunnel test as shown in Fig. 5.10. The upcoming wind speed was 10 m/s, and the same measurement system mentioned in section 2.1 was utilized. Six aerodynamic coefficients of truck model were estimated on the upper and lower deck.

The two coefficients, side force and rolling moment coefficients, measured on upper and lower deck are demonstrated in Fig. 5.11. In the case of upper

deck, small decrements were observed on leeward lanes even though wind barrier was installed only on the lower deck. However, the coefficients on windward lane is almost same, so overall vulnerability of upper deck does not seem to be changed by the installation of wind barrier. On the other hand, more than 30 % of decrements in aerodynamic coefficients were observed on all traffic lanes of lower deck. All aerodynamic coefficients reduced to similar level which means that there was large decrement especially on the windward lane due to the disturbance effect by wind barrier. According to the test results, large decrement in wind load acting on the vehicle body is expected which can cause reduction of the vulnerability level.

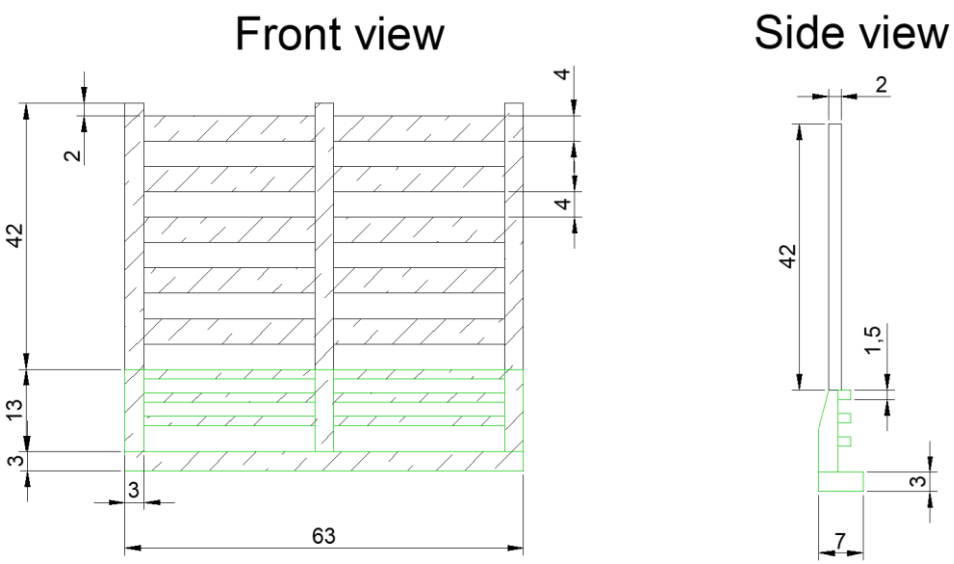

Fig. 5.9. Configuration and dimension of the wind barrier model (unit: mm)

Fig. 5.10. Wind barrier model on the lower deck of approaching span

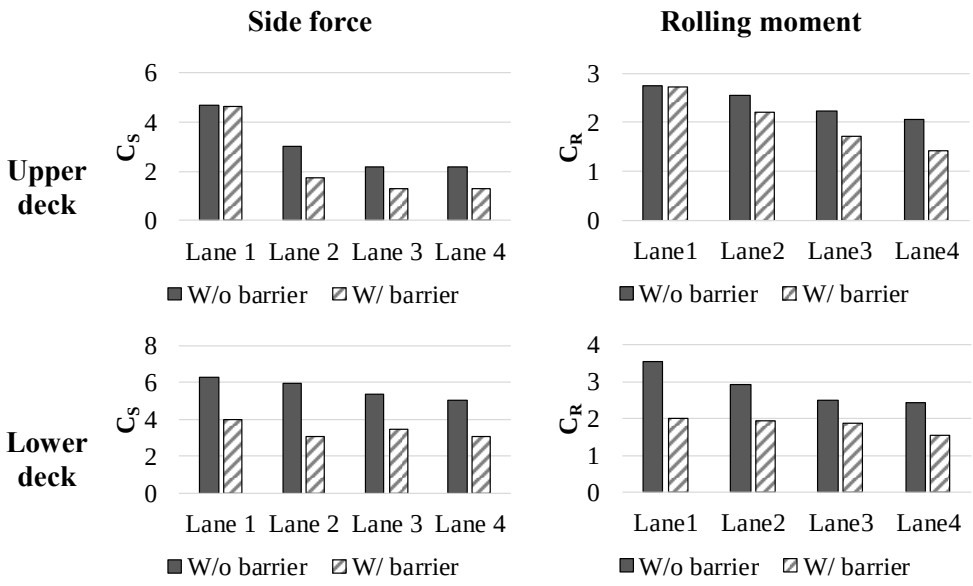

Fig. 5.11. Side force and rolling moment coefficients of the truck for the cases without and with the wind barrier

5.3.2 Effect of wind barrier on vulnerability index

The vulnerability index N_E was estimated for the case that wind barrier is installed on the both side of lower deck of approaching span 1. Because the straight section of approaching span 1 which is located in the inside of the bridge makes almost parallel angle with north-east direction, very low contribution on the vulnerability level was expected. Accordingly, installation of wind barrier was only considered for other area as shown in Fig. 5.12, and the estimation results are shown in Fig. 5.13. According to the figure, the large decrements about 77%, 76%, 73%, and 85 % were observed on Lane 1, 2, 3 and 4, respectively, due to the installation of the wind barrier. The decrement was largest on the outside traffic lane, and all the vulnerability index of the four lanes became the similar level.

As a result, overall vulnerability of Gwangan Bridge became much lower than before that the largest expected number of exceeding critical level reduced from 15 to 4 which is the vulnerability index obtained from approaching span 2. This results shows that installation of wind barrier at specific area can efficiently reduce the overall threat from the strong wind.

However, installation of wind barrier is also matter of economic issue. Also, wind barrier can block the passenger's view toward the sea which is quite an important issue in the case of Gwangan Bridge, so the decision should be made by meditating all these social issue. Nevertheless, the estimated

vulnerability index provides very useful insight in terms of driver's safety which is the most important factor during decision-making process.

Fig. 5.12. Construction area of wind barrier

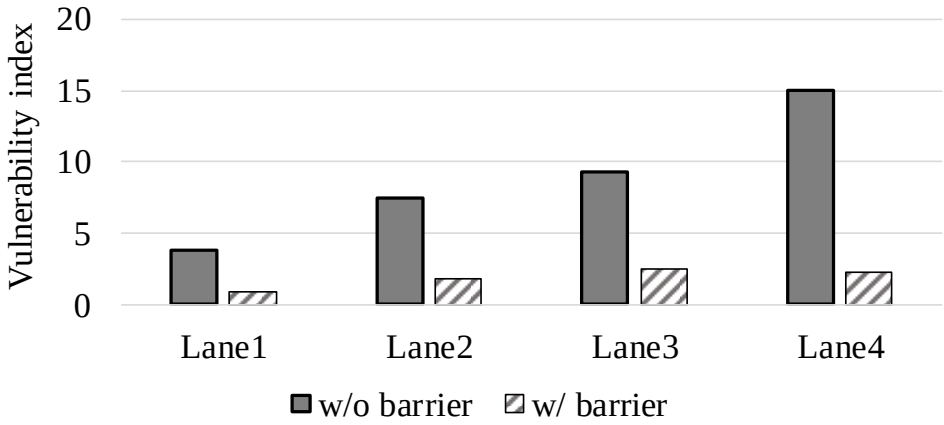

Fig. 5.13. Vulnerability index N_E of the truck on the lower deck of approaching span 1 for the cases without and with the barrier

CHAPTER 6

CONCLUSIONS AND RECOMMENDATIONS FOR FURTHER STUDY

This study aimed to propose a probabilistic methodology for evaluating vehicle stability on a bridge for strong wind which can provide valuable information for decision-making related to traffic restriction. Two main indices, critical wind speed and exceedance frequency of critical level were considered for quantification of vehicle stability. The developed method especially focuses on the stability of vehicles running on bridges by considering the effect of girder shape on the aerodynamic coefficients of vehicles. Another various important factors are also considered such as road geometry, wind turbulence effects, and wind environment. The developed method contains three main items: 1) estimation of aerodynamic coefficients of vehicles on a bridge girder through wind tunnel test, 2) estimation of critical wind speed of vehicles through vehicle simulations, and 3) vulnerability evaluation using long-term wind data. As an application, the developed evaluation method was applied to Gwangan Bridge which is a double-deck truss type suspension bridge.

A measurement system and method were introduced which is to estimate six aerodynamic coefficients of vehicles. The adequacy of the developed system was examined by comparing the coefficients measured under uniform wind conditions with the results of literatures. Comparison results showed

that the developed measurement system provided reliable coefficients although there was certain level of differences from the literatures due to the details of test set-up and Reynolds effects. Utilizing the developed measurement system, the aerodynamic coefficients of three vehicle models, a sedan, a truck and a tractor-trailer were successfully measured for various wind incident angles on the upper and lower decks of the main and approaching sections of Gwangan Bridge. In the case of approaching span, wind increment phenomenon was observed on the lower deck due to the limited flow area between the two decks. Due to this effect, the side force and rolling moment coefficients became larger than those of the uniform wind case. In contrast, a decrement in side force and rolling moment coefficients were observed on the lower deck of the main span due to the wind disturbance by the truss members. This result indicates that wind loads acting on a vehicle body can be largely effected by the shape of the girder. Parameterization of aerodynamic coefficients was performed using two sinusoidal functions for the simulation of turbulent wind loads during vehicle simulations. Since the coefficients of vehicle on the decks were obtained for limited range of wind angle, an extrapolation method was proposed which utilizes the variation of coefficients obtained under uniform wind condition. The curve-fitting results generally showed good fitting performance with the experiment results.

Two vehicle simulation methods were introduced: dynamic and quasi-static approaches. The well-known commercial software CarSim and TruckSim were adopted for the dynamic approach which can simulate realistic vehicle

system. On the other hand, a quasi-static approach was developed by the author for two vehicle types: a vehicle with two axles, and a tractor-trailer with three axles. The feasibility of using these two quasi-static models was examined by comparing the simulation results of the quasi-static approach with that of dynamic approach. According to the comparison result, the feasibility of the quasi-static approach for estimation of tire reactions was successfully demonstrated under both uniform and turbulent wind conditions.

A new methodology to estimate critical wind speed and determine wind speed for traffic control was proposed. Critical wind speed was estimated by a probabilistic approach using one-hundred generated time histories of turbulent in order to consider the uncertainty of turbulence. Applying this method, it was able to obtain critical wind speed curve (CWC) which corresponds to specific fragility level. In order to determine wind speed for traffic control, a procedure which uses both quasi-static and dynamic approaches was introduced. The CWCs of all traffic lanes were estimated using quasi-static approach, and the most dangerous traffic lane could be identified. Then, applying dynamic approach, CWCs of the selected lane were re-estimated according to road conditions and vehicle speeds. Based on the those obtained CWCs, traffic control guideline was established.

According to the application results, the critical wind speed was highly dependent on the wind direction and vehicle location. Critical wind speed was large when wind blew parallel to driving direction whereas it dramatically decreased when wind and driving direction made angle between 40~70°. Also,

the critical wind speed was generally smaller on the windward traffic lane than that on the leeward which is consistent with the results of wind tunnel test. Road geometry was also one of the influential factors which governed the shape of CWC. For example, a wide constant region was observed in the CWCs of approaching spans which could not find in the CWC of the main span. This was due to the characteristic of curved road that driving direction changes on the approaching span at every moment which consequently increases the possibility to encounter dangerous wind incident angle.

Also, the critical wind speed was highly dependent on the vehicle speed and road condition. Critical wind speed had proportional relation with vehicle speed, whereas significant decrements in critical wind speed were observed as the tire-road coefficient decreased from 0.85 (dry road) to 0.2 (snowy road). The difference of critical wind speed between dry and wet road was small whereas large gabs were observed between wet and snowy roads due to the small lateral friction force. Therefore, special attention seems to be necessary especially on a snowy day.

An evaluation method of vulnerability level with consideration of the wind environment at the bridge site was developed. The probability density functions of wind speed were obtained for 16 directions. Then, the frequency of exceeding the critical level per year, which is the vulnerability index, was estimated for each road section by probabilistic assessment combining the probability functions of wind speed with the fragility curves of vehicles. According to the application results, the vulnerability index of the lower deck

of approaching span 1 was estimated as 15 times per year which was much higher than that of other road sections. The distribution of strong wind according to the direction was the main reason for this difference. According to the wind environment analysis, strong wind which exceeds 15 m/s mostly appear at the north-east direction, and this is one of the most dangerous direction for the vehicles running on the lower deck of approaching span 1. This result shows that the vulnerability level depends not only on vehicle dynamics but also on road geometry. Applying the proposed method, it was also able to examine the effect of the construction of wind barrier for reducing vulnerability level. In the case of the Gwangan bridge, 75% reduction of the vulnerability level was observed by installing wind barrier on the lower deck of the approaching span 1.

The proposed methodology provides a powerful tool to evaluate vehicle stability for the strong wind and to establish a traffic control strategy. However, there are several improvement points which can be considered for the further studies. First, the interaction between bridge-vehicle can be included during vehicle simulation because wind-induced bridge vibration also effects on vehicle stability. Bridge aeroelastic analysis program can be utilized to simulate the displacement of wheelsets of vehicles. Second, more uncertain factors can be considered during CWC estimation. In this study, only uncertainty of turbulent wind was considered, but uncertainties of other factors can be additionally included such as tire-road friction, vehicle speed, and even aerodynamic coefficients. As the third point, it is necessary to

examine and re-define accident criteria especially for the overturning accident. In this study and many other literatures, critical wind speed for the overturning accident was determined when one of vertical tire reactions becomes 0. This criteria is appropriate if vehicle weight is similarly distributed on the front and rear axles. In general cases, however, vehicle weight is biased on the one of the axles, so the other axle can lose its contact force of windward tire under quite low wind speed compared to the equally distributed case. This means currently adopted criteria can provide quite conservative result for the overturning accident. Therefore, developing criteria which can reasonably predict wind speed which induces overturning of a vehicle could be one of meaningful research topic for the further study.

REFERENCE

Andersson, E., Häggström, J., Sima, M., & Stichel, S. (2004). Assessment of train-overturning risk due to strong cross-winds. Proceedings of the Institution of Mechanical Engineers, Part F: Journal of Rail and Rapid Transit, 218(3), 213-223.

Baker, C. J. (1986a). A simplified analysis of various types of wind-induced road vehicle accidents. Journal of Wind Engineering and Industrial Aerodynamics, 22(1), 69-85.

Baker, C.J., (1986b), Train aerodynamic forces and moments from moving model experiments. Journal of wind engineering and Industrial Aerodynamics, 31, 67-85

Baker, C. J. (1987). Measures to control vehicle movement at exposed sites during windy periods. Journal of Wind Engineering and Industrial Aerodynamics, 25(2), 151-161.

Baker, C. J. (1991a). Ground vehicles in high cross winds part I: steady aerodynamic forces. Journal of Fluids and Structures, 5(1), 69-90.

Baker, C. J. (1991b). Ground vehicles in high cross winds part II: unsteady aerodynamic forces. Journal of fluids and structures, 5(1), 91-111.

Baker, C. J. (1991c). Ground vehicles in high cross winds part III: The interaction of aerodynamic forces and the vehicle system. Journal of fluids and structures, 5(2), 221-241.

Baker, C. J., & Reynolds, S. (1992). Wind-induced accidents of road vehicles. Accident Analysis & Prevention, 24(6), 559-575.

Baker, C. J., & Humphreys, N. D. (1996). Assessment of the adequacy of various wind tunnel techniques to obtain aerodynamic data for ground vehicles in cross winds. Journal of Wind Engineering and Industrial Aerodynamics, 60, 49-68.

Baker, C. J., Jones, J., Lopez-Calleja, F., & Munday, J. (2004). Measurements of the cross wind forces on trains. Journal of Wind Engineering and Industrial Aerodynamics, 92(7-8), 547-563.

Baker, C. J. (2009). The effect of unsteady crosswind forces on train dynamic behavior. In Proceedings of the Fifth European and African Conference on Wind Engineering, Florence (Vol. 7, pp. 19-23).

Baker, C. J. (2010). The simulation of unsteady aerodynamic cross wind forces on trains. Journal of wind engineering and industrial aerodynamics, 98(2), 88-99.

Baker, C. (2013). A framework for the consideration of the effects of crosswinds on trains. Journal of Wind Engineering and Industrial Aerodynamics, 123, 130-142.

Baker, C. (2015). Risk analysis of pedestrian and vehicle safety in windy environments. Journal of Wind Engineering and Industrial Aerodynamics, 147, 283-290.

Batista, M., & Perkovič, M. (2014). A simple static analysis of moving road vehicle under crosswind. Journal of Wind Engineering and Industrial Aerodynamics, 128, 105-113.

Carrarini, A. (2007). Reliability based analysis of the crosswind stability of railway vehicles. Journal of Wind Engineering and Industrial Aerodynamics, 95(7), 493-509.

Cheli, F., Ripamonti, F., Sabbioni, E., & Tomasini, G, 2011a. Wind tunnel tests on heavy road vehicles: cross wind induced loads –part 1. Journal of Wind Engineering and Industrial Aerodynamics, 99(10), 1000-1010.

Cheli, F., Ripamonti, F., Sabbioni, E., & Tomasini, G. 2011b. Wind tunnel tests on heavy road vehicles: cross wind induced loads—part 2. Journal of Wind Engineering and Industrial Aerodynamics, 99(10), 1011-1024.

Chen, F., & Chen, S. (2013). Probabilistic assessment of vehicle safety under various driving conditions: a reliability approach. Procedia-Social and Behavioral Sciences, 96, 2414-2424.

Chen, N., Li, Y., Wang, B., Su, Y., & Xiang, H. (2015). Effects of wind barrier on the safety of vehicles driven on bridges. Journal of Wind Engineering and Industrial Aerodynamics, 143, 113-127.

Chen, S. R., & Cai, C. S. (2004). Accident assessment of vehicles on long-span bridges in windy environments. Journal of Wind Engineering and Industrial Aerodynamics, 92(12), 991-1024.

Chen, S., & Chen, F. (2009). Simulation-based assessment of vehicle safety behavior under hazardous driving conditions. Journal of transportation engineering, 136(4), 304-315.

Chen, S. R., & Wu, J. (2011). Modeling stochastic live load for long-span bridge based on microscopic traffic flow simulation. Computers & Structures, 89(9-10), 813-824.

Chu, C. R., Chang, C. Y., Huang, C. J., Wu, T. R., Wang, C. Y., & Liu, M. Y. (2013). Windbreak protection for road vehicles against crosswind. Journal of Wind Engineering and Industrial Aerodynamics, 116, 61-69.

Coleman, S. A., & Baker, C. J. (1992). The reduction of accident risk for high sided road vehicles in cross winds. Journal of Wind Engineering and Industrial Aerodynamics, 44(1-3), 2685-2695.

Cooper, R. K. (1984). Atmospheric turbulence with respect to moving ground vehicles. Journal of wind engineering and industrial aerodynamics, 17(2), 215-238.

Diana, G., Burlando, M., Cheli, F., Freda, A., Ratto, C. F., Rocchi, D., & Tomasini, G. (2008). A new methodology to perform the risk analysis of cross wind on high speed lines. In 8th World Congress on Railway Research (WCRR 2008) 1.-12.

Dorigatti, F., Sterling, M., Rocchi, D., Belloli, M., Quinn, A. D., Baker, C. J., & Ozkan, E. (2012). Wind tunnel measurements of crosswind loads on high sided vehicles over long span bridges. Journal of Wind Engineering and Industrial Aerodynamics, 107, 214-224.

Dorigatti, F., Sterling, M., Baker, C. J., & Quinn, A. D. (2015). Crosswind effects on the stability of a model passenger train—A comparison of static and moving experiments. Journal of Wind Engineering and Industrial Aerodynamics, 138, 36-51.

Fujii, T., Maeda, T., Ishida, H., Imai, T., Tanemoto, K., & Suzuki, M. (1999). Wind-induced accidents of train/vehicles and their measures in Japan. Quarterly Report of RTRI, 40(1), 50-55.

Ghandour, R., Victorino, A., Doumiati, M., & Charara, A. (2010). Tire/road friction coefficient estimation applied to road safety. In 18th Mediterranean Conference on Control and Automation, 1485-1490.

Gillespie, T.D. (1992). Fundamentals of Vehicle Dynamics; Society of Automotive Engineers: Warrendale, PA, USA.

Grip, H. F., Imsland, L., Johansen, T. A., Kalkkuhl, J. C., & Suissa, A. (2009). Vehicle sideslip estimation. IEEE control systems magazine, 29(5), 36-52.

Gustafsson, F. (1997). Slip-based tire-road friction estimation. Automatica, 33(6), 1087-1099.

Han, Y., Cai, C. S., Zhang, J., Chen, S., & He, X. (2014). Effects of aerodynamic parameters on the dynamic responses of road vehicles and bridges under cross winds. Journal of Wind Engineering and Industrial Aerodynamics, 134, 78-95.

Imai, T., Fujii, T., Tanemoto, K., Shimamura, T., Maeda, T., Ishida, H., & Hibino, Y. (2002). New train regulation method based on wind direction and velocity of natural wind against strong winds. Journal of wind engineering and industrial aerodynamics, 90(12-15), 1601-1610.

Kim, D. H., Kwon, S. D., Lee, I. K., & Jo, B. W. (2011). Design criteria of wind barriers for traffic-Part 2: decision making process. Wind and Structures, 14(1), 71-80.

Kim, S. J., Yoo, C. H., & Kim, H. K. (2016). Vulnerability assessment for the hazards of crosswinds when vehicles cross a bridge deck. Journal of Wind Engineering and Industrial Aerodynamics, 156, 62-71.

Kim, S. J., & Kim, H. K. (2019). Feasibility of a Quasi-Static Approach in Assessing Side-Wind Hazards for Running Vehicles. Applied Sciences, 9(16), 3377.

Korean Society of Civil Engineers, (2006). Design Guidelines for Steel Cable-Supported Bridges, Korea.

Kwon, S. D., Kim, D. H., Lee, S. H., & Song, H. S. (2011). Design criteria of wind barriers for traffic. Part 1: wind barrier performance. Wind and Structures, 14(1), 55.

Mechanical Simulation Corporation. (2016). TruckSim User Manual; Mechanical Simulation Corporation: Ann Arbor, MI, USA.

Misu, Y., & Ishihara, T. (2018). Prediction of frequency distribution of strong crosswind in a control section for train operations by using onsite measurement and numerical simulation. Journal of Wind Engineering and Industrial Aerodynamics, 174, 69-79.

Proppe, C., & Wetzel, C. (2010). A probabilistic approach for assessing the crosswind stability of ground vehicles. Vehicle system dynamics, 48(S1), 411-428.

Salati, L., Schito, P., & Cheli, F. (2017). Wind tunnel experiment on a heavy truck equipped with front-rear trailer device. Journal of Wind Engineering and Industrial Aerodynamics, 171, 101-109.

Sigbjörnsson, R., & Snæbjörnsson, J. T. (1998). Probabilistic assessment of wind related accidents of road vehicles: A reliability approach. Journal of Wind Engineering and Industrial Aerodynamics, 74, 1079-1090.

Simiu, E., & Scanlan, R.H. (1996). Wind Effects on Structures: Fundamentals and Applications to Design, 3rd ed.; John Wiley & Sons Inc. New York, NY, USA.

Snæbjörnsson, J. T., Baker, C. J., & Sigbjörnsson, R. (2007). Probabilistic assessment of road vehicle safety in windy environments. Journal of Wind Engineering and Industrial Aerodynamics, 95(9-11), 1445-1462.

Sterling, M., Quinn, A. D., Hargreaves, D. M., Cheli, F., Sabbioni, E., Tomasini, G. & Morvan, H. (2010). A comparison of different methods to evaluate the wind induced forces on a high sided lorry. Journal of Wind Engineering and Industrial Aerodynamics, 98(1), 10-20.

Strømmen, E. (2010). Theory of Bridge Aerodynamics, 2nd ed. Springer Science & Business Media: Berlin, Germany.

Suzuki, M., Tanemoto, K., & Maeda, T. (2003). Aerodynamic characteristics of train/vehicles under cross winds. Journal of Wind Engineering and Industrial Aerodynamics, 91(1-2), 209-218.

The Weather Network. (2018) SCARY: Vehicles are thrown around on bridge in Japan during Typhoon Jebi. Available online: https://www.youtube.com/watch?v=9yLx3mOxeVQ (accessed on 4 September 2018).

Thomas, D., Diedrichs, B., Berg, M., & Stichel, S. (2010). Dynamics of a high-speed rail vehicle negotiating curves at unsteady crosswind. Proceedings of the Institution of Mechanical Engineers, Part F: Journal of Rail and Rapid Transit, 224(6), 567-579.

Wang, M., Li, X. Z., Xiao, J., Zou, Q. Y., & Sha, H. Q., (2018). An experimental analysis of the aerodynamic characteristics of a high-speed train on a bridge under crosswinds. Journal of Wind Engineering and Industrial Aerodynamics, 177, 92-100.

Wu, M., Li, Y., Chen, X., & Hu, P. (2014). Wind spectrum and correlation characteristics relative to vehicles moving through cross wind field. Journal of Wind Engineering and Industrial Aerodynamics, 133, 92-100.

Xiang, H., Li, Y., Chen, S., & Li, C. (2017). A wind tunnel test method on aerodynamic characteristics of moving vehicles under crosswinds. Journal of Wind Engineering and Industrial Aerodynamics, 163, 15-23.

Xu, Y. L., & Guo, W. H. (2003). Dynamic analysis of coupled road vehicle and cable-stayed bridge systems under turbulent wind. Engineering structures, 25(4), 473-486.

Zhu, L.D., Li, L., Xu, Y.L., & Zhu, Q., (2012). Wind tunnel investigations of aerodynamic coefficients of road vehicles on bridge deck. J. Fluid. Struct. 30, 35-50.

APPENDIX

A. Parameterization results of the vehicles on the approaching span of Gwangan Bridge

Table A.1 Estimated parameters of the sedan on the approaching span

Upper deck							
		C_D	C_S	C_L	C_R	C_P	C_Y
Lane 1	M_1	0.72	0.10	3.00	0.20	-2.98	0.14
	M_2	0.72	-1.02	2.70	-0.04	0.16	0.10
	Z	0.00	0.00	-1.10	0.00	-2.20	0.14
Lane 2	M_1	0.40	0.02	3.00	0.40	0.98	0.00
	M_2	0.38	-0.96	2.70	-0.24	0.22	0.08
	Z	0.00	0.00	-1.20	0.00	0.30	0.00
Lane 3	M_1	0.24	0.02	2.32	0.04	1.54	0.00
	M_2	0.20	-0.52	2.12	-0.20	0.36	0.08
	Z	0.00	0.00	-0.80	0.00	0.60	0.00
Lane 4	M_1	0.34	0.04	3.00	0.10	2.90	0.04
	M_2	0.30	-0.20	2.76	-0.08	0.38	0.14
	Z	0.00	0.00	-1.00	0.00	1.40	0.00
Lower deck							
		C_D	C_S	C_L	C_R	C_P	C_Y
Lane 1	M_1	0.80	0.76	3.00	1.42	-2.72	0.94
	M_2	0.70	-0.10	2.82	-0.36	0.40	0.42
	Z	0.10	0.10	-0.50	-0.20	-2.00	0.10
Lane 2	M_1	0.74	0.82	3.00	1.68	-2.34	0.96
	M_2	0.68	0.36	2.58	0.10	0.78	0.60
	Z	0.00	0.10	-0.50	-0.20	-3.00	0.10
Lane 3	M_1	0.90	0.82	-3.00	1.12	-2.76	0.94
	M_2	0.90	0.84	-2.66	1.46	1.92	0.70
	Z	0.00	0.10	2.40	0.10	-3.00	0.10
Lane 4	M_1	0.82	0.72	3.00	1.20	-2.66	0.88
	M_2	0.82	0.94	2.70	0.84	2.06	0.72
	Z	0.00	0.10	-0.40	0.00	-3.00	0.00

Table A.2 Estimated parameters of the truck on the approaching span

Upper deck							
		C_D	C_S	C_L	C_R	C_P	C_Y
Lane 1	M_1	0.91	1.05	0.65	0.56	0.71	0.96
	M_2	0.70	0.08	0.65	0.03	0.59	0.66
	Z	0.00	-0.20	-0.20	0.80	0.40	-0.40
Lane 2	M_1	0.82	0.72	0.75	0.68	0.86	0.70
	M_2	-0.27	0.02	0.35	0.29	0.51	0.54
	Z	0.00	-0.20	0.80	0.60	-1.80	-0.20
Lane 3	M_1	0.81	0.52	0.25	0.55	0.25	0.54
	M_2	-0.41	0.55	-0.24	0.17	-0.17	0.53
	Z	0.00	0.00	0.80	0.60	-1.80	-0.20
Lane 4	M_1	0.83	0.50	0.33	0.46	0.32	0.51
	M_2	-0.34	0.40	-0.12	0.07	-0.06	0.49
	Z	0.00	0.00	0.60	0.60	-1.40	-0.20
Lower deck							
		C_D	C_S	C_L	C_R	C_P	C_Y
Lane 1	M_1	1.78	1.42	0.75	0.72	0.57	1.23
	M_2	-0.52	-0.23	0.29	0.05	0.43	0.91
	Z	0.20	-0.40	0.00	1.00	-0.20	-0.40
Lane 2	M_1	0.11	1.35	0.92	0.83	0.59	1.19
	M_2	0.21	0.47	0.56	0.45	0.58	0.86
	Z	-0.20	-0.20	-0.20	0.60	0.60	-0.60
Lane 3	M_1	0.06	1.20	0.33	1.00	0.47	1.14
	M_2	0.48	0.77	0.36	0.88	0.53	1.04
	Z	-0.20	0.00	-0.20	0.20	0.20	-0.40
Lane 4	M_1	0.07	1.16	0.59	0.78	0.66	1.09
	M_2	0.30	0.48	0.66	0.53	0.70	1.06
	Z	-0.20	-0.20	-0.20	0.40	0.40	-0.40

Table A.3 Estimated parameters of the tractor-trailer on the approaching span

Upper deck							
		C_D	C_S	C_L	C_R	C_P	C_Y
Lane 1	M_1	0.84	1.02	0.60	0.46	0.64	1.14
	M_2	0.92	0.22	-0.54	0.36	0.56	0.78
	Z	-0.10	-0.10	0.00	0.40	0.50	-0.20
Lane 2	M_1	0.72	0.86	0.88	0.68	0.70	1.10
	M_2	0.26	-0.32	-0.20	0.56	0.64	0.62
	Z	-0.10	-0.20	0.20	0.50	-0.40	-0.20
Lane 3	M_1	0.58	0.70	0.28	0.74	0.70	1.08
	M_2	-0.48	0.04	-0.14	0.62	0.02	0.54
	Z	-0.10	-0.10	0.50	0.50	-1.20	-0.10
Lane 4	M_1	0.72	0.62	0.14	0.68	0.58	0.96
	M_2	-0.22	0.40	0.80	0.56	-0.34	0.54
	Z	0.00	0.00	0.40	0.50	-1.50	0.00
Lower deck							
		C_D	C_S	C_L	C_R	C_P	C_Y
Lane 1	M_1	1.06	1.42	1.12	0.38	0.24	1.30
	M_2	-0.54	-0.84	0.96	0.18	0.84	1.02
	Z	-0.10	0.30	-0.40	0.80	0.00	-0.10
Lane 2	M_1	0.84	1.30	0.56	0.38	0.34	1.26
	M_2	1.42	0.02	1.46	0.26	0.56	1.16
	Z	-0.20	-0.20	-0.30	0.50	0.40	-0.10
Lane 3	M_1	0.84	1.22	0.46	0.80	0.56	1.20
	M_2	1.76	0.72	0.62	0.76	0.50	1.06
	Z	-0.20	-0.10	0.40	0.20	-0.10	-0.10
Lane 4	M_1	0.70	1.10	0.66	0.84	0.48	1.14
	M_2	1.28	0.90	-0.28	0.82	0.48	0.98
	Z	-0.20	0.00	0.50	0.10	-0.10	-0.10

국 문 초 록

김세진
건설환경공학부
서울대학교 대학원

이 연구에서는 강풍에 대한 교량상 차량의 주행안정성을 확률론적으로 평가할 수 있는 방법론을 제시하며, 이를 통하여 주행안정성 확보를 위한 통행제한전략 수립 및 방풍벽 설치를 검토할 수 있는 공학적 툴을 제공하는 것을 목표로 한다. 제시된 평가방법은 풍동실험을 통한 교량상 차량의 공기력계수 측정, 차량 시뮬레이션을 통한 위험풍속 및 통행제한풍속 도출, 그리고 교량현장의 풍환경을 고려한 주행취약도 평가로 크게 세 단계로 구분된다. 본 연구에서는 사례분석을 위하여 복층현수교인 광안대교를 예제 교량으로 선정하였으며, 승용차, 트럭 및 트랙터 트레일러를 대상으로 분석을 수행하였다.

풍동실험시 차선 및 입사각에 따른 교량상 차량의 공기력계수 분포를 측정하기 위한 특수 지그 및 측정시스템을 구축하였으며, 교량 거더형상에 의한 유동장변화의 영향을 고려하기 위하여 2 차원 거더 섹션을 제작하여 차선별/입사각별 차량의 공기력계수를 측정하였다. 광안대교의 경우, 주경간 및 접속교의 풍동모형을 제작하여 차량의 공기력계수 분포를 측정하였다. 케이스별 측정결과를 비교 분석을

수행한 결과, 차량의 위치에 따른 공기력계수의 큰 변동을 관측하였고 데크 위 풍속분포를 측정함으로서 그 원인을 규명하였다.

차량 시뮬레이션을 수행하기 위한 동적 및 준정적 해석 모델을 제시하였다. 동적 해석 모델의 경우 상용프로그램인 CarSim 및 TruckSim을 활용하였으며, 준정적 해석 모델의 경우 6축에 대한 평형방정식들을 기반으로 차량 모델을 직접 구축하였다. 준정적 해석 모델의 적정성을 검토하기 위하여 동적 해석을 통해 산정된 바퀴 반력이력과의 비교 분석을 수행하였으며, 그 결과 바퀴 반력을 기반한 위험도 평가시에는 준정적 해석 모델이 신뢰할 만한 결과를 주는 것을 확인하였다.

차량시뮬레이션을 통하여 교량의 위험풍속그래프을 산정하고 통행제한전략을 구축할 수 있는 방법론을 제시하였다. 위험풍속그래프 산정시 편경사나 곡률과 같은 도로특성들을 반영할 수 있도록 하였으며, 난류의 불확실성을 고려함으로서 확률적인 방법으로 풍향별 위험풍속을 산정하였다. 위험풍속그래프는 모든 차선 및 도로 구간에 대하여 산정되었으며, 동적 및 준정적 해성방법을 모두 활용함으로 전체 교량에 대한 시뮬레이션 소요시간을 최소화 할 수 있는 알고리즘을 제시하였다. 위험풍속그래프는 또한 차량의 속도 및 도로조건에 따라 다르게 산정하였으며, 이렇게 산정된 위험풍속그래프를 활용하여 강풍대응 통행제한전략을 구축하였다. 광안대교의 경우, 주경간 및 양측 접속교로 나누어 분석을 수행하였으며, 상/하부로 데크가 나뉘어 있으므로 이를 고려하여 총 4단계로 통행제한기준을 제시하였다.

마지막으로 현장풍환경을 고려한 상시주행취약도 평가기법을 개발하였다. 기상대 및 현장계측데이터를 활용하여 16 방향 각각의 풍속확률분포를 획득하고, 앞서 산정된 위험풍속그래프를 통해 연간 위험수준 초과 빈도를 산출하였다. 초과 빈도는 각 차선별로 산정되었으며, 결과를 통하여 가장 강풍에 취약한 차선을 판별할 수 있었다. 광안대교의 경우, 해운대 방향 하부데크가 다른 도로구간 대비 훨씬 취약한 구간인 것으로 판정이 되었으며, 이는 도로방향과 현장의 풍속분포간의 관계가 주요 원인인 것으로 파악되었다. 추가 실험 및 분석을 통하여 해당 구간에 방풍벽을 설치함으로서 75% 이상의 취험도 감소효과를 얻을 수 있음을 또한 확인하였다.

제안된 프레임워크는 강풍시 교량상 주행차량 안전확보를 위한 대책 마련 및 의사결정시 유용하게 활용가능한 근거자료를 제공할 수 있을 것으로 기대된다.

주요어: 강풍; 교량; 차량 안정성 평가; 풍동실험; 통행제한;

Student Number: 2015-30275